Electronic Structure of Alloys and Compounds

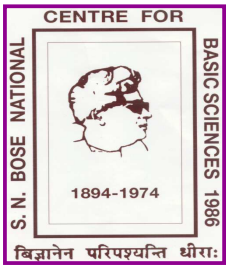

Moshiour Rahaman

S.N. Bose National Centre for Basic Sciences

West Bengal University of Technology

A thesis submitted for the degree of

Doctor of Philosophy (Science)

December, 2010

Thesis Certificate

This is to certify that the thesis entitled **"Study of the electronic structure of alloys and compounds"** submitted by Moshiour Rahaman to the West Bengal University of Technology for the award of the degree of Philosophy, is a bona fide record of the research work done by him under my supervision in the duration of five years from September 2005 to January 2011. He has completed the work truthfully and successfully to the best of my knowledge. The contents of this thesis, in full or in part, have not been submitted to any other Institute or University for the award of any degree or diploma.

Abhijit Mookerjee
(Supervisor)
Distinguished Professor,
Satyendranath Bose National Centre For Basic Sciences,
JD Block, Sector III, Salt Lake City, Kolkata 700 098
India

To my wife Nasrina Bulbul

ACKNOWLEDGMENTS

I am very happy to express my gratitude to Prof. Abhijit Mookerjee who has been a wonderful thesis adviser. His patience and persistence, insights into various problems, critical thinking and insistence on clarity have been most useful and inspiring. Working with him has been a rich and rare experience and I am indebted to him for reasons much beyond the pages of this thesis.

I would like to express my thanks to my collaborators with whom I had interacted directly at work. I am grateful to Prof. Manoj K Harbola of Indian Institute of Technology, Kanpur for his active involvement in the work on first-principles calculation of band gap for semiconductors. I am also grateful to Dr. Andrei Ruban of APM, Material Science and Engineering, Royal Institute of Technology, Stockholm for his active involvement in the work on first-principles calculation of phase transition of disordered alloys.

I would like to thank Prof. Igor Abrikosov of IFM, Linköping University, Sweden for a month's visit to his place and an enthusiastic discussion on KKR-CPA first principles calculations. I also would like to thank Prof. Börje Johansson of APM, Material Science and Engineering, Royal Institute of Technology, Stockholm for giving me the opportunity to work with his group for one year.

I would like to thank my colleagues : Aftab (now at University of Illinois at Urbana-Champaign), Kartick (at Uppsala University, Sweden), Manoj Kumar Yadav (Nepal),as well as Shreemoyee, Mitali, Rudra, Prasant, Ambika Jena and Rajiv of our Centre. I have had a nice time with many friends in the Centre - have been particularly close. It has been fun interacting with them and other students over all these years.

I would like to acknowledge financial support from the Third World Academy of Science (TWAS) and Government of India during the period of this work.

My sincerest thanks go to my parents, sister and especially to my wife for sharing my dreams and for giving me encouragement to work for my goal.

Moshiour Rahaman
S.N.Bose National Centre for Basic Sciences,
Kolkata, India.

Contents

List of Figures

List of Tables

Chapter 1

Introduction

All materials that surround us are built out of atoms. Atoms are themselves built out of a positively charged nuclei surrounded by negativity charged electrons. In solids, the atoms are closely packed and arranged in either a regular lattice or a random network. The atoms are so closely packed that the outer electronic shells of neighbouring atoms start to overlap. The atomic picture of electronic structure breaks down and a new picture emerges, in which the outer electrons are no longer attached to a single nucleus. In metals for instance, these electrons can jump from one atom to another, and can more or less move freely through the solid. The electronic structure of a solid can, however, still be deduced from the constituent atoms. The energy levels of the atomic orbitals spread out into the energy bands for solids. At T=0K, the highest energy filled by electrons is called the Fermi level, which marks the separation between occupied and unoccupied states. Many properties of solids are determined by the behaviour of the electrons in the bands that have energies close to the Fermi level. This is schematically shown in Fig. 1.1.

Assuming a knowledge of the types of atoms comprising any given material, a computational approach enables us to answer two basic questions:

- What is the atomis structure of the material ?
- What are its electronic properties ?

A number of methods to derive answers to these questions have been developed. These methods for computing the structure and properties of materials can conditionally be divided into two classes

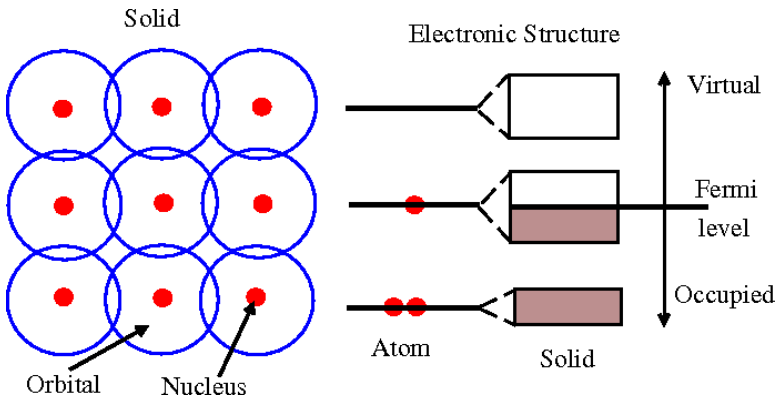

Figure 1.1: Solid - Schematic diagram of electronic structure of solid

- The empirical or semi-empirical methods, which directly depend on empirical or experimental derived quantities.
- The first principle or ab initio methods, which do not use any empirically or experimentally derived quantities.

First principles electronic structure calculations begin with the basic Schrödinger equation which governs all quantum phenomenon at a non-relativistic level. Clearly the calculation for a material is truly a many-body problem. The Hamiltonian of the system contains kinetic energy of the nuclei and electrons as well as all kind of interactions between electron-electron, electron-nuclei, nuclei-nuclei. Let us begin by considering system consisting of N_c ion-cores bonded in a solid by N_e valence electrons. The many body non-relativistic Hamiltonian (1) is :

$$H = \sum_{I=1}^{N_c} \frac{\nabla_I^2}{2M_I} + \sum_{i=1}^{N_e} \frac{\nabla_i^2}{2m_e} + V_{ee}(\{\mathbf{r}\}) + V_{eI}(\{\mathbf{r}_i\}, \{\mathbf{R}_I\}) + V_{II}(\{\mathbf{RI}_I\}) \tag{1.1}$$

where V_{ee}, V_{II} and V_{eI} are the Coulomb interactions between the electrons, the ions themselves and between the electrons and ions. The many-particle wave function of the system Ψ depends on both electron and nucleus coordinates

$$\Psi = \Psi(\mathbf{r}_1, \mathbf{r}_2, \ldots, \mathbf{r}_{N_e}; \mathbf{R}_1, \mathbf{R}_2, \ldots, \mathbf{R}_{N_c}) \tag{1.2}$$

According to Born-Oppenheimer approximation the nuclei is much heavier than electrons, move relatively slowly and may be treated as stationary while electrons move

relative to them. Hence, the nuclei can be thought as being fixed, which makes it possible to solve the Schrödinger equation for the wave function of electrons alone. However, the electron energy depends on the nucleus positions

$$\Psi(\{\mathbf{R}_I\},\{\mathbf{r}_i\}) \approx \chi(\{\mathbf{R}_I\})\psi(\{\mathbf{R}_I\}|\{\mathbf{R}_I\}) \tag{1.3}$$

Thus, the Schrodinger equation for the electrons leads

$$\left[-\sum_{i=1}^{N_e}\frac{\nabla_i^2}{2m} + V_{eI}(\{\mathbf{r}_i\}|\{\mathbf{R}_I\}) + V_{ee}(\{\mathbf{r}_i\})\right]\psi(\{\mathbf{r}_i\}|\{\mathbf{R}_I\}) = E_e(\{\mathbf{R}_I\})\psi(\{\mathbf{r}_i\}|\{\mathbf{R}_I\}) \tag{1.4}$$

The total energy of the system is a sum of electron and nucleus energies. The problem in trying to solve this equation is the number of variables involved. This is $\sim O(10^{20})$! We have to therefore bypass the difficulty by trying to describe physical properties not in terms of the many-body wave-function with enormous degrees of freedom but describe them with respect to a function of a few variables only.

1.1 Density Functional Theory

Most electronic structure calculations for solids are based on density functional theory (DFT), which results from the work of Hohenberg, Kohn and Sham. In DFT, the electronic orbitals are solutions to a Shrodinger equation which depends on the electron density rather than on the individual electron orbitals.

1.1.1 Definition of the problem

Density-functional theory in its earliest formulation by Hohenburg, Kohn and Sham (2, 3) aims at a description of ground state properties of many-electron systems in terms of the electron density. Consider a Hamiltonian of a stationary many-body system

$$\hat{H}_v = \hat{T} + \hat{V} + \hat{W} \tag{1.5}$$

where $\hat{T}$ is the kinetic energy of the electrons, $\hat{V}$ the external potential, and $\hat{W}$ the two-particle interaction. We denote the Hamilton operator $\hat{H}_v$ with a subindex v to indicate that we will consider the Hamiltonian as a functional of the external potential v. The constituent terms are explicitly given by :

$$\hat{T} = \sum_{i=1}^{N} -\frac{1}{2}\nabla_i^2 \quad ; \quad \hat{V} = \sum_{i=1}^{N} v(\mathbf{r}_i) \quad ; \quad \hat{W} = \sum_{i>j}^{N} w(|\mathbf{r}_i - \mathbf{r}_j|)$$

We are interested in electronic systems, i.e. molecules and solids. For all these systems the kinetic energy operator $\hat{T}$ and two-particle interaction $\hat{W}$ are identical. They only differ in the form of the external potential $v(r)$ and the number of electrons N. The properties of all these systems can therefore be regarded as a functional of the external potential v. So, the corresponding wave function $|\Psi[v]\rangle$ and the total energy $E[v]$, which are of course related by the Schrodinger equation

$$(\hat{T} + \hat{V} + \hat{W})|\Psi[v]\rangle = E[v]|\Psi[v]\rangle \tag{1.6}$$

where the external potential specifically can be written as

$$\hat{V} = \int d^3 r v(r)\hat{n}(r) \tag{1.7}$$

where we defined the density operator by

$$\hat{n}(r) = \sum_{i=1}^{N} \delta(r - r_i) \tag{1.8}$$

The expectation value of $\hat{V}$ is given by

$$\langle\Psi|\hat{V}|\Psi\rangle = \int d^3 r n(r)v(r) \tag{1.9}$$

where $n(r)$ the electron density.

1.1.2 Conditions on the electron density and external potentials

It is necessary to define function and functional space [1]before discussing about density and density functional.

[1] **The Lebesgue spaces** Let $\Omega \subset R^d$ be measurable and let $0 < p < \infty$. We denote by $L_p(\Omega)$ the class of all measurable functions $f : \Omega \to R$ such that

$$\int_\Omega |f(x)|^p \, dx < \infty$$

and also

$$\|f\|_p = \left\{ \int_\Omega |f(x)|^p \, dx \right\}^{\frac{1}{p}} \tag{1.10}$$

Definition: A measurable function $f : \Omega \to C$ is essentially bounded on Ω by K if $|f(x)| \leq K$ for almost everywhere $x \in \Omega$. The infimum of such K is the essential supremum of $|f|$ on Ω, and denoted $esssup_{x\in\Omega}|f(x)|$. For $p = \infty$, We define $\|f\|_\infty = esssup_{x\in\Omega}|f(x)|$. Then for all $0 < p < \infty$,

$$L_p(\Omega) = \{f : \|f\|_p < \infty\}$$

Sobolev Spaces

The electron density corresponding to a normalized N-electron wave function is defined as

$$n(r) = N \sum_{\sigma} \int |\Psi(r\sigma_1, r_2\sigma_2, ..., r_N\sigma_N)|^2 \, dr_2 ... dr_N \tag{1.11}$$

We first put some constraints on the wave function. First of all because of the probability interpretation, we know the wavefunction to be normalizable to one, so we require $\|\Psi\| \leq \infty$ where the norm is defined as

$$\|\Psi\| = \sum_{\sigma} \int |\Psi(r_1\sigma_1, ...r_N\sigma_N)|^2 \, dr_1 ... dr_N \tag{1.12}$$

Secondly because of the superposition principle in quantum mechanics we know that also some infinite linear combinations exist and are normalizable. More precisely we first define

$$\Psi_M = \sum_{i=1}^{M} a_m \Psi_m \tag{1.13}$$

with $\|\Psi_m\| = 1$ and

$$\sum_{i=1}^{M} |a_i|^2 = 1 \tag{1.14}$$

A third requirement on wavefunctions is that their kinetic energy expectation value must be finite. So we require that

$$T[\Psi] = \frac{1}{2} \sum_{i=1}^{N} \sum_{\sigma} \int |\nabla_i \Psi(r_1\sigma_1 ... r_N\sigma_N)|^2 \, dr_1 ... dr_N < \infty \tag{1.15}$$

Let $\Omega \subset R^d$ be a domain, $1 \leq p < \infty$, and $m \geq 0$ be an integer. The sobolev space of m derivatives in $L_p(\Omega)$ is

$$W^{m,p}(\Omega) = \{f \in L_p(\Omega) : D^\alpha f \in L_p(\Omega)$$

for all multi-indices α such that $|\alpha| \leq m\}$. We denote the m^{th} order Sobolev space in $L_2(\Omega)$ by

$$H^m(\Omega) = W^{m,2}(\Omega)$$

For $m = 1$ the Sobolev space $H^1(R)$ as the Banach space

$$H^1(R) = \left\{ f \in L_2(R) : \int_R (|f(x)|^2 + |\nabla f(x)|^2) \, dx < \infty \right\}$$

with corresponding norm

$$\|f\| = \left[\int (|f(x)|^2 + |\nabla f(x)|^2) \, dx \right]^{\frac{1}{2}}$$

This implies that

$$\sum_{\sigma} \int |\Psi(r_1\sigma_1 ... r_N\sigma_N)|^2 + \sum_{i=1}^{N} |\nabla_i \Psi(r_1\sigma_1 ... r_N\sigma_N)|^2 dr_1 ... dr_N < \infty \tag{1.16}$$

All these constraints on Ψ have consequences for the constraints on the electron density n which means that the Lebesque integral of the electron density is finite

$$\int n(r)\, dr < \infty \tag{1.17}$$

The finiteness of the kinetic energy implies that n must also be in $L_3(R^3)$ which together with the previous results implies that $n \in L_1(R^3) \cap L_3(R^3)$. Using the Schwarz inequality, we find that the von Weiszacker kinetic energy functional

$$T_W[n] = \frac{1}{2} \int |\nabla \sqrt{n(r)}|^2\, dr = \frac{1}{2} \int \frac{(\nabla n(r))^2}{n(r)}\, dr \leq T[\Psi] < \infty \tag{1.18}$$

Therefore $\sqrt{n(r)} \in H^1(R^3)$. If we now use the Sobolev inequality for the functions $f \in H^1(R^3)$

$$\int |\nabla f(r)|^2\, dr \geq 3(\frac{\pi}{2})^{\frac{4}{3}} [\int |f(r)|^6\, dr]^{\frac{1}{3}}$$

we find that

$$\int n^3(r)\, dr \leq \frac{1}{3}(\frac{2}{\pi})^{\frac{4}{3}} \int |\nabla \sqrt{n}|^2 < \infty \tag{1.19}$$

so we conclude that $n \in L_3(R^3)$ which together with $n \in L_1(R^3)$ implies $n \in L_1(R^3) \cap L_3(R^3)$. We define the sets

$$S_N = \{n | n(r) \geq 0, \sqrt{n} \in H^1(R^3), \int n\, dr = N\} \tag{1.20}$$

and

$$R_N = \{n | n(r) \geq 0, n \in L_3(R^3), \int n\, dr = N\} \tag{1.21}$$

The set R_N and S_N are convex. In particular it follows that the von Weiszacker kinetic energy functional equation (1.18) is a convex functional. We now turn to the expectation values of the external potential $\hat{V}$. From the condition

$$|\int n(r)v(r)\, dr| < \infty \tag{1.22}$$

and $n \in L_1(R^3) \cap L_3(R^3)$ we can deduce some constraints on the external potential $v(r)$. If $n \in L_1(R^3)$ then the above integral exists for bounded potentials,i.e. for potentials $v \in L_\infty(R^3)$. This follows directly from

$$|\int n(r)v(r)\, dr| \leq esssup|v(r)| \int n(r)\, dr < \infty \tag{1.23}$$

if $v \in L_\infty(R^3)$. If $n \in L_3(R^3)$ then the above integral exists for potentials in the set $L_{\frac{3}{2}}(R^3)$. Then by using Holder inequality, we have

$$\int n(r)v(r)\,dr| = \|nv\|_1 \leq \|n\|_3\|v\|_{\frac{3}{2}} < \infty \tag{1.24}$$

The most general set of potentials for which the expectation value $\langle\Psi|\hat{V}|\Psi\rangle$ exists is therefore the set

$$L_{\frac{3}{2}}(R^3) + L_\infty(R^3) = \{v|v = u + w, u \in L_{\frac{3}{2}}(R^3), w \in L_\infty(R^3)\} \tag{1.25}$$

1.1.3 Properties of the energy functional $E[v]$

For the external potentials in the set $L_{\frac{3}{2}}(R^3) + L_\infty(R^3)$ we define the total energy functional $E[v]$ as

$$E[v] = \inf\langle\Psi|\hat{H}|\Psi\rangle \tag{1.26}$$

where $\Psi \in H^1(R^{3N})$ and where the wave function Ψ is normalized to $\|\Psi\| = 1$. We can analyze some properties of this functional. First of all we have that $E[v]$ is concave, that is

$$E[\lambda_1 v_1 + \lambda_2 v_2] \geq \lambda_1 E[v_1] + \lambda_2 E[v_2] \tag{1.27}$$

for all $v \in L_{\frac{3}{2}}(R^3) + L_\infty(R^3)$ and $0 \leq \lambda_1, \lambda_2 \leq 1$ and $\lambda_1 + \lambda_2 = 1$. This follows directly from the variational principle. If Ψ is a wave function corresponding to the infimum in equation (1.27) then

$$E[v] = \langle\Psi|\hat{T} + \hat{V} + \hat{W}|\Psi\rangle = \lambda_1\langle\Psi|\hat{T} + \hat{V}_1 + \hat{W}|\Psi\rangle + \lambda_2\langle\Psi|\hat{T} + \hat{V}_2 + \hat{W}|\Psi\rangle$$

$$\Rightarrow E[v] \geq \lambda_1 E[v_1] + \lambda_2 E[v_2] \tag{1.28}$$

where we used $\lambda_1 + \lambda_2 = 1$. A second property of $E[v]$ is that it is monotonously decreasing, that is, if $v_1(r) \leq v_2(r)$ for all r (almost everywhere) then $E[v_1] \leq E[v_2]$. This follows again from the variational property. If Ψ is a wave function corresponding to the infimum in equation (1.26) then

$$E[v_2] = \langle\Psi|\hat{T} + \hat{V}_2 + \hat{W}|\Psi\rangle = \langle\Psi|\hat{T} + \hat{V}_1 + \hat{W}|\Psi\rangle + \langle\Psi|\hat{V}_1 - V_2 + \hat{W}|\Psi\rangle$$

$$E[v_2] \geq E[v_1] + \int n(r)(v_2(r) - v_1(r))\,dr \geq E[v_1] \tag{1.29}$$

1.1.4 The Hohenbergh-Kohn functionals $F_{HK}[n]$ and $F_{EHK}[n]$

We will try to understand the Hohenberg-Kohn functional which has been introduced by Hohenberg and Kohn in their well-known paper(2). Suppose that Ψ_1 and $\Psi_2 \in H^1(R^{3N})$ are non-degenerate ground state wave functions corresponding to external potentials v_1 and $v_2 \in L_{\frac{3}{2}}(R^3) + L_\infty(R^3)$ with corresponding electron densities n_1 and n_2. Then if $v_1 \neq v_2 + C$ where C is constant then $n_1 \neq n_2$. As a first step we have that if $v_1 \neq v_2 + C$ that $\Psi_1 = \Psi_2$. This follows by contradiction. Suppose by subtraction of the Hamiltonian for Ψ_1 and Ψ_2 we find that

$$(v_1 - v_2)\Psi = (E_1 - E_2)\Psi \tag{1.30}$$

If $v_1 - v_2$ is not constant in some region then Ψ must vanish in this region for the above equation to be true. However if $v_1, v_2 \in L_{\frac{3}{2}}(R^3) + L_\infty(R^3)$ then Ψ cannot vanish on an open set by the unique continuation theorem. So we obtain a contradiction and we find $\Psi_1 \neq \Psi_2$. So different potentials give different wavefunctions. We denote $\Psi_1 = \Psi[v_1]$ and $\Psi_2 = \Psi[v_2]$. These different wave functions also yield different densities. This follows again by contradiction. If $n_1 = n_2 = n$ then

$$\begin{aligned} E[v_1] = \langle [v_1]|\hat{T} + \hat{V}_1 + \hat{W}|\Psi[v_1]\rangle &< \langle [v_2]|\hat{T} + \hat{V}_1 + \hat{W}|\Psi[v_2]\rangle \\ \langle [v_2]|\hat{T} + \hat{V}_2 + \hat{W}|\Psi[v_2]\rangle &+ \int n(r)(v_1(r) - v_2(r))\, dr \\ \Rightarrow E[v_1] &< E[v_2] + \int n(r)(v_1(r) - v_2(r))\, dr \end{aligned} \tag{1.31}$$

Similarly, we have

$$E[v_2] < E[v_1] + \int n(r)(v_2(r) - v_1(r))\, dr \tag{1.32}$$

Adding the both inequalities yields the contradiction

$$E[v_1] + E[v_2] < E[v_1] + E[v_2] \tag{1.33}$$

So we conclude that $n_1 \neq n_2$, which proves our statement. We now define the set A_N as

$A_N = \{n | n$ comes from a non-degenerate ground stateg $\}$

The set A_N is a subset of the previously defined set S_N. The densities in the set A_N

we call pure state v-representable densities or denote as PS-V-densities. On the set of PS-V densities we can therefore define the Hohenberg-Kohn functional F_{HK} as

$$F_{HK}[n] = \langle \Psi[n] | \hat{T} + \hat{W} | \Psi[n] \rangle \tag{1.34}$$

We can then define the energy functional E_v as

$$E_v[n] = \int n(r)v(r)\,dr + F_{HK}[n] \tag{1.35}$$

Therefore

$$E_v[n] = \inf_{n \in A_N} \left\{ \int n(r)v(r)\,dr + F_{HK}[n] \right\} \tag{1.36}$$

The functional F_{HK} has some mathematical inconveniences. First of all its domain A_N is not convex however the functional F_{HK} is convex. There are convex combinations of PS-V ground state densities which are not in A_N. An example of this is a convex combination of densities corresponding to a q-fold degenerate ground state multiplet

$$n = \sum_{i=1}^{q} \lambda_i n_i, \sum_{i=1}^{q} \lambda_i = 1, 0 \leq \lambda_i \leq 1 \tag{1.37}$$

which in general is not in A_N. We define
$B_N = \{n = \sum_i \lambda_i n_i | n_i \text{ comes from the same } v \text{ for all } i, \sum_i \lambda_i = 1, 0 \leq \lambda_i \leq 1\}$
We call these densities ensemble v-representable densities or E-V-densities. We can now extend the functional F_{HK} to the ensemble functional F_{EHK} on the set B_N of ensemble v-representable densities. For a degenerate ground state multiplet $\{\Psi_i\}$ with q-fold degeneracy corresponding to some external potential v we define the ensemble density matrices

$$\hat{D} = \sum_{i=1}^{q} \lambda_i |\Psi_i\rangle\langle\Psi_i|, \sum_{i}^{q} \lambda_i = 1, (0 \leq \lambda_i \leq 1) \tag{1.38}$$

the corresponding ensemble density is given by

$$n(r) = Tr\hat{D}\hat{n}(r) \tag{1.39}$$

where $\bar{n}(r)$ is the density operator.For every E-V-density n we can therefore unambiguously define

$$F_{EHK}[n] = Tr\hat{D}[n](\hat{T} + \hat{W}) \tag{1.40}$$

where $\hat{D}[n]$ is any of the ground state ensemble density matrices corresponding to n. We can now define an extension of the energy functional E_v to the set of E-V-densities

$$E_v[n] = \int n(r)v(r)\,dr + F_{EHK}[n] = Tr\hat{D}[n]\hat{H} \tag{1.41}$$

Similarly, as for F_{HK} we easily can prove

$$E[n] = \inf_{n\in B_N}\left\{\int n(r)v(r)\,dr + F_{EHK}[n]\right\} \tag{1.42}$$

1.1.5 The Levy and Lieb functionals $F_{LL}[n]$ and $F_L[n]$

The functionals F_{HK} and F_{EHK} have the unfortunate mathematical difficulty that their domains of definition A_N and B_N, although they are well-defined, are difficult to characterize, i.e. it is difficult to know if a given density n belongs to A_N or B_N. It is therefore desirable to extend the domains of definition of F_{HK} and F_{EHK} to an easily characterizable (preferably convex) set of densities. This can be achieved using the constrained search procedure introduced by Levy (5) and further investigated by Lieb (4). The Levy-Lieb functional F_{LL} is defined as

$$F_{LL}[n] = \inf_{\Psi\to n}\langle\Psi|\hat{T}+\hat{W}|\Psi\rangle \tag{1.43}$$

where the infimum is searched over all normalized anti-symmetric N-particle wave functions in $H^1(R^{3N})$ yielding density n. As we have shown earlier such a density is always in the convex set S_N which is again a subspace of $L_1 \cap L_3$. The functional F_{LL} is an extension of the Hohenberg-Kohn functional F_{HK} which was defined on A_N to the larger set S_N. We define a corresponding energy functional

$$E_v[n] = \int n(r)v(r)\,dr + F_{LL}[n] \tag{1.44}$$

If n_0 is the ground state density corresponding to v with corresponding ground state wave function $\Psi[n_0]$ then

$$E_v[n] = \inf_{\Psi\to n}\langle\Psi|\hat{H}|\Psi\rangle \geq \langle\Psi[n_0]|\hat{H}|\Psi[n_0]\rangle = E_v[n_0]$$

Minimizing E_v over the set S_N therefore yields the ground state density n_0 corresponding to external potential v. The functional F_{LL} has however one inconvenient property, it is not convex. We find

$$\int \bar{n}(r)v(r)\,dr + F_{LL}[\bar{n}] = \inf_{\Psi\to n}\langle\Psi|\hat{H}|\Psi\rangle$$

$$> \frac{1}{2L+1}\sum_{i=1}^{2L+1}\langle\Psi[n_i]|\hat{H}|\Psi[n_i]\rangle = \frac{1}{2L+1}\sum_{i=1}^{2L+1}F_{LL}[n_i] + \int \bar{n}(r)v(r)\,dr$$

and we find

$$F_{LL}[\bar{n}] > \frac{1}{2L+1}\sum_{i=1}^{2L+1}F_{LL}[n_i]$$

which proves the non-convexity of F_{LL}. Therefore, we can now define a different but related functional with the same domain S_N which is also convex. This is the Lieb (4) functional F_L defined as

$$F_L[n] = \inf_{\hat{D}\to n} Tr\hat{D}(\hat{T}+\hat{W}) \tag{1.45}$$

where the infimum is searched over all N-particle density matrices

$$\hat{D} = \sum_{i=1}\lambda_i|\Psi_i\rangle\langle\Psi_i|, \sum_{i=1}\lambda_i = 1, |\Psi_i\rangle \in H^1(R^{3N}) \tag{1.46}$$

which yield the given density $n(r) = Tr\hat{D}\hat{n}(r)$ where $|\Psi_i\rangle$ is an orthonormal set. This functional is an extension of F_{EHK} to the larger set S_N, that is $F_L[n] = F_{EHK}[n]$ if $n \in B_N$ We can again define an energy functional

$$E_v[n] = \int n(r)v(r)\,dr + F_L[n] \tag{1.47}$$

which similar as F_{LL} assumes its minimum at the ground state density corresponding to potential v. We further have the following relations

$F_L[n] = F_{LL}[n]$ if $n \in A_N$

and

$F_L[n] < F_{LL}[n]$ if $n \in B_N$ and $n \notin A_N$

The first relation follows from the fact that is the density n is a pure state v-representable density then the minimizing density matrix for F_L is a pure state density matrix. The second relation follows from the fact that if n is an ensemble v-representable density there is a ground state ensemble density matrix $\hat{D}[n]$ Any wave function yielding density n can not be a linear combination of these ground state wave-functions otherwise n would be pure state v-representable. Therefore its expectation value with the Hamiltonian must be larger, i.e

$$\langle\Psi_i|\hat{H}|\Psi_i\rangle < \inf_{\Psi\to n}\langle\Psi|\hat{H}|\Psi\rangle = \int n(r)v(r)\,dr + F_{LL}[n]$$

Which proves our statement. We can prove another important property of F_L, which is its convexity. If $n = \lambda_1 n_1 + \lambda_2 n_2$ then we have

$$\lambda_1 F_L[n_1] + \lambda_2 F_L[n_2] = \lambda_1 \inf_{\hat{D}_1 \to n_1} Tr\hat{D}_1(\hat{T} + \hat{W}) + \lambda_2 \inf_{\hat{D}_2 \to n_2} Tr\hat{D}_2(\hat{T} + \hat{W})$$

$$= \inf_{\hat{D_1,D_2} \to n_1, n_2} Tr(\lambda_1 \hat{D}_1 + \lambda_2 \hat{D}_2)(\hat{T} + \hat{W}) \geq \inf_{\hat{D} \to n} Tr\hat{D}(\hat{T} + \hat{W}) = F_L[n]$$

We therefore now have established that F_L is a convex functional on a convex space. This is important information which enables one to derive the differentiability of the functional F_L at the set B_N of ensemble v-representable densities.

1.1.6 Kohn-Sham theory by Legendre transforms

The method described here the work of De Dominics and Martin(6) and Fukuda(7). We have seen from equation (1.6) the ground state energy $E[v]$ and wave function $|\Psi[v]\rangle$ are functional of external potential. We have

$$(\hat{T} + \hat{V} + \hat{W})|\Psi[v]\rangle = E[v]|\Psi[v]\rangle \tag{1.48}$$

Now multiply $\langle\Psi|$ on both side of the above eqaution, we get

$$E[v] = \langle\Psi[v]|H_v|\Psi[v]\rangle[v] \tag{1.49}$$

Our goal is now to go from the potential as our basic variable, to a new variable, which will be the electron density. The deeper reason that this is possible that the density and the potential are conjugate variables. With this means that the contribution of the external potential to the total energy is simply an integral of the potential times the density. We make use of this relation if we take the functional derivative of the energy functional $E[v]$ with respect to the potential v

$$\frac{\delta E}{\delta v(r)} = \langle \frac{\delta \Psi}{\delta v(r)}|\hat{H}|\Psi\rangle + \langle\Psi|\hat{H}|\frac{\delta\Psi}{\delta v(r)}\rangle + \langle\Psi|\frac{\delta \hat{H}_v}{\delta v(r)}|\Psi\rangle$$

$$\Rightarrow \frac{\delta E}{\delta v(r)} = E[v]\frac{\delta}{\delta v(r)}\langle\Psi|\Psi\rangle + \langle\Psi|\hat{n}(r)|\Psi\rangle$$

$$\Rightarrow \frac{\delta E}{\delta v(r)} = \langle\Psi|\hat{n}(r)|\Psi\rangle = n(r) \tag{1.50}$$

where we used the Schrodinger equation $\hat{H}_v|\Psi\rangle = E[v]|\Psi\rangle$ and the normalization condition $\langle\Psi|\Psi\rangle = 1$. Note that the equation above is nothing but a functional generalization

of the well-known Hellmann-Feynman(8, 9) theorem. Now we can go to the density as our basic variable by defining a Legendre transform

$$F[n] = E[v] - \int d^3r n(r)v(r) = \langle \Psi[v]|\hat{T} + \hat{W}|\Psi[v]\rangle \tag{1.51}$$

where v must now be regarded as a functional of n. The uniqueness of such a mapping is garanteed by the Hohenbergh-Kohn(2) theorem. The set of densities for which the functional $F[n]$ is defined is the set of so-called v-representable densities. These are ground state densities for a Hamiltonian with external potential v. The question which constraints one has to put on a density to make sure that it is v-representable[8] is known as v-representability problem. Again, take derivative of the above equation (1.51) with respect to n, we have

$$\frac{\delta F}{\delta n(r)} = -v(r) \tag{1.52}$$

This is our basic relation. In order to derive the Kohn-Sham equations we define the following energy functional for a system of noninteracting particles with external potential v_s and with ground state wave function $|\Phi[v_s]\rangle$,

$$E_s[v_s] = \langle \Phi[v_s]|\hat{T} + \hat{V}_s|\Phi[v]\rangle \tag{1.53}$$

with Legendre transform

$$F_s[n] = E[v_s] - \int d^3r n(r)v_s(r) = \langle \Phi[v_s]|\hat{T}|\Phi[v_s]\rangle \tag{1.54}$$

and derivatives

$$\frac{\delta E_s}{\delta v_s(r)} = n(r) \tag{1.55}$$

$$\frac{\delta F_s}{\delta n(r)} = -v_s(r) \tag{1.56}$$

We see that $F_s[n]$ in equation (1.54) is the kinetic energy of a noninteracting systems with potential v_s and density n. For this reason the functional F_s is usually denoted by T_s. Finally, we define the exchange-correlation functional $E_{xc}[n]$ by the equation

$$F[n] = F_s[n] + \frac{1}{2}\int d^3r d^3r' n(r)n(r')w(|r - r'|) + E_{xc}[n] \tag{1.57}$$

This equation assumes that the functionals $F[n]$ and $F_s[n]$ are defined on the same domain of densities. We thus assume that for a given ground state density of an

interacting system there is a noninteracting system with the same density. Inother words, we assume that the interacting density is noninteracting-v-representable. If we differentiate equation(1.57) with respect to the density n, we obtain

$$v_s(r) = v(r) + \int d^3r' n(r') w(|r - r'|) + v_{xc}(r) \tag{1.58}$$

where

$$v_{xc}(r) = \frac{\delta E_{xc}}{\delta n(r)}$$

defines the exchange-correlation potential. Now the state$|\Phi[v_s]\rangle$ is a ground state for a system of noninteracting particles, and can therefore be written as an antisymmetrized product of single-particle orbitals $\varphi_i(r)$. If we now collect our results we see that we have converted the ground state problem into the following set of equations

$$E[v] = \sum_{i=1}^{N} -\frac{1}{2}\int d^3r \varphi_i^*(r)\nabla^2\varphi_i(r) + \int d^3r n(r)v(r) + \frac{1}{2}\int d^3r d^3r' n(r)n(r')w(|r-r'|) + E_{xc}[n] \tag{1.59}$$

$$(-\frac{1}{2}\nabla^2 + v(r) + \int d^3r' n(r')w(|r - r'|) + v_{xc}(r))\varphi_i(r) = \epsilon_i(r) \tag{1.60}$$

$$n(r) = \sum_{i=1}^{N} |\varphi_i(r)|^2 \tag{1.61}$$

The above equations (1.59,1.60,1.61) constitute the ground state Kohn-Sham equations, These equations turn out to be of great practical use. If we can find a good approximation for the exchange-correlation energy, we can calculate the exchange-correlation potential v_{xc} and solve the orbital equations self-consistently. The density we find in this way can then be used to calculate the ground state energy of the system. Various approximations for the exchange-correlation exist in literature. In our calculations we shall specify the particular approximation used.

1.2 Basic assumptions of electronic band theory

The large number of electrons contained in a macroscopic crystal prohibits a direct solution of the Schrödinger equation for such a system. Reduction to the single particle-like Kohn-Sham equation is a starting point. Fortunately, the solid may have lattice periodic symmetry in the bulk, and this can be exploited to reduce the size of the problem significantly, using Bloch's theorem, which enables us to replace the problem

of solving the Kohn-Sham equation for electrons in an infinite periodic solid by that of solving the equation in a unit cell (see Fig.1.2). The Kohn-Sham equation for an

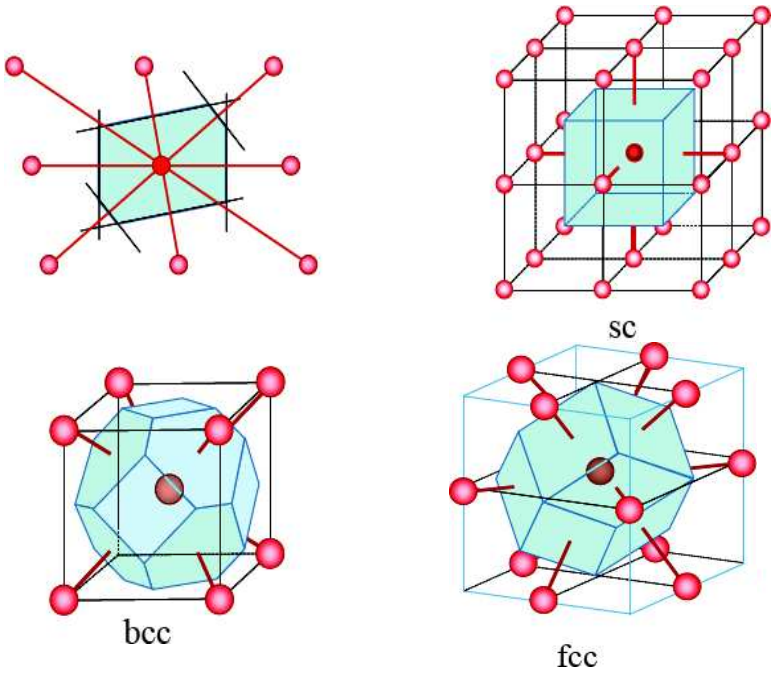

Figure 1.2: Unit cell - Unit cell of the rhombic, simple cubic, body-centered cubic and face-centered cubic lattices.

electron in a crystal can be solved in two limiting cases:

- the nearly free electron approximation, in which the potential is considered to be weak everywhere and
- the tight-binding approximation, in which it is assumed that the states are tightly bound to the nuclei.

In ab initio methods, potential is usually determined self-consistently with the electron density according to the density functional scheme. In a general electronic structure calculation we must give the basis functions a good deal of attention since we know that by cleverly choosing the basis states we can reduce their number, which has a huge impact on the computer time needed as the latter is dominated by matrix diagonalisations. To solve the Kohn-Sham equation (1.4) with a periodic potential we can distinguish two main approaches based on the expansion of basis wave function.

- Energy independent basis set such as plane waves in the pseudo-potential method, plane waves orthogonalized to core states in the orthogonalized plane wave method, linear combination of the atomic orbitals in the tight-binding method.
- Energy dependent partial wave like the cellular method, the augmented plane wave method, the Korringa-Kohn-Rostoker (KKR) method and its linearized version the linear muffin-tin orbitals method (LMTO).

As a part of our work we shall use the KKR and LMTO methods.

1.2.1 The KKR and LMTO methods

Korringa (1947), Kohn and Rostoker(1954) (KKR) introduce the Green' function method (or KKR method) for expansion inside the muffin tin sphere and in the interstitial region, the wave functions are expanded in phase shifted spherical waves. The boundary conditions are then expressed as the condition for the self consistent multiple scattering between the MT spheres.

It is clear form the discussion in the earlier section that LDA reduces the many-body Hamiltonian of the valence electron cloud in the presence of a 'frozen' array of ion-cores. The effective potential seen by an electron within LDA looks like:

$$V(r) = \sum_R v(r - R)$$

where R and r are the position of the ion-cores and electron respectively. In the neighborhood of an ion-core the potential seen by the electron in a solid is not very different from that in focused atoms ion-core. A radius s_r can be define around R within which the potential is spherically symmetric. The spheres with radius s_r around R is called *muffin-tin spheres*, In the interstitial the potential varies very slowly and one can replace the potential in this region by a constant. The resulting potential is called the *Muffin-tin Potential*. Detail description of this method has already been given in Andersen and Jepsen (10). Here we shall give a short summary and discuss the main results that we have used.

After muffin-tin(MT) approximation the solution inside the MT can be obtained from the numerical solution of the radial Schrödinger equation

$$[r\phi_{Rl}(\varepsilon, r)]'' = \left[V_R(r) + \frac{l(l+1)}{r^2} - \varepsilon\right] r\phi_{Rl}(\varepsilon, r) \tag{1.62}$$

In the outside(interstitial) solutions for constant potential can be represented as linear combination of the spherical Bessel $j_l(\kappa, r)$ and Neumann functions $n_l(\kappa, r)$. To make the basis functions to be well behaved all over the space we add $P_{Rl}(\varepsilon, \kappa)\ j_l(\kappa, r_{_R})$ to the partial wave. This makes the tail (in the interstitial) independent of the muffin-tin potential within the muffin-tin sphere. The muffin tin orbitals are then looks like

$$\chi_{RL}(\varepsilon, \kappa, r_{_R}) = Y_L(\hat{r}_{_R}) \times \begin{cases} \phi_{Rl}(\varepsilon, r_{_R}) + P_{Rl}(\varepsilon, \kappa)\ j_l(\kappa, r_{_R}), & r_{_R} \leq s_{_R} \\ n_l(\kappa, r_{_R}), & r_{_R} > s_{_R} \end{cases} \tag{1.63}$$

where L is the combined index for $\{lm\}$ and r_R refers to $|\mathbf{r} - \mathbf{R}|$. $\kappa = \varepsilon - V_{_0}$ can be interpreted as the "kinetic energy in the interstitial region". The tail represented by Neuimann function $n_L(\kappa, r_{_R})$ can be expanded in terms of canonical structure constants $S_{R'L',RL}(\kappa)$ which depends only upon the relative position of R' with respect to R as :

$$n_L(\kappa, \mathbf{r}_{\mathbf{R}'}) = \sum_{L'} j_{L'}(\kappa, \mathbf{r}_{\mathbf{R}'})\ S_{R'L',RL}(\kappa) \tag{1.64}$$

The MTO-tails from neighboring sites (R') cancel the "unphysical" term $P_{Rl}(\varepsilon, \kappa) j_L(\kappa, r_{_R})$ of the MTO at the site R which directly leads to the KKR set of homogeneous linear equations

$$\sum_{RL} \Big[P_{_{R'l'}}(\varepsilon, \kappa)\delta_{R'R}\ \delta_{L'L} - S_{_{R'L',RL}}(\kappa) \Big]\ c_{_{RL}}(\varepsilon)\ = 0, \qquad \text{for each } R', L'. \tag{1.65}$$

Solving for $c_{_{RL}}$ we get the KKR secular equation:

$$\det \mid P(\varepsilon, \kappa) - S(\kappa) \mid = 0 \tag{1.66}$$

The KKR equation is a non-linear equation in energy and there is not any priory idea that how many root one can expect nor whether all roots are physically permissible. Since the equation is not of the type of eigen value equation so there is no proof of reality of the roots.

Most importantly the canonical structure constants $S(\kappa)$ are strongly energy dependent and are long ranged in real space. Typical wavelength of the partial wave is of the order of $2\pi/\kappa$. If this is much larger then the distance between the neighboring muffin-tin spheres, the structure matrix has a very weak energy dependence. For close-packed solids and low energies, one often uses the atomic-spheres approximation (ASA), which substitutes the MT-spheres with slightly overlapping atomic spheres and sets $\kappa = 0$, so that the envelope functions become simple multipole potentials $r^{-l-1}Y_{lm}(\hat{r})$.

In open structures, also the potentials in the voids are also taken to be spherically symmetric. It has been experienced that the overlap between the Wigner-Seitz spheres is less than 15% is good approximation within ASA and gives reliable results. In ASA we integrate out a bit more up to the WS sphere instead of integrating the atomic potential out as far as the MT sphere that is in apparently we include the flat potential region.It is also possible to calculate the exact difference between the integrals of the interstitial functions over the WS polyhedron and the sphere. This is called the combined correction term.

The long range of the envelopes with $\kappa = 0$ can be got rid of by screening with multipoles on the neighboring sites and it is possible to generate the structure matrix in real space. The screened structure matrix $\mathbf{S}^\alpha$ can be obtained from the canonical structure matrix $\mathbf{S}^0$ by the unitary transformation :

$$\mathbf{S}^\alpha = \mathbf{S}^0 \left(1 - \mathbf{Q}^\alpha \, \mathbf{S}^0\right)^{-1}$$

$\mathbf{Q}^\alpha$ is the diagonal screening matrix, which defines the uniqueness of the above transformation for all closely packed structures, and yields the most localized structure constant with exponential decay rather than the usual power law behavior. In the most tight-binding representation, a LMTO basis orbital centered at site R, is given in the ASA, by the expression :

$$\chi^\alpha_{RL}(r_R) = \phi_{RL}(r_R) + \sum_{R'L'} \dot{\phi}^\alpha_{R'L'}(r_{R'}) \; h^\alpha_{R'L',RL} \tag{1.67}$$

where $L = (lm)$ is the collective angular momenta index. The function ϕ_{RL} is the solution of the wave-equation inside the spheres of radius S_R at R for some reference energy $E_{\nu RL}$ and is normalized within the sphere. The potential inside the sphere is calculated using the local density functional approximation (LDA). The radial part of the $\dot{\phi}^\alpha_{RL}$ is related to the energy derivative of $\phi^\alpha_{RL}(r_R)$ at the reference energy :

$$\dot{\phi}^\alpha_{RL}(r_R) = \dot{\phi}_{RL}(r_R) + \phi_{RL}(r_R) o^\alpha_{RL}$$

The quantity $o^\alpha = \langle \phi_{Rl} \mid \dot{\phi}^\alpha_{Rl} \rangle$ is the overlap. The expansion coefficients h_α are given by

$$h^\alpha_{RL,R'L'} \;=\; (C^\alpha_{RL} - E_{\nu RL})\, \delta_{RR'} \delta_{LL'} + \sqrt{\Delta^\alpha_{RL}} S^\alpha_{RL,R'L'} \sqrt{\Delta^\alpha_{RL}} \tag{1.68}$$

Where C^{α}_{RL} and Δ^{α}_{RL} are the potential parameters to be obtained from the potential function at the reference energy $E_{\nu RL}$. $S^{\alpha}_{RL,R'L'}$ is the screened structure matrix whose elements in the most tight-binding representation are essentially zero beyond the second shell of neighbors in all closed packed structures.

From the expression of TB-LMTO orbital in equation(1.67) the summation over the composite angular momentum index suggest that orbitals are not preserving pure L character. Further $\dot{\phi}^{\alpha}_{RL}(r_R)$ and $\phi^{\alpha}_{RL}(r_R)$ are truncated outside the Wigner-Seitz spheres and the expansion coefficients vanish beyond the second shell of neighbors in all closed packed structures. Therefore all TB-LMTO orbitals are short ranged and in this representation the Hamiltonian is sparse. This is ideal for real space calculations based on the recursion method witch we shall discuss latter in details . The Hamiltonian and overlap matrices for this basis are given by :

$$H = h + hoh + (I + ho)E_{\nu}(I + ho) \tag{1.69}$$

$$o = \langle\chi|\chi\rangle = (I + ho)(I + ho) \tag{1.70}$$

Summation indices RL in the above equation are suppressed for convenience. The matrix o is diagonal in RL representation and its value is determined by the logarithmic derivative of the function $\dot{\phi}$ at the sphere boundary. The orbital wave function in equation1.67 are not orthogonal. Orthogonalized them (Löwdin orthonormalization) the Hamiltonian in the ASA is given by :

$$H = E_{\nu} + h - hoh + hohoh - \cdots \tag{1.71}$$

and for the first order approximation

$$H^{(1)} = E_{\nu} + h \tag{1.72}$$

The parameter o determines the degree of non-orthogonality of the basis. Again o^{-1} has the dimension of energy and provides a measure of the energy window about the reference energy E_{ν} for which the density of states obtained with $H^{(1)}$ are reliable.

1.3 Green Function formalism

In systems like random alloys, surfaces and interfaces, defects in solids, spin-glasses,amorphous materials the conventional Bloch theorem is no longer valid due to lack of periodicity

of the lattice. In this situation Greens function is the alternative approach for the electronic structure calculation. The Greens function is nothing but a propagator. For a given Hamiltonian H the time-dependent Schrödinger equation determines the time evolution of the wave function $\psi(t)$ as

$$i\frac{\partial}{\partial t}\psi(t) = H\psi(t) \tag{1.73}$$

with formal solution

$$\psi(t) = \exp^{-iHt}\psi(0) \tag{1.74}$$

with $\psi(0)$ is the initial wave function. Corresponding to the above Schrödinger equation we can define two propagators $G^R(t)$(retarded) and $G^A(t)$ (advanced) as

$$\left(i\frac{\partial}{\partial t} - H\right) G^{R(A)}(t) = \delta(t) \tag{1.75}$$

with boundary conditions

$$\begin{aligned} G^R(t) &= 0 \qquad t < 0 \\ G^A(t) &= 0 \qquad t > 0 \end{aligned}$$

and the formal solution of these equation is:

$$\begin{aligned} G^R(t) &= -\Theta(t) i e^{-iHt} \\ G^A(t) &= \Theta(-t) i e^{-iHt} \end{aligned}$$

for all t, where $\Theta(t)$ is zero for $t < 0$ and unity for $t > 0$. Clearly the greens function coincides with the time evolution operator(up to a factor). To propagate the wave function forward in time one use $G^R(t)$ and $G^R A(t)$ for the backward in time. Now for a given perturbing potential $V(\vec{r})$ to the Hamiltonian H_0, The Green's function G_1 corresponding to the perturb Hamiltonian $H = H_0 + V$ can be written in terms of the Greens function G_0 corresponding to H_0 via Dyson integral as:

$$G_1(t) = G_0(t) + \int_0^t G_0(t - t')VG_1(t')dt' \tag{1.76}$$

and the wave function $\psi_0(t)$ of system without interaction evolves into the wave function $\psi_1(t)$ by the *Lippmann-schwinger equation* as

$$\psi_1(t) = \psi_0(t) + \int_0^t G_0(t - t')V\psi_1(t')dt' \tag{1.77}$$

Taking the Fourier transformation of the $G(t)$ we can write the energy dependent Greens function as:

$$G(z) = (z - H)^{-1} \tag{1.78}$$

where $z = E + i\delta$ is a complex number with very small imaginary part δ. Clearly the energy dependent Green's function is the resolvent of the time dependent Hamiltonian and it's singularities determines the eigenvalue spectrum; in particular it has poles at the eigen energies of the bound states, and branch cut along the energies of the continuous spectrum. For $Im(z) > 0$, $G(z)$ is an analytical function of z and has certain analytic properties witch are collectively called the Harglotz properties

1. $\mathrm{Im}G(z) < 0 \quad$ when $z > 0$
2. Singularities of $G(z)$ lie on the real axis.
3. $G(z) \to \frac{1}{z}$ when $\mathrm{Re}(z) \to \infty$

Using the complete basis set of eigen function $|\psi_i\rangle$ corresponding to the eigenvalues ϵ_i of the Hamiltonian, the spectral representation of the Green's function can be written as:

$$G(z) = \sum_i |\psi_i\rangle \frac{1}{z - \epsilon_i} \langle\psi_i| \tag{1.79}$$

and in real space it is represented as

$$G(\vec{r}, \vec{r}', z) = \sum_i \frac{\psi_i(\vec{r})\psi_i^*(\vec{r}')}{z - \epsilon_i} \tag{1.80}$$

in the limit of the $\mathrm{Im}(z) = \delta \to 0$ for an outgoing wave vector at $\vec{r}$ with a source term at $\vec{r}'$. It is known that for $z = E \pm i\delta$ and $\delta \to 0$

$$\frac{1}{z - \epsilon_i} \to \mathrm{P}\left(\frac{1}{E - \epsilon_i}\right) \mp i\pi\delta(E - \epsilon_i)$$

Where P denotes the principal part. So from the spectral representation of the greens function in the real space the imaginary part is directly related to the spectral and space resolved density of state.

$$n(r; E) = -\frac{1}{\pi} \lim_{\delta \to 0} \mathrm{Im}G(\vec{r}, \vec{r}, E + i\delta) \tag{1.81}$$

and the spectral density of state is then given by

$$n(E) = -\frac{1}{\pi} \lim_{\delta \to 0} \mathrm{Im} \int G(\vec{r}, \vec{r}, E + i\delta) d^3r = -\frac{1}{\pi} \lim_{\delta \to 0} \mathrm{Tr}G(E + i\delta) \tag{1.82}$$

Also the charge density is found as an integral of $n(\vec{r};E)$ over the energies upto fermi level E_f

$$\rho(\vec{r}) = -\frac{1}{\pi}\lim_{\delta\to 0}\mathrm{Im}\int_{-\infty}^{E_f} G(\vec{r},\vec{r},E+i\delta)dE \;= -\frac{1}{\pi}\lim_{\delta\to 0}\mathrm{Im}\int_{-\infty}^{E_f}\mathrm{Tr}(\hat{r}G(\vec{r},\vec{r},E+i\delta))dE \tag{1.83}$$

with $\hat{r}$ is the position operator. In general the expectation value of any physical quantity represented by an operator $\hat{O}$ can be obtain by the relation

$$\langle O\rangle = -\frac{1}{\pi}\lim_{\delta\to 0}\mathrm{Im}\int_{-\infty}^{E_f}\mathrm{Tr}(\hat{O}G(\vec{r},\vec{r},E+i\delta))dE \tag{1.84}$$

From the above relations we can say that the greens function contains all the informations about the system. Therefore, if it is possible to calculate the greens function of the system then we can able to obtain all the physical properties of the system.

1.4 The Recursion method

The recursion method introduced by Haydock(11) is basically a scheme for the calculation of the local properties of a system. For the system like disordered materials, amorphous system, spin-glass etc. where the enormous simplification of the Bloch theorem is no longer valid due to the lack of the periodicity, one has to invoke the *"Black Body Theorem"* discussed by Heine and Friedel(12). Particularly from their discussion it implies that the most of the physical properties are govern by the local environments. In the recursion scheme Haydock concentrated on a local atom witch couples with its first nearest neighbor and through them to the second nearest neighbor and through them to the more distant neighbor and so on. Mathematically it transform the basis in such a way that the Hamiltonian of the system becomes tirdiagonal from which one can easily calculate the elements of the Greens function in a continued fraction from. A new orthonormal basis set $|n\rangle$ in which the Hamiltonian is tridiagonal is constructed by a three term recurrence formula. We start with the initial state $|0\rangle$. Choice of the starting state $|0\rangle$ of recursion plays an important role in determining the specific physical property which we shall discuss in our subsequent chapter later. For example, in case of local density of states calculation, atomic type orbitals are chosen as the starting stat.

Now, we define the new state $|1\rangle$ as,

$$\beta_1|1\rangle = \mathbf{H}|0\rangle - \alpha_0|0\rangle \tag{1.85}$$

The whole set of orthonormal states are generated by the following three term recurrence relation:

$$\beta_{n+1}|n+1\rangle = \mathbf{H}|n\rangle - \alpha_n|n\rangle - \beta_n|n-1\rangle \tag{1.86}$$

α_n and β_n are the coefficients to orthogonalize $\mathbf{H}|n\rangle$ to the preceding vectors $|n\rangle$, $|n-1\rangle$ and β_{n+1} is the coefficient to normalize $|n+1\rangle$ to unity. β_0 is assumed to be unity. In the new basis, the Hamiltonian matrix elements are,

$$\begin{aligned} \langle n|\mathbf{H}|n\rangle &= \alpha_n \\ \langle n-1|\mathbf{H}|n\rangle &= \beta_n \\ \langle n|\mathbf{H}|m\rangle &= 0 \end{aligned} \tag{1.87}$$

In this new representation, the Hamiltonian has the following tridiagonal form,

$$\begin{pmatrix} \alpha_0 & \beta_1 & 0 & 0 & 0 & 0 & 0 \\ \beta_1 & \alpha_1 & \beta_2 & \ddots & 0 & 0 & 0 \\ 0 & \beta_2 & \alpha_2 & \beta_3 & \ddots & 0 & 0 \\ 0 & \ddots & \beta_3 & \alpha_3 & \beta_4 & \ddots & 0 \\ 0 & 0 & \ddots & \ddots & \ddots & \ddots & 0 \\ 0 & 0 & \ddots & \ddots & \ddots & \ddots & 0 \end{pmatrix} \tag{1.88}$$

The above transformation can be graphically represented as the transformation of a d-dimensional system to a semi-infinite linear chain. $\{\alpha_n\}$ and $\{\beta_n\}$ are represented as the on-site term and the coupling between two sites.

From the above tridiagonal Hamiltonian one can easily calculate the matrix representation of the Green's function as:

$$G(z) = (zI - H)^{-1} = \begin{pmatrix} z-\alpha_0 & -\beta_1 & 0 & 0 & 0 & 0 & 0 \\ -\beta_1 & z-\alpha_1 & -\beta_2 & \ddots & 0 & 0 & 0 \\ 0 & -\beta_2 & z-\alpha_2 & -\beta_3 & \ddots & 0 & 0 \\ 0 & \ddots & -\beta_3 & z-\alpha_3 & -\beta_4 & \ddots & 0 \\ 0 & 0 & \ddots & \ddots & \ddots & \ddots & 0 \\ 0 & 0 & \ddots & \ddots & \ddots & \ddots & 0 \end{pmatrix}^{-1} \tag{1.89}$$

Now if we define $D_n(z)$ as the determinant of the tridiagonal matrix constructed out of equation (1.89) with first n rows and n columns removed then the first diagonal element of the Greens function can easily be obtained in a continued fraction as:

$$\begin{aligned} G_{00}(z) &= D_1(z)/D_0(z) \\ &= \cfrac{1}{z-\alpha_0-\cfrac{\beta_1^2}{z-\alpha_1-\cfrac{\beta_2^2}{z-\alpha_2-\cfrac{\beta_3^2}{z-\alpha_3-\cfrac{\beta_4^2}{\ddots}}}}} \end{aligned} \tag{1.90}$$

and the local density of state is then given by:

$$n(E) = -\frac{1}{\pi}\lim_{\delta\to 0}\mathrm{Im}\ G_{00}(z) \quad , \quad z = E + i\delta \tag{1.91}$$

If the system of our interest is large enough then the dimension of the Hamiltonian matrix is infinitely large. So we have to calculate in principle, infinite number of coefficients $\{\alpha_n, \beta_n\}$. In practice, we can only evaluate the continued fraction up to a finite number of recursion steps. Haydock (13) has shown that contributions of the continued fraction coefficients (α_n, β_n) can be map to self-avoiding walks on the underlying lattice, where α_n and β_n contain information about only the irreducible paths of length (2n-1) and 2n respectively i.e. those closed paths that do not return to the initial site at any intermediate stage. He has also shown that the dominant contribution comes from the path that wind around the initial starting state. This allows us to work only on the finite part of the Hilbert space. Thus, if we try to model an infinitely extended system, the recursion algorithm after n steps contains contributions only from a central cluster consisting of O (n^3) atoms. For numerical purposes, this limits the number of atoms that can be modeled, and also implies that we are studying a finite system. The terminating continued fraction obtained in this process yields a finite number poles of the Green's function corresponds to a finite number of isolated bound states of the system which is appropriate for a finite cluster. For most purposes this is an unphysical approximation to the problem under investigation and we need to overcome these finite size effects by embedding the cluster in an infinite medium. That is we need to determine suitable terminator to the continued fraction, so as to obtain a Green function with a branch cut, rather than a finite set of simple poles. In

this termination procedure we have to careful about terminator so that the analytic properties (*herglotz properties*) of the Green's function should be preserve.

Several terminators are available in the literature which reflect the asymptotic properties of the continued fraction expansion of the Green function accurately. The advantage of using such terminators is that the approximate resolvent not only retains the analytic properties (*herglotz properties*) of the Green's function but also preserves the first 2n moments of the density of states exactly and maintains the correct band-widths, band-weights and the correct singularity at the band edges.

1.5 Terminating schemes

After calculating a set finite of $\{\alpha_n, \beta_n\}$ when we apply the termination scheme to approximate the tail of the continued fraction (representing the diagonal element of G), we have to ensure that the approximate resolvent (which replaces G) should be such that the corresponding approximate Hamiltonian should have a similar energy spectrum as the original Hamiltonian H. In other words, the resulting approximate density of states should preserve the singularities (singularities at the band-edges and Van Hove singularities) of the density of states of the system one is examining.

Applications to a system with a single band of states, it was found that the $\{\alpha_n, \beta_n\}$ rapidly convergent to some (α, β). So for $n \geq N$ we can set $\alpha_n = \alpha$ and $\beta_n = \beta$. Finally we can sum up the remainder of the infinite continued fraction analytically as follows:

$$T(E) = \cfrac{\beta_n^2}{E - \alpha_n - \cfrac{\beta_{n+1}^2}{E - \alpha_{n+1} - \ldots}}$$

is replaced by

$$T(E) = \cfrac{\beta^2}{E - \alpha - \cfrac{\beta^2}{E - \alpha - \ldots}} = \frac{\beta^2}{E - \alpha - T(E)}$$

we can solve for

$$T(E) = \frac{1}{2}\left(E - \alpha - \sqrt{(E-\alpha)^2 - 4\beta^2}\right) \tag{1.92}$$

This terminator $T(E)$ is called quadratic termination proposed by Haydock. In more complex systems involving a number of isolated bands (For example, semiconductors

and transition metal compounds), the quadratic terminator came out to be unsuitable and the quadrature method proposed by Nex (14) is found to be more useful. It has been found that given the band-edges and the truncated continued fraction, the analytic terminator proposed by Haydock (16) and later improved by Luchini and Nex (15) produces much better results as compared to the quadrature method. Here we shall outline the features of the analytic terminator schemes for a solid with a single band. A set of coefficients $\{\alpha_n, \beta_n\}$ is first generated recursively from the three term recurrence relation. We generate such coefficients upto n=n_2 steps. We now generate orthogonal polynomials of the first and second kinds: P_n (z) and Q_n (z) for the above recurrence relation. These are the solutions of:

$$\begin{aligned} P_{n+1}(z) &= (z-\alpha_n)\ P_n(z) - \beta_n^2\ P_{n-1}(z) \\ Q_n(z) &= (z-\alpha_n)\ Q_{n-1}(z) - \beta_n^2\ Q_{n-2}(z) \end{aligned} \tag{1.93}$$

with P_{-1}=Q_{-1}=0, P_0=Q_0=1

The next step is to locate accurately, from the generated continued fraction coefficients (n<n_2), the lower (left) band edge a, the bandwidth r and the weight w. From this we construct a model herglotz function with square-root band edge singularities:

$$F(z) = 8w\left[z-(a+r/2)-\sqrt{(z-a)(z-a-r)}\right]/r^2 \tag{1.94}$$

We now run the recursion again with the Hamiltonian replaced by z, the state vectors by polynomials described by equation (2-21), the inner product by a union of Gauss-Chebyshev quadrature:

$$f(z)\odot g(z) = \sum_{i=1}^{n} \Omega_i f\left(\alpha_i^{'}\right) g\left(\alpha_i^{'}\right) \tag{1.95}$$

where,

$$\begin{aligned} \Omega_i &= \frac{\pi w}{(n+1)\,sin^2\theta_i} \\ \alpha_i^{'} &= a+(1-\cos\theta_i)\,r/2 \\ \theta_i &= \frac{i\pi}{n+1} \end{aligned}$$

This will generate a set of recursion coefficients $\{c_n, d_n\}$ and a set of mutually orthogonal polynomials $\{R_n(z)\}$ and $\{S_n(z)\}$.The terminator is then given by,

$$T(z) = \frac{S_{n-2}(z) - F(z)\,R_{n-1}(z)}{d_{n-1}^2\left(S_{n-3}(z) - F(z)\,R_{n-2}(z)\right)} \tag{1.96}$$

Again, from the fact that R_n and S_n are polynomials of order n and $F(z)$ is a herglotz function, it follows immediately that the terminator is itself herglotz. The Green function is given by,

$$G(z) = \frac{Q_{n-2}(z) - \beta_{n-1}^2 T(z) Q_{n-3}}{P_{n-1}(z) - \beta_{n-1}^2 T(z) P_{n-2}} \tag{1.97}$$

Using very similar arguments as before, the Green function is herglotz if $T(z)$ is herglotz.

This method of analytic termination of Haydock and Nex was further improved by Luchini and Nex (15) . It is easy to understand that in a chain with constant parameters if one appends a constant terminator with infinite band-width then the spectrum will consist of delta functions. When the band edge mismatch is reduced these delta-functions broaden into Lorentzians and finally only show up as oscillations superimposed on the semi-elliptic local density of states resulting from such constant coefficients. In such a simple picture, one can consider the chain parameters α_n and β_n to represent the potentials on the one-dimensional chain and one can regard the eigenstates of the computed chain as being initially unable to tunnel out through the potential barrier of the terminator. As the height of the barrier is reduced they become resonances superposed on the local density of states. The situation is analogous to the coherent reflection of the eigenstates by the step function in the potential represented by the discontinuous join to the terminator. The method of Luchini and Nex suggests linear interpolation between the computed and the analytic terminator coefficients to reduce the spurious oscillations arising out of this coherent reflection. The method is analogous to splicing as opposed to butt-joining pieces of wood.

We start with computed continued fraction coefficients α_n, β_n up to n_2 levels and with terminator coefficients α_n^t and β_n^t. The method of Luchini and Nex now suggests to linearly interpolate between the computed coefficients and that of the analytic terminator in the following manner:

$$\alpha_n = \begin{cases} \alpha_n & n \leq n_1 \\ \left[\alpha_n (n_2 - n) + \alpha_n^t (n - n_1)\right] / (n_2 - n_1) & n_1 \leq n \leq n_2 \\ \alpha_n^t & n_2 < n \end{cases}$$

where n_1 is the start and n_2 is the end of the interpolation. Similarly β_n can be obtained by replacing α_n with β_n in the above expression. Again, such a termination procedure retains the herglotz properties of the Green function.

1.6 Comments

In this chapter we have described the basic theoretical tools for the study of electrons in a solid : the density functional theory which reduces the many-body Schrödinger equation with a plethora of variables to a single-electron like Kohn-Sham equation; the electronic band theory and the linear muffin-tin orbitals method which allows us to obtain the solutions of the Kohn-Sham equations in a minimal basis set; the method of Green functions and the physical quantities we derive from it and the recursion method which allows us to calculate the Green function matrix elements. These techniques will form the basis of the applications we shall describe in our thesis.

In the next chapter we shall go on to describe those techniques which will allow us to address the problem of disorder.

Chapter 2

Electronic structure calculation in random binary alloys

2.1 Introduction

The concept of disorder is primitive and intuitive ; it belongs with statistical terms such as 'random', 'stochastic', 'unpredictable', which can only be defined within a specific context of what is already known or can be taken for granted. In the crystalline state, long-range order for positions of atoms and orientations of atomic rows apparent; in alloys, the positional order for atomic sites remains, but the occupation of atomic sites by different species of atoms is somewhat random. The effect of disorder is always to break some symmetry. In the physics of disordered systems we can no longer rely upon the most powerfull mathematical tool in the theory of the solid state. Theorems and principles that we cheerfully prove and accept for crystalline materials may not be taken for granted in the study of disordered systems. There are several different ways in which disorder may be present in material.

- Substitutional disorder : The binary alloy is formed by replacing atoms of element A in a perfect crystal by that of another element B randomly with almost with almost no disturbance in the crystal lattice.
- Topologically disorder : The topology of the lattice itself may be perturbed and the crystalline lattice replaced by a random network.

- Magnetic disorder : In a magnetic material, the Rth site (or unit cell) of a regular crystal can carry a net magnetic moment. If this moment varies randomly in magnitude or direction or both, from site to site (or cell to cell) we have magnetic disorder.

- Other kinds of disorder : disorder can also enter through randomness in local polarization or random distribution in local strains. Good examples are multiferroic glasses.

This has been schematically shown in Fig. 2.1. The reason for the increased interest

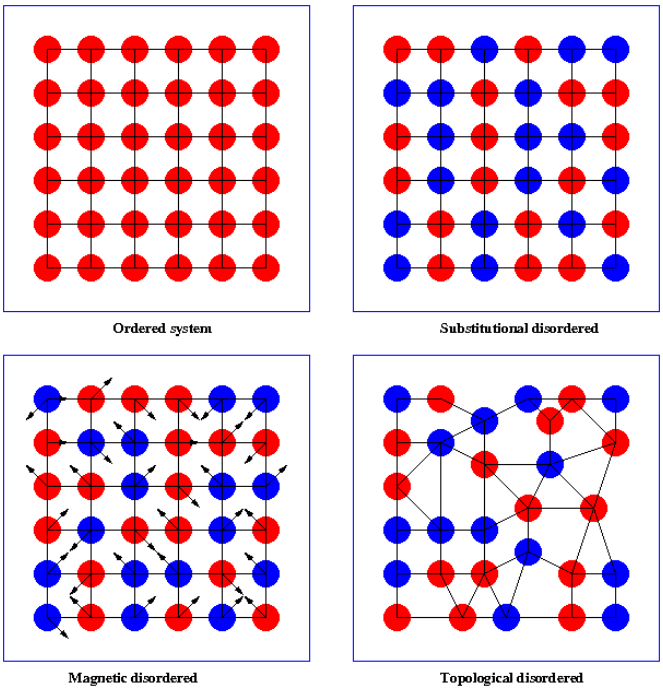

Figure 2.1: Different types of disorder: - (from top left clockwise) Ordered lattice,substitutional disorder, topological disorder and magnetic disorder.

in disordered materials are many and varied. The interest in disordered systems is growing up due to the technological importance of such systems in our modern world. Steel alloys, amorphous semiconductors, liquid metals and glasses, to mention only a handful, are at the core of further technological progress, and the properties of such systems like electrical, magnetic, optical, structural, elastic are important to verify the systems. A detail understanding based on the microscopic, parameter free approach is

thus necessary for the future development in the material science. In a solid the outer most electrons of the atoms plays important role as they bind each atom to it's neighbor and determines the properties of the resulting materials. So one of the important aim of the condensed matter theory is thus calculation of the electronic structure of the solids. This is not only helpful in understanding and interpreting experiment, but also a predictive tool of the condensed matter and materials science. In case of disorder system the calculation of such properties is much more difficult compare to that of the order system. Difficulties arising due to the involvement of the random variables and we have to carry out averages for physical observables over different configurations. In this chapter we shall first overview some of the conventional mean field theories for the configuration averaging. We shall also discuss their limitations and probable extensions. Then we shall introduce the concept of averaging in configuration space and the augmented space method, which is a powerful technique in this regard and we shall extended this idea in our subsequent chapter for the calculation of the response functions. Then we combine this method with TB-LMTO method to calculate the electronic structure of the real binary alloys. Finally we shall discuss a fully self-consistent scheme of TB-LMTO-ASR calculation for realistic systems.

2.2 Rigid Band Model (RBM) and Virtual Crystal Approximation (VCA)

The first attempt for the calculation for the electronic structure of disordered alloy was made by Jones in 1934 with his rigid band model (RBM). In this model the electronic states of one constituent is assumed to be identical to the other and to those of any binary alloy formed by them. This is an oversimplified model which neglects the difference between alloy constituents and only accounts for the number of electrons per atom which is different for different alloys. In that time this model was success for a very few cases like $CuNi$ system where potentials of constituents are nearly identical. Almost all types of alloy the eigen value distribution is qualitatively very different from that of the constituents materials and the model does not work. Korringa in 1958 made the modification of RBM which is called Virtual Crystal Approximation (VCA). He assumed that the potential associated with every lattice site in the alloy is same

and which is equal to the concentration average potential $\langle V \rangle$ of the constituents.

$$V_{alloy} = \langle V \rangle = xV_A + (1-x)V_B$$

where x is the concentration of one-type of atom. System with weak scattering and consisting of nearly equal concentration of the constituent, this model is fairly successful. In this model the self energy consisting of only the lowest order term $\langle V \rangle$, witch is independent of wave-vector k. Therefore the life-time of the Bloch states are infinite as in the pure materials.

2.3 Average t-matrix approximation (ATA)

Fpr systems with large difference between the potential of the constituents atoms VCA can not able to produce good results. It also fails in large concentration fluctuation. In case of small concentration one deals with averaging the scattering matrix (t-matrix) associated with individual scatterers (potential) instead of using average potential. We shall illustrate it by a very simple model Hamiltonian :

$$H_{ij} = \epsilon_i \delta_{ij} + t_{ij} \tag{2.1}$$

where $\epsilon_i = \epsilon_A$ or ϵ_B randomly with probabilities x and $1-x$.

Using the Dyson's equation(1.76) of discussed in the previous chapter we can express the Green's function in terms of the scattering matrix as:

$$\begin{aligned} G_1(r-r', t-t') \quad &= G_0(r-r', t-t') + \\ &\int_0^t dt_1 \int_0^{t_1} dt_2 \int dr_1 \int dr_2 G_0(r-r_1, t-t_1) T(r_1, r_2; t_1, t_2) G_0(r_2-r', t_2-t') \end{aligned}$$

where G_0 is the unperturbed Green's function and

$$T = \sum_{i,j} T_{ij} \tag{2.2}$$

is the total system t-matrix with

$$\begin{aligned} T_{ij} &= V_i \delta_{ij} + V_i G_0 V_j (1-\delta_{ij}) + \sum_k V_i G_0 V_k G_0 V_j + \dots \\ &= V_i \delta_{ij} + V_i \sum_k G_0 T_{kj} \end{aligned} \tag{2.3}$$

Separating $k = i$ term we can write

$$T_{ij} = t_i \delta_{ij} + t_i \sum_k G_0 T_{kj} \tag{2.4}$$

t_i are the single site scattering matrix and these are replaced by the average value $\langle t \rangle$. If we considering VCA medium as the host material, then perturbation is $V_i - \langle V \rangle$ and correspondingly $\langle t \rangle$ becomes

$$\langle t \rangle^{ATA} = \frac{x(\epsilon_A - \langle \epsilon \rangle)}{1 - (\epsilon_A - \langle \epsilon \rangle) G_0^{VCA}} + \frac{(1-x)(\epsilon_B - \langle \epsilon \rangle)}{1 - (\epsilon_B - \langle \epsilon \rangle) G_0^{VCA}} \tag{2.5}$$

with $\langle \epsilon \rangle = x\epsilon_A + (1-x)\epsilon_B$. The configuration averaged Green's function is given by

$$\langle G \rangle = G_0 + G_0 \left[\langle t \rangle^{ATA} (1 - G_0 \langle t \rangle^{ATA})^{-1} \right] G_0$$

Compare to VCA, ATA shows the impurity bands and Bloch-states with finite life times

2.4 Coherent Potential Approximation

The VCA and the ATA fails primarily because they leads to choices of a translationally invariant effective medium that is either incorrect or not very accurate. As we have mentioned before that for the disordered system the main thrust goes to obtain the configuration averaged quantity. Also the greens function contains all informations about the system. Therefor the main aim goes to the calculation of configuration averaged greens function for a disordered system. The coherent potential approximation(CPA) was introduced simultaneously by Soven(17) in connection with disordered electronic systems and Taylor(18) in connection with the lattice dynamics of mass disordered alloys in 1967. In case of totally random alloy their basic idea was to obtain a translationally symmetric effective Hamiltonian (H^{eff}) and the representation of it's greens function G^{eff} which are good approximation of the average greens function of the random Hamiltonian. If we write the total Hamiltonian as $H = H_0 + V$ where $V = \sum_i V_i$ is the superposition of the real individual site potential $V_i(z)$ then in terms of self energy operator $\Sigma(z)$ one can write the average Green's function as:

$$\langle G(z) \rangle \;=\; \langle (z - H)^{-1} \rangle \;=\; [z - H_0 - \Sigma(z)]^{-1} \tag{2.6}$$

In a translationally invariant medium $\Sigma(z)$ the total Hamiltonian can be written as

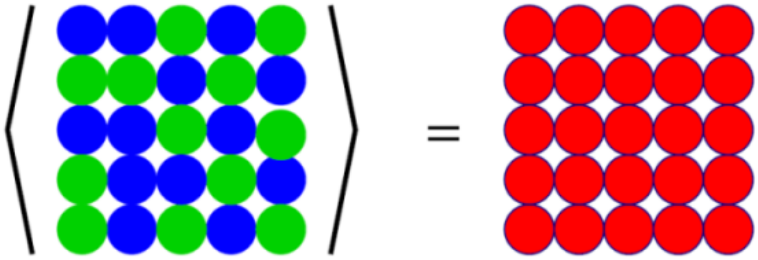

Figure 2.2: CPA - The schematic representation of the CPA mean-field approximation.

$$H(z) \;=\; H^{eff}(z) + V(z) - W(z) \quad \text{with} \quad H^{eff}(z) \;=\; H_0(z) + W(z)$$

where $W(z) = \sum_i W_i(z)$ is the translationally invariant site-dependent quantities $W_i(z)$. Defining $\mathcal{V}(z) = \sum_i (V_i - W_i)$ and $G^{eff}(z) = (z - H^{eff})^{-1}$ we can express the resolvent $G(z)$ and corresponding T operator $T(z)$ as :

$$\begin{aligned} G(z) &= G^{eff}[1 - \mathcal{V}(z)G^{eff}] \\ T(z) &= \mathcal{V}(z) + \mathcal{V}(z)G^{eff}\mathcal{V}(z) \\ G(z) &= G^{eff} + G^{eff}T(z)G^{eff} \end{aligned}$$

Clearly G^{eff} is translationally symmetric and therefore the average $G(z)$ becomes

$$\begin{aligned} \langle G(z)\rangle &= G^{eff}(z) + G^{eff}(z)\langle T(z)\rangle G^{eff}(z) \\ &= [1 + G^{eff}(z)\langle T(z)\rangle]G^{eff}(z) \end{aligned} \tag{2.7}$$

and hence to get the average greens $\langle G(z)\rangle$ function as the effective greens function $G^{eff}(z)$ i.e.

$$\langle G(z)\rangle = G^{eff}(z) \tag{2.8}$$

We need to satisfy

$$\langle T(z)\rangle = 0 \tag{2.9}$$

Now the self energy becomes

$$\Sigma(z) \;=\; z - H_0(z) - [\langle G(z)\rangle]^{-1}$$

$$
\begin{aligned}
&= z - H_0(z) - G^{eff}(z)^{-1}\{1 - G^{eff}(z)\langle T(z)\rangle \left[1 + G^{eff}(z)\langle T(z)\rangle\right]^{-1}\} \\
&= z - H_0(z) - G^{eff}(z)^{-1} + \langle T(z)\rangle \left[1 + G^{eff}(z)\langle T(z)\rangle\right]^{-1} \\
&= W(z) + \langle T(z)\rangle \left[1 + G^{eff}(z)\langle T(z)\rangle\right]^{-1} = W(z) + \Sigma_1(z)
\end{aligned}
$$

With the help of equation 2.4 in the previous section we can write

$$\langle T(z)\rangle = \sum_i \langle Q_i(z)\rangle \tag{2.10}$$

where $\langle Q_i\rangle$ can be represents as

$$
\begin{aligned}
\langle Q_i\rangle &= \langle t_i(z)\rangle \left[1 + G^{eff}(z)\sum_{i\neq j}\langle Q_j(z)\rangle\right] \\
&+ \langle [t_i(z) - \langle t_i(z)\rangle]\, G^{eff}(z)\sum_{i\neq j}[Q_j(z) - \langle Q_j(z)\rangle]\rangle
\end{aligned}
$$

The first term of the above expression contains only the single site quantities but the second one is kind of correlation term. In CPA The second term is neglected and therefore it is single site approximation. But neglecting second term means that, excluding the local environmental effect like short-ranged ordering. So in CPA $\langle Q_i(z)\rangle$ becomes

$$\langle Q_i(z)\rangle = \langle t_i\rangle \left[1 + G^{eff}(z)\sum_{j\neq i}\langle Q_j(z)\rangle\right] \tag{2.11}$$

So in the single site coherent potential approximation condition in equation(2.9) namely $\langle T(z)\rangle = 0$ reduces to

$$\langle Q_i(z)\rangle = 0 \implies \langle t_i(z)\rangle = 0 \quad \text{for all } i \tag{2.12}$$

This condition implies that the average scattering produces on a site is zero. It is possible to prove that this approximation preserves the analytic properties of the greens function and gives first eight moment of the density of state exactly. It is also reproduces several limiting cases like dilute limit where it is exact up to first order. In the atomic limit it can be shown that the approximation is exact up to second order term by using the locator formalism.

CPA is one of the most extensively used successful methods in the study of electronic structure of disordered solids. It has been used in conjunction with almost all the electronic structure techniques starting from pseudo-potentials to KKR, LMTO and APW.

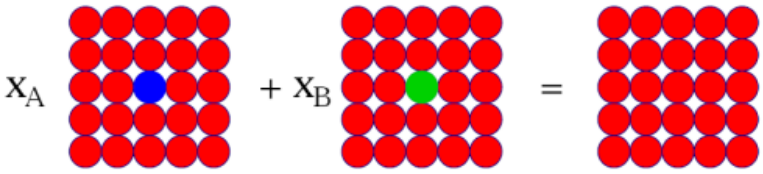

Figure 2.3: Average - Average over single-site approximation in cpa

2.5 Beyond single site CPA

Although CPA produces excellent results in many cases and no doubt it is a very good approximation and is widely used but it has several limitations. As we have discussed before that being single site approximation, CPA cannot take into account the local environmental effects and off-diagonal randomness. It also fails to describe local lattice distortions. In case of low dimensionality for example surfaces it cannot able to produce fine structures in the density of states. There have been several attempts by many authors to generalized this approximation to overcome those limitations. These are basically the cluster generalization of the CPA. Generalizing scattering t-matrix approach Nickel and Krummhansl (20) and Leath(19)(1970,1972) tried to include all cross scattering diagrams involving two sites. This diagram summation is extremely cumbersome and intractable for a bigger cluster. After partitioning the system into subunits, Tsukada(21, 22) suggested tho carry out CPA by replacing single site by such subunits. This is the easiest way to include some of the effects of scattering from cluster of atoms. This procedure is called the molecular coherent potential approximation (MCPA). However in case of homogeneous disorder this violets the lattice translational symmetry of the configuration averaged greens function. Butler(23) suggested a further approximation to overcome this difficulty. He assumed that every cluster has a central site and the CPA equations are applied only to the central site. In the weak scattering limit the 'central site approximation' produces good results. However in the strong scattering limit the density of state becomes many-valued and negative in some energy range and the sum rule for the integrated density of state violated. After that he applied

the the CPA equations in the boundary sites instead of central site witch also gave unphysical results in the strong scattering limits. The traveling cluster approximation (TCA) proposed by Kaplan and Gray (24) using augmented space formalism which we shall discuss subsequently, is a major breakthrough in this direction. This method based on the fact that instead of summing all possible diagrams necessary for consistent treatment of scattering event one should sum up certain type of diagrams so that the corresponding self energy satisfy the condition : $Im(\Sigma(z)) \leq 0 \quad$ for $Im(z) \geq 0$, which is necessary (but not sufficient) for the annaliticity. The TCA formalism provides a consistent rule for summing such class of diagrams so that the self energy and Green's function with proper analytic properties can be obtain. Also the diagrammatic consistency generates all higher order graphs associated with a given type of scattering and includes such scattering through out the material. In the two site version, this method not only retains the analytic properties of the Greens function but also the lattice translational symmetry of the configuration averaged greens function, however this method is also suffers some limitations. The method is computationally extremely difficult for a bigger cluster size and is nearly impossible to implement for a realistic system. TCA beyond a pair approximation has not been implemented as yet.

2.6 Augmented space formalism

2.6.1 The Configuration Space

Let us first start with clarifying the mathematical concept of the configuration space of a set of random variables. Depending on the nature of random variables, it assumes different values for different circumstances. The set containing all possible values that the random variables assume is called the configuration space of those random variables. If their are N-number of independent binary random variables, then each random variable assumes two values therefore the set where all possible arrangements of these N variables contains 2^N sequences and hence the dimension of the space in this case is 2^N . The idea will be more clear if we take a particular example of the Ising model. This model consists of a set of *spins* $\{\sigma_R\}$ arranged on a discrete lattice labeled by $\{R\}$. Each spins can have two possible states or *configurations* : $|\uparrow_R\rangle$ and $|\downarrow_R\rangle$. For a single lattice site it only occupied by either $|\uparrow_R\rangle$ or $|\downarrow_R\rangle$, i.e the configuration space in this case is $[(|\uparrow_R\rangle), (|\downarrow_R\rangle)]$. Let us call this space ϕ_R. Now if we consider

there are only two lattice sites, then possible distribution of spins in this two sites are $[(|\downarrow_1\rangle,|\downarrow_2\rangle),\ (|\downarrow_1\rangle,|\uparrow_2\rangle),\ (|\uparrow_1\rangle,|\downarrow_2\rangle),\ (|\uparrow_1\rangle,|\uparrow_2\rangle)]$, which is the configuration space for the sites with two random spins. The set of N-spins then have 2^N possible configurations, each of which can be written as a sequence of p-up states and (N-p) down-states. The number (N-p) is defined as the *cardinality* of the configuration and the sequence {C} of sites $\{R_{i1}, R_{i2}, R_{i3}, \ldots R_{i_{N_p}}\}$ where the down states sit is called the *cardinality sequence* of configuration. For example take a particular configuration of 6-spins $\{\uparrow_1 \downarrow_2 \uparrow_3 \downarrow_4 \downarrow_5 \downarrow_6\}$. It has a cardinality 4 and a cardinality sequence {2 4 5 6}. Another configuration $\{\downarrow_1 \uparrow_2 \uparrow_3 \downarrow_4 \downarrow_5 \downarrow_6\}$ also has cardinality 4 but its cardinality sequence is {1 4 5 6} which is distinct from the previous one. For a set of N-spins, the configuration space Φ is of rank 2^N and can be written as the direct product of the configuration spaces of individual spins

$$\Phi = \prod_R^{\otimes} \phi_R$$

It is quite straight forward to generalize these ideas when random variables assumes more then two values. The configuration of an individual random variables can be labeled as $|\kappa_R\rangle$ where $\kappa_R = 1, 2, \ldots\ldots, n$. The rank of ϕ_R is now n. Also the set of N-variables will have n^N possible configurations.

2.6.2 The formalism

The augmented space method was first introduce by Mookerjee(25, 26) is a feasible technique for carrying out configuration averaging in disordered systems. Here we shall discuss briefly about this formalism. Let us consider a set of independently distributed binary random variables $\{n_R\}$ with probability densities $p_R\{n_R\}$ and assume that the $p_R\{n_R\}$ has finite moment of all order. Clearly it is a reasonable assumption for almost all physical distributions. Since probability densities are positive definite functions therefore it can always be possible to express them as spectral densities of positive definite operator N_R as:

$$p_R(n_R) = -\frac{1}{\pi}\, \Im m \left[\langle \uparrow_R |(z\mathbf{I} - \mathbf{N}^R)^{-1}| \uparrow_R\rangle\right] \tag{2.13}$$

where $z \to n_R + i\ \delta\ ; \delta \to 0$, and $|\uparrow_R\rangle$ is the *average* state defined in such a way that the for any related quantity containing n_R, $\langle \uparrow_R |\eta| \uparrow_R\rangle$ gives average value of η

Since the resolvent of N^R $(z\mathbf{I} - \mathbf{N}^R)^{-1}$ is Herglotz, and $p_R\{n_R\}$ is assumed to be such that it has finite moment of all order exists, so one can expand it as a continued fractional form,

$$p_i(n_i) = -\frac{1}{\pi}\Im m \quad \cfrac{1}{z - a_0 - \cfrac{b_1^2}{z - a_1}} \tag{2.14}$$

For a binary distribution if n_R takes the value 0 and 1 with probabilities $x,\ y = (1-x)$ then $p_R(n_R) = x\delta(n_R - 1) + x\delta(n_R)$ we have : $a_0 = x, a_1 = y$ and $b_1 = \sqrt{xy}$, and a representation of N^R is

$$\begin{pmatrix} x & \sqrt{xy} \\ \sqrt{xy} & y \end{pmatrix}$$

In general if n_R takes k different values with probability x_k , then the configuration space is spanned by k *states* : $|k\rangle$ which are the eigenstates of N_R with eigenvalue k. In that case the *average state* $|\emptyset_R\rangle$, which is the equivalent of $|\uparrow_R\rangle$ is $\sum_k \sqrt{x_k}|k\rangle$ where x_k is the probability of the variable N_R to take the value k. The other members of the countable basis $|n\rangle$ may be obtained recursively from the average state through :

$$\begin{aligned} |0\rangle &= |\emptyset_R\rangle \\ b_1|1\rangle &= \mathbf{N}^R\,|0\rangle - a_0|0\rangle \\ \dots &\quad \dots \quad \dots \quad \dots \\ b_n|n\rangle &= \mathbf{N}^R\,|n-1\rangle - a_{n-1}|n-1\rangle - b_{n-1}|n-2\rangle \end{aligned}$$

In this basis, the operator $\mathbf{N}^R$ thus has the traditional form,

$$\begin{pmatrix} a_0 & b_1 & 0 & 0 & 0 & \dots \\ b_1 & a_1 & b_2 & 0 & 0 & \dots \\ 0 & b_2 & a_2 & b_3 & 0 & \dots \\ 0 & 0 & b_3 & a_3 & b_4 & \dots \\ \dots & \dots & \dots & \dots & \dots & \dots \end{pmatrix}$$

We can see that there is a close relationship between the above procedure and the recursion method described in the previous chapter. This is not surprising, since the projected density of states and the probability density are both positive definite and integrable functions. and in both the cases finite moments to all orders exists.

2.6.3 Augmented Space Theorem

The problem addressed involves the configuration averaging of a function of many independent random variables. e.g. $\ll f(\{n_R\}) \gg$ where R labels a set of lattice points. The first step is to associate with each random variable n_R an operator N^R such that the spectral density of this operator is the probability density of the random variable :

$$p(n_R) = -(1/\pi)\langle\uparrow_R |(n_R\mathrm{I} - \mathrm{N}^R)^{-1}| \uparrow_R\rangle$$

Also to each variable n_R there is associated a *configuration* space ϕ_R spanned by the *states* $\{| \uparrow_R\rangle\}$ then the augmented space theorem states that the average of any physical quantity $f(n_R)$, which is a function of the set of random variables $\{n_R\}$ is given by

$$\ll f(\{n_R\}) \gg = \langle\emptyset|\widetilde{\mathbf{f}}(\{\mathbf{N}^R\})|\emptyset\rangle \tag{2.15}$$

where $\widetilde{\mathbf{f}}(\{N^R\})$ is an operator which is a functional of $\{\mathbf{N}^R\}$ and has the same form as function $f(\{n_R\})$ of n_R has. Further, $|\emptyset\rangle = \prod_R^{\otimes} | \uparrow_R\rangle$ is the *average configuration state* in the product space $\Phi = \prod_R^{\otimes} \phi_R$. Therefore information about all possible configurations of the disordered system with random variables n_R are kept in the product space Φ. The statement of the theorem will be clear if we see the following mathematical steps.

Let us start with a function $f(n_R)$ of a single random variable n_R. The generalization for a function of the set of many random variables is quite straight forward. The average value of $f(n_R)$ can be expressed as:

$$\begin{aligned} \ll f(n_R) \gg &= \int_{-\infty}^{\infty} f(n_R)\ p_R(n_R) dn_R \\ &= -\frac{1}{\pi}\Im m \int_{-\infty}^{\infty} f(n_R)\langle\uparrow_R |(n_R I - \mathbf{N}^R)^{-1}| \uparrow_R\rangle dn_R \end{aligned}$$

Since the eigen vectors of the operator N^R on the configuration space is a complete set, we can write

$$\ll f(n_R) \gg = -\frac{1}{\pi}\Im m \sum_k \sum_{k'} \int_{-\infty}^{\infty} f(n_R)\langle\uparrow_R |k\rangle\langle k|(n_R I - \mathbf{N}^R)^{-1}|k'\rangle\langle k'| \uparrow_R\rangle dn_R$$

But $(n_R I - \mathbf{N}^R)^{-1}$ is diagonal in the eigen basis of N^R and is equal to $\frac{\delta_{kk'}}{n_R - k}$, so

$$\begin{aligned} \ll f(n_R) \gg &= \sum_k \int_{-\infty}^{\infty} f(n_R) \langle \uparrow_R |k\rangle \left[-\frac{1}{\pi} \Im m (n_R - k)^{-1} \right] \langle k| \uparrow_R \rangle dn_R \\ &= \langle \uparrow_R | \sum_k |k\rangle \int_{-\infty}^{\infty} [f(n_R)\delta(n_R - k) dn_R] \langle k| \uparrow_R \rangle \\ &= \langle \uparrow_R | \{ \sum_k |k\rangle f(k) \langle k| \} | \uparrow_R \rangle \end{aligned} \tag{2.16}$$

Now $\sum_k |k\rangle f(k) \langle k|$ is nothing but the spectral representation of the functional $\tilde{\mathbf{f}}(\mathbf{N}^R)$ of the operator N^R constructing by simply replacing the variable n_R with the associated operator $\mathbf{N}^R$ in $f(n_R)$. Hence

$$\ll f(n_R) \gg \quad = \quad \langle \emptyset_R | \tilde{\mathbf{f}}(\mathbf{N}^R) | \emptyset_R \rangle \tag{2.17}$$

In general if there are independent random variables $\{n_R\}$ involved then the joint probability distribution is given by :

$$P(n_{R_1}, n_{R_2}, \ldots n_{R_i} \ldots) = \prod_i p_i(n_{R_i})$$

Proceeding in the same way we shall get average of functions of the set of random variables as.

$$\ll f(\{n_R\}) \gg = \langle \emptyset | \tilde{f}(\{\widetilde{\mathbf{N}}^R\}) | \emptyset \rangle$$

The operator $\widetilde{\mathbf{N}}^R$ are built up from the operators $\mathbf{N}^R$ as :

$$\widetilde{\mathbf{N}}^R = \mathbf{I} \otimes \mathbf{I} \otimes \ldots \otimes \mathbf{N}^R \otimes \mathbf{I} \otimes \ldots$$

and $|\emptyset\rangle$ is the average state in the full configuration space Φ.

Clearly this is a very powerful theorem as it reduce the problem of configuration averaging to just a calculation of a spatial matrix element of an operator in the configuration space constructed according to the given prescription above by using probability distribution of the random variables. One can visualize in a way that the space where disordered function or operators are defined is extended to a bigger space by including the configuration space and in this enlarge space functions or operators are ordered one. In this formalism any approximation has not yet been done so far for averaging , therefore the expressions are exact. Also the formalism preserves all intrinsic properties of the function for example in case of greens function Harglotz properties are preserve

which ensures positive density of states. One of the main advantage of this formalism is that we can generalize it also for a system with correlated random variables. In practice there are lots of alloys where this kind of randomness exists which comes mainly due to the different chemical affinities of the constituent atoms. Formulation and use of generalized version of this formalism will be discussed in our subsequent chapter. In the following section we shall discuss how to perform configuration averaged electronic structure calculations for a real system using augmented space formalism.

2.6.4 Augmented space recursion in TB-LMTO formulation

We have already showed in our previous section that the augmented space theorem maps a disordered operator described in a space on to an ordered function in the augmented space. For a real physical system the disordered Hamiltonian defined in a real Hilbert space maps onto the configuration space Ψ which is nothing but the direct product of the real Hilbert space and the configuration space of the random variables. i.e. $\Psi = \mathcal{H} \otimes \Phi$ If the binary disordered system consisting of N number of sites then the dimension of Ψ is $N \times 2^N$. For the calculation of real binary disordered alloy using TB-LMTO method, we first need to express the TB-LMTO Hamiltonian in the augmented space Ψ.

In terms of potential parameter and screened structure matrix, upto the second-order TB-LMTO Hamiltonian in the most localized β representation is expressed as:

$$\begin{aligned} \mathcal{H} &= E_\nu + h - hoh \\ \text{with} \quad h &= \sum_\nu (C_\nu - E_\nu)\mathcal{P}_\nu + \sum_{\nu\nu'} \Delta_\nu^{1/2} S_{\nu\nu'} \Delta_{\nu'}^{1/2} \mathcal{T}_{\nu\nu'} \end{aligned} \tag{2.18}$$

where ν, ν' are the composite indices of the position(R) and orbital(L) quantum numbers and $\mathcal{P}_\nu = |\nu\rangle\langle\nu|$, $\mathcal{T}_{\nu\nu'} = |\nu\rangle\langle\nu'|$ are projection and translation operators respectively in the Hilbert space spanned by the tight binding basis $\{|\nu\rangle\}$. Now if we only consider diagonal disordered then C, Δ, and o are random at each site and one can express them in terms of the binary random variables n_R as:

$$\begin{aligned} \tilde{C}_\nu &= C_\nu^A n_R + C_\nu^B (1 - n_R) &&= C_\nu^B + \delta C_\nu n_R \\ \tilde{\Delta}_\nu^{1/2} &= (\Delta^A)_\nu^{1/2} n_R + (\Delta^B)_\nu^{1/2} (1 - n_R) &&= (\Delta^B)_\nu^{1/2} + \delta\Delta_\nu^{1/2} n_R \\ \tilde{o}_\nu &= o_\nu^A n_R + o_\nu^B (1 - n_R) &&= o_\nu^B + \delta o_\nu n_R \\ \text{where} \quad \delta C_\nu &= C_\nu^A - C_\nu^B \quad \text{and so on} \end{aligned}$$

The representation of the Hamiltonian in the augmented space can be obtain simply by replacing the local site occupation variable $\{n_R\}$ by corresponding operator $\{N^R\}$. Hence the form of the first order Hamiltonian in the augmented space is

$$\begin{aligned}\tilde{\mathcal{H}} &= \sum_{\nu}(C_{\nu}^{B}\tilde{\mathfrak{J}} + \delta C_{\nu}N^{R}) \otimes \mathcal{P}_{\nu} \\ &\quad + \sum_{\nu\nu'}[(\Delta^{B})_{\nu}^{1/2}\tilde{\mathfrak{J}} + \delta\Delta_{\nu}^{1/2}N^{R}]S_{\nu\nu'}[(\Delta^{B})_{\nu'}^{1/2}\tilde{\mathfrak{J}} + \delta\Delta_{\nu'}^{1/2}N^{R}] \otimes \mathcal{T}_{\nu\nu'} \qquad (2.19)\end{aligned}$$

We have already shown that in $\{|\uparrow_R\rangle\}$ basis N^R has the representation of

$$N^{R} = x\mathcal{P}_{\uparrow}^{R} + y\mathcal{P}_{\downarrow}^{R} + \sqrt{xy}(\mathcal{T}_{\uparrow\downarrow}^{R} + \mathcal{T}_{\downarrow\uparrow}^{R}) \qquad (2.20)$$

where $\mathcal{P}_{\uparrow}^{R} = |\uparrow_R\rangle\langle\uparrow_R|$ and $\mathcal{T}_{\uparrow\downarrow}^{R} = |\uparrow_R\rangle\langle\downarrow_R|$ are the projection and transfer operator respectively in the configuration space Φ.

Now replacing the form of N^R in equation(2.20) in the Hamiltonian in (2.19) we get the Hamiltonian operator in the enlarge space (augmented space)spanned by the basis $\{|\nu\rangle \otimes |\uparrow_R\rangle\}$. Using this Hamiltonian we perform the recursion process in the augmented space and calculate the configuration averaged greens function as single element of the greens function in this enlarge space.

2.6.5 DFT Self Consistency in the TB-LMTO-ASR

In this section we shall describe a fully self consistent scheme to perform first principle electronic structure calculation for the disordered alloy by using TB-LMTO and ASR. The whole scheme is divided into two parts. First we determine the structure constant matrices $\bar{S}$ for a given system. The canonical structure matrices are calculated in the same way as the LMTO-ASA doses, that is expanding the tail of the envelop function at site R around the other site R', which are nothing but the expansion coefficient of that expansion. From this canonical structure matrices S^0 we obtain the structure matrices for the tight-binging representation using the same mixing parameter α by which LMTO-ASA reduces to its most localized representation via the transformation $\bar{S} = S^0(I - \bar{\alpha}S^0)^{-1}$. The values of $\bar{\alpha}$ were found to be independent of structure and are given for s, p, and d electrons by $\bar{\alpha}_s = 0.3485$, $\bar{\alpha}_p = 0.05303$ and $\bar{\alpha}_d = 0.00107$ Since structure matrices are only depends on the position of the atom and not the type of the atom therefore it does not change in the total self consistency process. Now to construct

the Hamiltonian we need potential parameters $\bar{C}_l,\ \bar{\Delta}_l$ in the most localized basis of the LMTO. These are obtain from the orthogonal potential parameters $C_l,\ \Delta_l, \alpha_l$ via the relation

$$\frac{\bar{C}_l - E_l}{C_l - E_l} = \frac{\bar{\Delta}_l}{\Delta_l} = 1 - (\alpha_l - \bar{\alpha}_l)\frac{C_l - E_l}{\Delta_l} \tag{2.21}$$

$C_l,\ \Delta_l, \alpha_l$ are obtain by solving Schrödinger equation inside the Wigner-sitz sphere for each type of atom. This part is called the atomic part and we treat this part of the problem in the same way as k-space LMTO-ASA formalism does. That is we use the same exchange and correlation term as one uses in LMTO-ASA formalism. The potential and the corresponding potential parameters inside the Wigner-Sitz sphere can be uniquely determined from the given occupation numbers of each local band, firs and second order moment of the density of states relative to E_ν and the logarithmic derivative of the orbital wave function at the sphere boundary. The spherical averaged charge density inside a WS sphere can be expressed in terns of the radial part of the Schrödinger equation inside the sphere and the moments of the local density of states. We choose the potential to be zero at the sphere boundary and corrected the total energy and potential by adding madelung term while constructing the Hamiltonian. Starting from a guess charge density we made the local density potential and $\phi_\nu(r), \dot{\phi}_\nu(r)$ are calculated to the given logarithmic derivative. Then we construct a new charge density by occupying the wave functions according to the moments and iterate this process until the self consistency achived in the atomic sphere. E_ν is chosen to be such that the first moment of the density of state for the occupied part of the band always zero. To start the self-consistency process, we give reasonable guess for the occupation, second moment and logarithmic derivatives and find nearly orthogonal potential parameters for each type of atom from the atomic part. then using equation 2.21 we calculate $\bar{C}_l,\ \bar{\Delta}_l$. Using $\bar{C}_l,\ \bar{\Delta}_l$ and the structure matrix $\bar{S}$ we construct the augmented space Hamiltonian in the same procedure discussed in the previous section. Now we solve the eigen value problem of the disordered Hamiltonian by using recursion technique in the augmented space and obtain the local density of state(LDOS) for each type of atom and for each orbital. From LDOS we calculate new E_ν, moments for each band of each type of atom. The logarithmic derivatives are calculated from the E_ν and old potential parameters. Finally we supply all these moment an logarithmic derivative in the atomic part for the calculation of new potential parameter which will use in the

next iteration. We iterate this process until desire self-consistent values of moment and the logarithmic derivative achived.

2.6.6 Problem of charge transfer, madelung potential and energy

Since the constituent atoms in an alloy are different, there should be charge transfer between them in the alloying process and the neutral atomic spheres are become charged. As a result there Madelung energy become a significant part of the total energy. But in this case Madelung potential is very difficult to define as it depends upon the far environment in a given configuration.

In a single site CPA Johnson (28, 29) assumed that all atom of the same kind have the same net charge Q_A or Q_B which does not affected by the environment. As a result

$$Q_i = n_R Q_A + (1 - n_R) Q_B$$

which follows on account for overall charge neutrality that

$$\langle Q_R Q_{R'} \rangle = \langle Q_R \rangle \langle Q_{R'} \rangle = 0$$

and hence $E_{mad} = 0$. This assumption works in many cases but if the for the system like $CuZn$ alloy where the charge-transfer plays a significant role, it produces qualitatively incorrect results. For a mean-field coherent potential approach, Kudrnovský and Drchal (27) have suggested using different atomic radii for the constituents in such a way that average total volume is conserved and the overlap is below the threshold value (15%), one can make these spheres approximately neutral and therefore ignore the Madelung contributions. In this procedure varying the ratio of the atomic spheres $r = R_A/R_B$ is very cumbersome, also Ruban and Skriver (30, 31) have shown that local environmental effects (beyond the CPA) destroys the strict charge-potential alignment, and hence the possibility of choosing electroneutral atomic spheres by a single ratio r. In our self consistency process we have chosen the procedure namely screened impurity model proposed by Ruban and Skriver (30, 31). According to their suggestion the net charge of the alloy component embedded in the effective CPA medium is completely screened by the first shell of its surrounding effective atoms and the screening charge is uniformly distributed among all the Z_1 nearest neighbor atoms. There for the Madelung potential of the impurity atom is

$$V_M^i = -e^2 \frac{Q_i}{R_1}$$

where, i = A or B (labels the constituents of the alloy), Q_i is the net charge of the alloy component i in its own atomic sphere of radius R_a and R_1 is the radius of the first co-ordination shell. Consequently the Madelung energy is given by :

$$E^i_{Madelung} \;=\; -\beta^* e^2 \frac{Q_i^2}{R_1} \tag{2.22}$$

where

$$\beta^* = 1 - \sum_{m=1}^{4} \frac{n_m}{2\varrho_m}$$

with ϱ_m is the ratio of the radius of the m-th and 1st co-ordination shell. In case of BCC and FCC structure the values of β^* are 0.69155 and 0.65735 respectively.

2.7 Comments

In the first two chapters, we have given overviews on the techniques which we shall use in our work : the density functional theory, the KKR and the tight-binding linear muffin-orbitals method and CPA and the augmented space recursion. These will form the backbone of the calculational techniques described in this thesis.

Chapter 3

Excited states and the band gap problem

3.1 Introduction

First-principles calculations based on the density functional theory (DFT) have been eminently successful for the study of ground state properties of electrons in a solid (32).[1] However, it has always been understood that the spectrum and wavefunctions of the associated one-electron like Kohn-Sham equation have no specific significance beyond the fact that they are used to obtain the ground-state density. Thus the unoccupied part of the Kohn-Sham spectrum cannot be expected to describe correctly the excitations of a many-electron system. On the other hand, the energy eigenvalue of the highest occupied orbital, i.e. the orbital energy correcponding to the top of the valence band, is (33) the exact ionization potential of the system. This is known as the ionization potential theorem. Since adding an extra electron at the bottom of the conduction band would hardly change the density of a bulk system, the ionization potential theorem leads one to expect that the difference in the Kohn-Sham orbital energies corresponding to the bottom of the conduction band and the top of the valence band should give the correct band gap of semiconductors and insulators. However it is well known that such an interpretation leads to gross underestimates of the band gaps of semiconductors in comparison to the experiments. This is true even in solids like Ge, Si and the III-V semi-conductors which are not "strongly correlated". This underestimate of the band

[1] The contents of this chapter has been published in Physica B403, 4111 (2008)

gap has been explained in terms of the derivative discontinuity (34, 35) of the exchange-correlation energy functional. To circumvent this difficulty, we propose to look at the calculation of the band gap as an excited-state problem. As such, the question we ask is: could we set up a DFT for excited states, calculate the total energy for appropriate excited-state and obtain the excitation energy as its difference from the ground state total energy. We may then go on to interpret the band gap in a semi-conductor as the difference of the energies between the ground state and an excited state where an electron in the highest occupied state of the ground state is removed from it and excited to the lowest unoccupied state.

The mathematical basis of a density functional theory for total energies in excited states had been set up by Görling (36) and Levy and Nagy (37, 38), based on the constrained search approach (4, 39). The theory has been put on a strong footing by Samal and Harbola (40). The energy of the excited state of electron s in a solid may be expressed as a bi-functional of both the excited state density and the ground state density.

$$E[\rho, \rho_0] \;=\; F[\rho, \rho_0] \;+\; \int d^3\underline{r}\; V(\underline{r})\rho(\underline{r})$$

where $V(\underline{r})$ is the ion-electron potential. $F[\rho, \rho_0]$ for the density $\rho(\underline{r})$ of an excited state is found from the constrained search formulation :

$$F[\rho, \rho_0] \;=\; \min_{\Phi \to \rho} \langle \Phi | (\hat{T} + \hat{V}_{ee}) | \Phi \rangle$$

where Φ is orthogonal to all the wavefunctions which determine ρ_0. The exchange-correlation energy functional is then :

$$E_{xc}[\rho, \rho_0] \;=\; F[\rho, \rho_0] - T_0[\rho] - V_H[\rho] \tag{3.1}$$

This makes the functional non-universal and state dependent. If we now assume that the excited-state density is non-interacting v-representable, we obtain the Kohn-Sham equation :

$$\left[-\frac{1}{2}\nabla^2 + v(r) + \int \frac{\rho(r)}{\mid r - r' \mid} + \frac{\delta E_{xc}}{\delta \rho(r)} \right] \phi_i(r) \;=\; \varepsilon_i \; \phi(r) \tag{3.2}$$

The excited state density is obtained from : $\rho(\underline{r}) \;=\; \sum_i \; f_i \; \mid \phi_i(r) \mid^2$ where the occupation number f_i are 0 or 1 depending on whether the state labelled by i are occupied or not.

As in the ground-state theory, the exchange-correlation energy functional in excited-state theory too has to be approximated. The problem of finding an excited-state exchange-correlation energy functional is a challenging one and is further compounded by the fact that the functional is not expected to be universal. Thus different functional may have to be constructed for different classes of the excited-states. Recently, Samal and Harbola (41) have proposed a local-density approximation (LDA) for the exchange energy functional of excited-state theory for excited-states with one gap. The functional has been applied to a large number of atomic excited-states to obtain very accurate excitetaion energies for single and double-electron excitations. The functional has precisely the form rquired to calculate band-gaps of semiconductors using excited-state DFT. The purpose of the present work is then to employ excited-state DFT to obtain the band-gaps of a number of semiconducting and insulating materials. In the following we give a brief description of the methodology employed by us and then present our results.

3.2 Formulation

3.2.1 Total energy within the Density Functional Theory

As we discussed in the earlier section, the band gap in a semiconductor or an insulator can be thought of as the lowest energy required to excite one electron out of a many-electron ground state to one of the excited states of the system. Thus, in terms of the transition energy,

$$\Delta E_g = E_{ex}[\rho, \rho_0] - E_{gr}[\rho_0] \tag{3.3}$$

where $E_{ex}[\rho, \rho_0]$ is the excited-state energy and $E_{gr}[\rho_0]$ is the ground-state energy corresponding to the configurations mentioned above.

To obtain the total energies we turn to the solution of the variationally obtained Kohn-Sham equation (3) :

$$\left(-\frac{\hbar}{2m}\nabla^2 + v_{eff}(r)\right)\ \varphi_i(r) = \epsilon_i\ \varphi_i(r) \tag{3.4}$$

where

$$v_{eff}(r) = v(r) + \int \frac{\rho(r')}{|r - r'|} dr' + \frac{\delta E_{xc}}{\delta \rho(r)} \tag{3.5}$$

where $v(r)$ is the ion-electron potential and the density is given by,

$$\rho(r) = \sum_{i=1}^{\infty} f_i \ |\varphi_i(r)|^2 \quad \text{with} \quad \sum_{i=1}^{\infty} \ f_i = N_e$$

For the ensemble $v-$representable densities, the non-interacting kinetic energy functional is given by

$$T[\rho] = \sum_{i=1}^{\infty} \ f_i \ \epsilon_i - \int \rho(r) \ v_{eff}(r)$$

This immediately leads to :

$$\begin{aligned} E[\rho] &= \sum_{i=1}^{\infty} \ f_i \ \epsilon_i - \frac{1}{2} \int \int \frac{\rho(r)\rho(r')}{|r-r'|} dr dr' - \int \frac{\delta E_{xc}}{\delta \rho(r)} \ \rho(r) dr \ + \ E_{xc}[\rho(r)] \\ &= E_{KS} - E_H - E_{xc}^{(1)} + E_{xc}^{(2)} \end{aligned} \tag{3.6}$$

3.2.2 Exchange Functional for excited states

There have been many attempts at obtaining accurate but approximate forms for the exchange-correlation functional for the ground state. The simplest of them - the LDA - follows the Dirac (42) approach and proposes the functional on the basis of exchange energy for the homogeneous electron-gas. As mentioned above, adopting the same approach, Samal and Harbola (41) proposed an excited-state functional for the exchange-energy and applied it to atoms to obtain accurate excited-state energies. In this work we construct first a similar exchange-energy functional for semiconductors and insulators and employ it to get the band gap of these materials as defined by 3.3 above. The accuracy or otherwise of our proposition will be evident from the applications to several semi-conductors and insulators.

As the first step towards setting up an excited-state functional, let us make a correspondence between the excited state configuration that we are cosidering and similar excitations in a homogeneous electron gas (HEG). This is shown in Fig. 4.1. In the semi-conductor or insulator in its ground state, the electrons are filled up to the Fermi level, that is, in reciprocal space electrons occupy states labelled by wave vectors from $k = 0$ to k_F. The same picture is true for the HEG, but in addition we have

$$k_F^3 \ = \ 3\pi^2 \rho_0(r) \tag{3.7}$$

where $\rho_0(r)$ is the almost uniform electron density in the ground state.

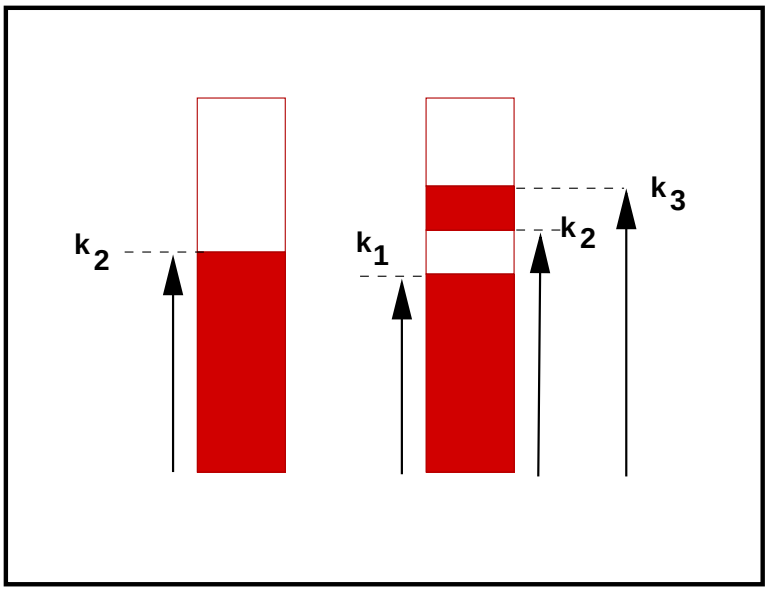

Figure 3.1: Schematic picture of band - (left) SC : Filled valence band and the unfilled conduction band in a semi-conductor or insulator for the ground and excited states.(right) HEG : An equivalent picture for the homogeneous electron gas

On the other hand, for the lowest excited state in the semi-conductor or insulator, the electron in the highest occupied state (HOS) in the ground state configuration (GSC) is removed from that state and now occupies the lowest unoccupied state (LUS) in the GSC. For the HEG this excited state configuration (ESC) corresponds to the following : first, all states which were occupied in the ground state as well as in the excited state we shall call the *core states*. If $\rho_c(r)$ is the electron density due to the electrons occupying the core states, then all states from $k = 0$ to k_1 are occupied, where

$$k_1^3 = 3\pi^2 \rho_c(r) \tag{3.8}$$

Next, if $\rho_r(r)$ is the electron density due to the electron in the HOS of GSC which has been removed in the ESC, then

$$k_2^3 - k_1^3 = 3\pi^2 \rho_r(r) \tag{3.9}$$

Finally, if ρ_a is the electron density due to the electron in the LUS of GSC, which has been added in the ESC, then

$$k_3^3 - k_2^3 = 3\pi^2 \rho_a(r) \tag{3.10}$$

The ground state density is $\rho_0(r) = \rho_c(r) + \rho_r(r)$ and the excited state density is $\rho_{ex}(r) = \rho_c(r) + \rho_a(r) = \rho_0(r) - \rho_r(r) + \rho_a(r)$. in an excited state of the system the electrons will occupy the k-space differently from the ground state. The exchange energy in the modified LDA (MLDA) can be obtained by integration over the reciprocal space equienergetic spherical shell surfaces.

$$E_x^{MLDA} = E_x^c + E_x^a + E_x^{a-c}$$

where

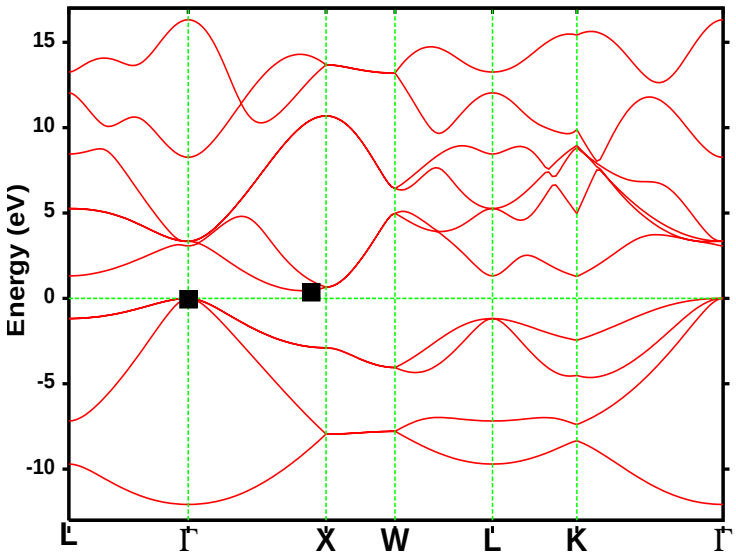

Figure 3.2: Band - The Kohn-Sham band structure of Si showing the highest occupied and and lowest unoccupied states used in our calculations

$$\begin{aligned}
E_x^c &= -\frac{1}{4\pi^3}\int k_1^4 dr \\
E_x^a &= \frac{1}{8\pi^3}\int \left[2(k_3^3 - k_2^3)(k_3 - k_2) + (k_3^2 - k_2^2)^2 \ln\left(\frac{k_3 + k_2}{k_3 - k_1}\right)\right] dr \\
E_x^{a-c} &= -\frac{1}{8\pi^3}\int \left[2(k_3 - k_2)k_1^3 + 2(k_1^3 - k_2^3)k_1 + (k_2^2 - k_1^2)^2 \ln\left(\frac{k_2 + k_1}{k_2 - k_1}\right)\right. \\
&\quad \left. -(k_3^2 - k_1^2)^2 \ln\left(\frac{k_3 + k_1}{k_3 - k_1}\right)\right] dr
\end{aligned} \tag{3.11}$$

It is easy to check from above that when $k_1 = k_2 = k_2 = k_F$, (3.11) reduces to the ground state exchange functional. Equations (3.8)-(3.11) will then provide the

basis for the calculation of the total energies. Assuming no change in the orbital eigenvalues corresponding to the ground- and excited-state configurations, which is a good assumption for bulk systens, the band gap will be given by :

$$\begin{aligned} \Delta E_g &= \Delta E_g^{KS} - \Delta E_H - \Delta E_{xc}^{(1)} \\ &+ E_x^{MLDA}[\rho_{ex};\rho_0] - E_x^{LDA}[\rho_{ex}] \end{aligned} \tag{3.12}$$

where ΔE_g^{KS} is the conventional Kohn-Sham gap, ΔE_H is the difference in the Hartree energy corresponding to the excited-state and the ground-state densities. Usually the sum of the second and third terms in (3.12) are very small, which is the basis for assigning the Kohn-Sham energy difference as the band gap. Thus we expect the major correction to the conventional Kohn-Sham gap to come from the last two terms. What these terms accomplish is to replace the LDA exchange energy corresponding to the excited-state density ρ_{ex} by the MLDA exchange energy. The latter is tailor-made - and therefore more appropriate - for getting exchnage energy for an excited-state of the kind considered for the band gap calculation. We note that the functional proposed by Samal and Harbola also has self-interaction-correction terms in it. For extended systems we expect these terms to be negligible and therefore do not include them in the functional above.

3.2.3 The band gap calculation

We shall base our calculations in solids on the tight-binding linear muffin-tin orbitals method within the atomic-sphere approximation (TB-LMTO-ASA) (43)-(46). In this method the muffin-tin spheres are inflated to the Wigner-Seitz cell volume and the interstitial contribution is neglected. The wavefunction is expanded in a basis of linearized muffin-tin orbitals :

$$\begin{aligned} \psi(r, E_{kn}) &= \sum_{RL} u_{RL}(E_{kn})\ \chi_{LR}(r) \\ \chi_{LR}(r) &= [\varphi_{R\ell}(r) + (E_{kn} - E_{\nu R\ell})\dot{\varphi}_{R\ell})]\, Y_L(\hat{r}) \end{aligned}$$

Here, the muffin-tin orbitals $\chi_{LR}(r)$ belong to a well of type R, the angular momentum L=(ℓ, m). On linearizing the energy dependent basis, the expression for the spherically averaged charge density contribution of an atomic sphere labelled by R for a state

labelled by (kn) is :

$$\rho^R_{kn}(r) = \frac{1}{4\pi}\sum_\ell \Big[\varphi_{R\ell}(r)^2\ n^{(0)}_{R\ell} + 2\varphi_{R\ell}(r)\ \dot{\varphi}^\gamma_{R\ell}(r)\ n^{(1)}_{R\ell} + \big\{\dot{\varphi}^\gamma_{R\ell}(r)^2 + \varphi_{R\ell}(r)\ \ddot{\varphi}^\gamma_{R\ell}(r)\big\}\ n^{(2)}_{R\ell}\Big] \tag{3.13}$$

in terms of the following energy-moments :

$$n^{(p)}_{R\ell} = (E_{kn} - E_{\nu RL})^p \sum_m |u_{RL}(E_{kn})|^2$$

From the Kohn-Sham band-structure we can identify the HOS and LUS states in reciprocal space. Uisng these values of (kn) we construct the removed and added electron densities. The core electron density is obtainted by integrating the expression in (3.13) over the states occupied in the core. These expressions are then used in (3.7)-(3.12) to obtain the band gap. We point out that both the ground- and the excited-state densities are constructed from a single ground-state calculation. This is justified since one does not expect LUS to change much even if an excited-state KS calculation is performed. An advantage of this is that the computational demand of our calculations is pretty much at the same level as the ground-state calculations.

3.3 Results and Discussion

We shall first illustrate our calculations with a specific example, i.e. that of Si. The Fig. 6.1 shows the Kohn-Sham band structure of Si and the HOS and LUS as obtained from the regular Kohn-Sham LDA calculation. In addition to the HOS and LUS, the calculations also gives the Kohn-Sham gap E_g^{KS} (see Eq. 3.12). These states are then used to construct the removed and added electron densities for the excited state. When employed in equation 3.12, these densities yield the band gap of silicon. The results are shown in Table 3.1. As is clear from the Table, our method improves the Kohn-Sham band gap subtantially, bringing it very close to the exact exchange (47, 48, 49) and experimental (50)-(57) band gap. Interestingly the correction to the band gap is 0.52 eV and arises essentially from the exchnage-energy difference between the ground- and the excited-state. This difference is very close to the derivative discontinuity in the exchange-correlation potential for Si obtained (58) from a GW calculation.

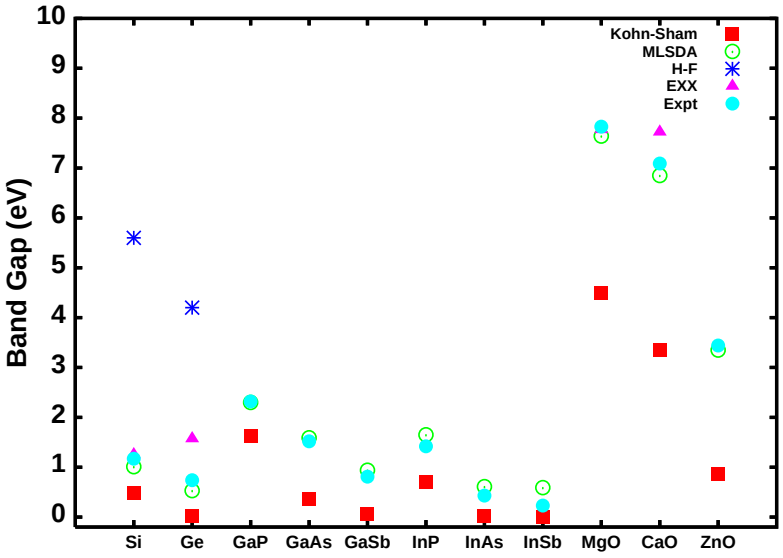

Figure 3.3: Band gap - Band gaps calculated by different methods compared with the experimental band gaps of a series of semi-conductors and insulators.

Having obtained accurate results for Si, we have performed similar calculations for Ge, the III-V zinc-blende semiconductors GaP, GaAs, GaSb, InP, InAs and InSb, two zinc-blende oxides MgO and CaO, and one Wurtzite structure oxide ZnO. The results are displayed in Table 3.1 and Fig. 6.2 It is evident from the results that our procedure yields uniformly accurate results for the band gaps of narrow band-gap to large band-gap materials. However, for semiconductors like InAs and InSb which actually turn out to be metals with zero Kohn-Sham gaps, our procedure is problematic. Therefore we did the initial calculation with a lattice constant slightly smaller than the equilibrium one, so that a very small Kohn-Sham gap appears and then redid our calculations. The estimated band gaps in the MLSDA are slight over-estimations.

As mentioned before, since the band gap is calculated as an energy difference, we expect the difference in SIC between the added and the removed states to be small. We have carried out SIC corrections, as proposed by Samal and Harbola (40, 41), for Si, GaSb and ZnO. For Si the gap changes from 1.01 eV to 1.02 eV; for GaSb from 0.94 eV to 1.06 eV and for ZnO from 3.35 eV to 3.37 eV. In all cases the correction is $\sim 1\%$

confirmig our assumption.

Our correction is to the exchange energy functional alone. However, even with the pure exchange correction major part of the correction to the Kohn-Sham gap is achieved.

Table 3.1: Comparison of the calculated band gap (ΔE) by the present work (LMTO-MLDA) with the TB-LMTO Kohn-Sham gap, the LMTO based Hartree-Fock (LMTO-HF) gap, the LMTO based exact exchange gap (LMTO-EXX) and the experimental (Exp) gap for diamond lattice Si and Ge, zinc-blende III-V semiconductors and wurzite oxides of Zn, Ca and Mg. Percentage deviation (%dev) of the pure exchange MLDA result without SIC obtained in the present work from experiment is also quoted.

System	Latt Par A	LMTO-KS eV	LMTO-MLDA eV	LMTO-HF eV	LMTO-EXX eV	Exp eV
Si	5.43(54)	0.49	1.01	5.6(50)	1.15(48)	1.17(52)
Ge	5.55	0.08	0.53	4.2(50)	1.57(48)	0.74(57)
GaP	5.45(57)	1.62	2.30	-	-	2.32(57)
GaAs	5.65(54)	0.37	1.59	-	-	1.52(57)
GaSb	6.00	0.07	0.94	-	-	0.81(57)
InP	5.87(54)	0.71	1.65	-	-	1.42(57)
InAs	6.04(54)	0.03	0.61	-	-	0.43(57)
InSb	6.48(54)	0.01	0.59	-	-	0.23(57)
MgO	4.21(56)	4.49	7.64	25.30(51)	7.77(47)	7.83(53)
CaO	4.80(56)	3.35	6.85	15.80(51)	7.72(47)	7.09(53)
ZnO	3.25,5.21(55)	0.87	3.35	-	-	3.44(57)

3.4 Comments.

We have proposed a new functional form for the exchange in excited state problems. Using our ideas we have obtained the band gap of a series of semi-conductors and insulators. Our results agree very well with experiment. Our future plan is to extend our ideas to obtain the entire excited state spectrum. This will form the groundwork for our work on optical response. This will be a part of our future research plan.

Chapter 4

Cluster Coherent Potential Approximation

4.1 Introduction

The search for successful approximations for the study of configuration averaging in disordered systems and ones: which preserve the Herglotz analytic properties [1] and lattice translational symmetry of the averaged Green functions has thrown up several alternative approaches. These methods to deal with disorder fall into four categories :

To the first category belongs the single-site mean-field coherent potential approximation CPA. This approximation has been eminently successful in dealing with a variety of disordered systems.

To the second category belong the generalizations of the CPA, of which, the augmented space based methods : the cluster CPA (CCPA) suggested by Razee and Prasad (59, 60), the itinerant CPA of Ghosh *et.al.*(61) (ICPA) and the augmented space recursion (ASR) (62), are foremost. They not only retain the necessary analytic (Herglotz) properties and lattice translational symmetry of the averaged Green function, as the CPA does, but also properly incorporate local environment effects.

To the third category belong the super-cell based calculations. Zunger (63) suggested that if we construct a super-cell and populate its lattice points randomly by the constituents so as to mimic the concentration correlations in the random alloy, a single

[1] A complex function $f(z)$ is called *Herglotz* if (a) its singularities lie on the real z axis (b) $Sgn(Imf(z)) = -Sgn(Imz)$ and (c) $f(z) \sim 1/z$ as $z \to \pm\infty + i0$.

calculation with this super-lattice should approximate the configuration average in the infinite random system.

The above methods are essentially real space approaches. There is a fourth class of techniques based on reciprocal-space renormalization : the non-local CPA (NL-CPA). The underlying idea was first suggested by Jarrel and Krishnamurthy (64) and applied to CuZn alloys by Rowlands *et.al.*(65). The method is capable of taking into account environmental effects and short-ranged ordering.

Of all the single-site approximations, the CPA alone maintains the essential Herglotz analytical properties and lattice translational symmetry of the averaged Green function. However, whenever there is either strong scattering due to disorder-induced configuration fluctuations, as in dilute, split-band alloys or when local environment effects like short-ranged ordering, clustering and segregation, or local lattice distortions due to size mismatch of the constituent atoms become important, the single-site based CPA becomes inadequate.

The aim of this communication will be to extend the ideas suggested by Razee and Prasad (59, 60) to realistic alloys and apply it to CuZn as a test case. The basic idea behind our method is to look at a particular site in the lattice, it does not matter which, and then estimate the effect of its random environment on a local electronic property at that site. Homogeneity of disorder ensures the the environment of any site is statistically equivalent to that of all others. We retain the randomness of the immediate environment and replace the far environment by an effective medium. The effect of the environment is obtained by downfolding it onto the chosen site using of the partitioning theorem The partitioning theorem states that if we partition a Hilbert space $\mathcal{H} = \mathcal{H}_1 \cup \mathcal{H}_2$ and $\mathcal{H}_1 \cap \mathcal{H}_2 = \emptyset$, then if H is an operator in $\mathcal{H}$, then $H^{-1} = (H_1 + H'^T\ H_2^{-P_2}\ H')^{-P_1}$, where $-P_j$ denotes the inverse in the subspace $\mathcal{H}_j$ while $H_j = P_j\ H\ P_j$ and $H' = P_j\ H\ P_{j'}$, P_j is the projection operator onto the subspace $\mathcal{H}_j$. The ASR has a very similar approach : choosing a site to begin recursion and then repeatedly downfolding further and further environments (66)-(11) on to it. The main difference between the two approaches is the way in which the far environment is estimated. In the ASR we do it through the 'terminating' procedure (68), while in the CCPA we approximate it with an effective medium which is self-consistently generated using mean-field ideas. We should note that our approach is different from

the embedded cluster approaches (69, 70) where the cluster is embedded in a CPA medium with no attempt to generate it self-consistently.

4.2 The TB-LMTO-ASR formalism for binary alloys

Our study of the electronic structure of disordered binary alloys will begin with the solution of the Kohn-Sham equation (3), where the effective one electron Hamiltonian will be represented in the minimal basis set of a linear muffin-tin orbitals (TB-LMTO) approach in the so-called most localized or β representation (71). The choice of the β representation is dictated by our subsequent application to substitutionally disordered alloys where the disorder is *local* and a real space formulation with a sparse Hamiltonian is most convenient. The Hamiltonian in this representation is given by :

$$\mathcal{H}^{\beta} = \sum_{\vec{R}} \underline{\underline{C}}^{\beta}_{\vec{R}} \, \mathcal{P}_{\vec{R}} \; + \; \sum_{\vec{R}} \sum_{\vec{R}'} \underline{\underline{\Delta}}^{\beta \, 1/2}_{\vec{R}} \, \underline{\underline{S}}^{\beta}_{\vec{R}\vec{R}'} \, \underline{\underline{\Delta}}^{\beta \, 1/2}_{\vec{R}'} \, \mathcal{T}_{\vec{R}\vec{R}'} \tag{4.1}$$

where $\vec{R}$, $\vec{R}'$ are the positions of the ion-cores, the potential parameters are matrices in angular momentum ($L = (\ell m \sigma)$) space, the operator $\mathcal{P}_{\vec{R}} = |\vec{R}\rangle\langle\vec{R}|$ and $\mathcal{T}_{\vec{R}\vec{R}'} = |\vec{R}\rangle\langle\vec{R}'| + |\vec{R}'\rangle\langle\vec{R}|$ are the projection and transfer operators on the space spanned by the muffin-tin orbital basis set $\{|\vec{R}\rangle\}$. The quantities $\underline{\underline{C}}^{\beta}_{\vec{R}}$ and $\underline{\underline{\Delta}}^{\beta}_{\vec{R}}$ are diagonal in angular momentum space and describe the positions and widths of the energy bands. The short-ranged structure matrix $\underline{\underline{S}}^{\beta}_{\vec{R}\vec{R}'}$ is dependent on the spatial arrangements of the muffin-tin potentials and in a substitutionally disordered alloy is usually non-random : $\underline{\underline{S}}^{\beta}_{\vec{R}\vec{R}} = \underline{\underline{S}}^{\beta}_{0}$ and $\underline{\underline{S}}^{\beta}_{\vec{R}\vec{R}'} = \underline{\underline{S}}^{\beta}(\vec{R}\text{-}\vec{R}')$. In what follows, the diagonal part $\underline{\underline{S}}^{\beta}_{0}$ has been incorporated within the diagonal potential parameter $\underline{\underline{C}}^{\beta}_{\vec{R}}$. If the constituents, however, have large differences in atomic size, there could be local lattice distortions which. are significant and lead to off-diagonal disorder in the structure matrix. The Green function may now be written as :

$$\begin{aligned} \underline{\underline{G}}_{\vec{R}\vec{R}'}(z) \;\; &= \;\; \underline{\underline{\lambda}}^{\beta}_{\vec{R}}(z) \; \delta_{\vec{R}\vec{R}'} + \ldots \\ &+ \;\; \underline{\underline{\Delta}}^{\beta}_{\vec{R}}(z)^{\,-1/2} \; \underline{\underline{T}}^{\beta}_{\vec{R}\vec{R}'}(z) \; \underline{\underline{\Delta}}^{\beta}_{\vec{R}}(z)^{\,-1/2} \end{aligned} \tag{4.2}$$

where

$$\mathcal{T}^{\beta}(z)^{-1} \;\; = \;\; \sum_{\vec{R}} \underline{\underline{P}}^{\beta}_{\vec{R}}(z) \; \mathcal{P}_{\vec{R}} - \sum_{\vec{R}} \sum_{\vec{R}'} \underline{\underline{S}}^{\beta}_{\vec{R}\text{-}\vec{R}'} \; \mathcal{T}_{\vec{R}\vec{R}'}$$

$$\underline{\underline{P}}^{\beta}_{\vec{R}}(z) = \underline{\underline{\Delta}}^{\beta\ -1/2}_{\vec{R}} \left(z\underline{\underline{I}} - \underline{\underline{C}}^{\beta}_{\vec{R}} \right) \underline{\underline{\Delta}}^{\beta\ -1/2}_{\vec{R}}$$

$$\underline{\underline{\lambda}}^{\beta}_{\vec{R}}(z) = (\underline{\underline{\gamma}} - \underline{\underline{\beta}})\ \underline{\underline{\Delta}}^{\gamma\ -1/2}_{\vec{R}}\ \underline{\underline{\Delta}}^{\beta\ 1/2}_{\vec{R}} \tag{4.3}$$

the values for the parameters $\beta_L = \beta_\ell$ for which we have maximum localization of the structure matrix are given by Andersen (71) while the parameters γ_ℓ are obtained through the LMTO procedure together with the other potential parameters.

In the absence of off-diagonal disorder in the structure matrices, all random 'potential parameters' in the Hamiltonian representation are *local* quantities and this representation is ideal for the description of substitutional randomness. We associate with each $\vec{R}$ labeled member of the basis set a random 'occupation' variable $n_{\vec{R}}$ such that

$$n_{\vec{R}} = \begin{cases} 1 & \text{if site } \vec{R} \text{ is occupied by a A atom,} \\ & \text{with probability } y \\ 0 & \text{if site } \vec{R} \text{ is occupied by a B atom,} \\ & \text{with probability } x = 1 - y \end{cases}$$

Putting this back in Eqn. (4.2) and taking configuration averaging we get,

$$\begin{aligned} \left\langle\!\left\langle G_{\vec{R}L,\vec{R}L} \right\rangle\!\right\rangle = \left\langle\!\left\langle \lambda^{\beta}_{\vec{R}L} \right\rangle\!\right\rangle + \mu_L^2(z)\ \left\langle\!\left\langle T^{\beta}_{\vec{R}L,\vec{R}L}(z) \right\rangle\!\right\rangle + \ldots \\ + \mu_L(z)\ \left\langle\!\left\langle T^{\beta}_{\vec{R}L,\vec{R}L}(z)\ n_{\vec{R}} \right\rangle\!\right\rangle\ \delta\mu_L(z) + \ldots \\ + \delta\mu_L(z)\ \left\langle\!\left\langle n_{\vec{R}}\ T^{\beta}_{\vec{R}L,\vec{R}L}(z) \right\rangle\!\right\rangle\ \mu_L(z) + \ldots \\ + \delta\mu_L(z)\ \left\langle\!\left\langle n_{\vec{R}}\ T^{\beta}_{\vec{R}L,\vec{R}L}(z)\ n_{\vec{R}} \right\rangle\!\right\rangle\ \delta\mu_L(z) \end{aligned} \tag{4.4}$$

where $\delta\mu_L(z) = \Delta^{\beta}_{AL}(z)^{\ -1/2} - \Delta^{\beta}_{BL}(z)^{\ -1/2}$ and $\mu_L(z) = \Delta^{\beta}_{AL}(z)^{\ -1/2}$.

We shall now introduce the augmented space formalism for configuration averaging. The ideas behind the approach have been described in great detail in a monograph (26). Here we shall briefly introduce only those essential points which will enable us to describe the cluster coherent potential approximation :

(i) The augmented space approach (25) replaces all the random variables $n_{\vec{R}}$ by operators $N_{\vec{R}}$ whose projected spectral density is the probability density of the variables $n_{\vec{R}}$. The eigenstates of $N_{\vec{R}}$ span the "configuration space" of $n_{\vec{R}}$.

(ii) We work in a new basis of representation : $|\emptyset_{\vec{R}}\rangle = \sqrt{y}|1_{\vec{R}}\rangle + \sqrt{x}|0_{\vec{R}}\rangle$, the average state, and $|\{1_{\vec{R}}\}\rangle = \sqrt{x}|1_{\vec{R}}\rangle - \sqrt{y}|0_{\vec{R}}\rangle$, which describes a fluctuation about the

average state. These two states span the configuration space $\phi_{\vec{R}}$ of $n_{\vec{R}}$ (of rank 2).

(iii) The full configuration space of all the variables $\{n_{\vec{R}}\}$ is $\Phi = \prod_{\vec{R}}^{\otimes} \phi_{\vec{R}}$ and the configuration states are labeled by the sequence of sites where we have a state $|1_{\vec{R}}\rangle$. For example, the configuration $\{0_{\vec{R}}, 1_{\vec{R}'}, 1_{\vec{R}''}, 0_{\vec{R}'''} \ldots\}$ is denoted by the sequence $\{\mathcal{C}\} \equiv \{\vec{R}', \vec{R}''\}$. This sequence is called the 'cardinality' sequence and it uniquely labels a given configuration. In configuration space : $\langle\{\mathcal{C}\}|\{\mathcal{C}'\}\rangle = \delta(\mathcal{C}, \mathcal{C}')$.

(iv) The operators in full configuration space corresponding to the binary random variables $\{n_{\vec{R}}\}$ $\Phi = \prod_{\vec{R}}^{\otimes}$ $\phi_{\vec{R}}$ are : [1]

$$\widehat{N}_{\vec{R}} = y\ \widehat{\mathcal{P}}^{\emptyset}_{\vec{R}} + x\ \widehat{\mathcal{P}}^{1}_{\vec{R}} + \sqrt{xy}\ \widehat{\mathcal{T}}^{01}_{\vec{R}} \tag{4.5}$$

here, $\widehat{\mathcal{P}}^{\lambda}_{\vec{R}} = I \otimes \ldots \otimes |\lambda_{\vec{R}}\rangle\langle\lambda_{\vec{R}}| \otimes \ldots$ and $\widehat{\mathcal{T}}^{\lambda\lambda'}_{\vec{R}} = I \otimes \ldots \otimes \Big(|\lambda_{\vec{R}}\rangle\langle\lambda'_{\vec{R}}| + |\lambda'_{\vec{R}}\rangle\langle\lambda_{\vec{R}}|\Big) \otimes \ldots$ where $\lambda \neq \lambda' = \emptyset, 1$

The projection operator counts the number of configuration fluctuations at the site $\vec{R}$, while the transfer operators create or annihilate configuration fluctuations at the site $\vec{R}$.

(v) Any random local potential parameter $X_{\vec{R}}$ in the Hamiltonian now can be expressed in terms of $n_{\vec{R}}$ as in Eqn. (5). The augmented space theorem replaces $n_{\vec{R}}$ by corresponding operator $\widehat{N}_{\vec{R}}$, so $X_{\vec{R}}$ is replaced by an operator $\widehat{X}_{\vec{R}}$ in the 'configuration' space spanned by the 'configuration' states of $N_{\vec{R}}$ and can be written as:

$$\widehat{X}_{\vec{R}} = A(X)\ \widehat{\mathcal{P}}^{0}_{\vec{R}} + B(X)\ \widehat{\mathcal{P}}^{1}_{\vec{R}} + F(X)\ \widehat{\mathcal{T}}^{01}_{\vec{R}} \tag{4.6}$$

where

$$\begin{aligned} A(X) &= \ll X \gg = yX_A + xX_B \\ B(X) &= xX_A + yX_B \\ F(X) &= \sqrt{xy}(X_A - X_B) \end{aligned} \tag{4.7}$$

[1] The following notation has been adopted : unmarked operators X act on the space $\mathcal{H}$ spanned by the LMTO basis. Hatted operators $\widehat{X}$ act on the configuration space Φ and tilded operators $\widetilde{X}$ act on the augmented space $\mathcal{H} \otimes \Phi$

(vi) The augmented space theorem (25) tells us that the configuration average of any function of $\{n_{\vec{R}}\}$ is :

$$\ll f[H(\{n_{\vec{R}}\}] \gg = \langle\{\emptyset\}|\ \widehat{f}[\widehat{H}(\{\widehat{N}_{\vec{R}}\})\ |\{\emptyset\}\rangle \tag{4.8}$$

where $|\{\emptyset\}\rangle = \prod_{\vec{R}}^{\otimes} |\{0_{\vec{R}}\}\rangle$.

(vii) Let us now apply the augmented space theorem to the different averages quoted in Eqn. (4.4) :

$$\left\langle\!\!\left\langle T^{\beta}_{\vec{R}L,\vec{R}L}(z) \right\rangle\!\!\right\rangle = \langle \vec{R}L \otimes \{\emptyset\}|\widetilde{\mathcal{T}}^{\beta}(z)|\vec{R}L \otimes \{\emptyset\}\rangle$$

$$\begin{aligned}\left\langle\!\!\left\langle T^{\beta}_{\vec{R}L,\vec{R}L}(z)\ n_{\vec{R}} \right\rangle\!\!\right\rangle = y\ &\langle \vec{R}L \otimes \{\emptyset\}|\widetilde{\mathcal{T}}^{\beta}(z)|\vec{R}L \otimes \{\emptyset\}\rangle \ldots \\ &+\sqrt{xy}\ \langle \vec{R}L \otimes \{\emptyset\}|\widetilde{\mathcal{T}}^{\beta}(z)|\vec{R}L \otimes \{\vec{R}\}\rangle\end{aligned}$$

$$\begin{aligned}\left\langle\!\!\left\langle n_{\vec{R}}\ T^{\beta}_{\vec{R}L,\vec{R}L}(z) \right\rangle\!\!\right\rangle = y\ &\langle \vec{R}L \otimes \{\emptyset\}|\widetilde{\mathcal{T}}^{\beta}(z)|\vec{R}L \otimes \{\emptyset\}\rangle \ldots \\ &+\sqrt{xy}\ \langle \vec{R}L \otimes \{\vec{R}\}|\widetilde{\mathcal{T}}^{\beta}(z)|\vec{R}L \otimes \{\emptyset\}\rangle\end{aligned}$$

$$\begin{aligned}\left\langle\!\!\left\langle n_{\vec{R}}\ T^{\beta}_{\vec{R}L,\vec{R}L}(z)\ n_{\vec{R}} \right\rangle\!\!\right\rangle = y^2\ &\langle \vec{R}L \otimes \{\emptyset\}|\widetilde{\mathcal{T}}^{\beta}(z)|\vec{R}L \otimes \{\emptyset\}\rangle \ldots \\ &+ y\sqrt{xy}\ \Big[\langle \vec{R}L \otimes \{\emptyset\}|\widetilde{\mathcal{T}}^{\beta}(z)|\vec{R}L \otimes \{\vec{R}\}\rangle \ldots \\ &+ \langle \vec{R}L \otimes \{\vec{R}\}|\widetilde{\mathcal{T}}^{\beta}(z)|\vec{R}L \otimes \{\emptyset\}\rangle\Big] \ldots \\ &+ xy\ \langle \vec{R}L \otimes \{\vec{R}\}|\widetilde{\mathcal{T}}^{\beta}(z)|\vec{R}L \otimes \{\vec{R}\}\rangle\end{aligned}$$

where

$$\begin{aligned}\widetilde{\mathcal{T}}^{\beta}(z)^{-1} \quad &= \quad \sum_{\vec{R}}\ A(\underline{\underline{P}}^{\beta})\ \mathcal{P}_{\vec{R}} \otimes \widehat{I} \ldots \\ &+ \quad \sum_{\vec{R}}\ B(\underline{\underline{P}}^{\beta})\ \mathcal{P}_{\vec{R}} \otimes \widehat{\mathcal{P}}^{1}_{\vec{R}} \ldots \\ &+ \quad \sum_{\vec{R}}\ F(\underline{\underline{P}}^{\beta})\ \mathcal{P}_{\vec{R}} \otimes \widehat{\mathcal{T}}^{\emptyset 1}_{\vec{R}} \ldots \\ &- \quad \sum_{\vec{R}}\sum_{\vec{R}'}\ \underline{\underline{S}}^{\beta}_{\vec{R}\text{-}\vec{R}''}\ \mathcal{T}_{\vec{R}\text{-}\vec{R}''} \otimes \widehat{I}\end{aligned}$$

the functions A, B and F are defined in the Eqn. (4.7).

We shall make two comments here : First, it is important to note that the result quoted above is *exact*. Although the mathematical formulation is attractive, it is not very useful for actual calculations in specific real alloy systems, since the dimension of the augmented space is essentially infinite and the representation of the operators are matrices of infinite rank. We need to introduce approximations which maintain the analytic and lattice translation properties of the configuration averaged Green functions. Several approximations have been proposed earlier. We shall discuss one such in the next section and present it in a way that will allow us to use it as the basis for a calculation algorithm for real alloy systems.

The second comment is that the above formulation closely follows the Kohn-Korringa-Rostocker (KKR) method, which is the parent method of the LMTO. A KKR-CCPA formulation can therefore be stated exactly along the same lines. The correspondences are :

$$P_{\vec{R}L}(z) \Longrightarrow \tau^{-1}_{\vec{R}L}(z) \qquad S_{\vec{R}L,\vec{R}'L'} \Longrightarrow -B_{\vec{R}L,\vec{R}'L'}$$
$$T_{\vec{R}L,\vec{R}'L'}(z) = \left[(P(z)-S)^{-1}\right]_{\vec{R}L,\vec{R}'L'} \Longrightarrow$$
$$\left[(\tau^{-1}(z)+B)^{-1}\right]_{\vec{R}L,\vec{R}'L'}$$

4.3 The cluster coherent potential approximation

We shall begin by the basic assumption of *all* mean-field theories : we suppose that there is a lattice translation symmetric effective system with a 'Hamiltonian' :

$$\mathcal{T}^{\rm eff}(z) = H^{\rm eff}(z)^{-1} =$$
$$\left(\sum_{\vec{R}} \underline{\underline{P}}^{\rm eff}(z)\ \mathcal{P}_{\vec{R}} - \sum_{\vec{R}} \sum_{\vec{R}'} \underline{\underline{S}}^{\rm eff}(\vec{R}\text{-}\vec{R}'\ ;z)\ \mathcal{T}_{RR'} \right)^{-1}$$

such that :

$$\left\langle\!\left\langle \underline{\underline{T}}^{\beta}_{\vec{R}\vec{R}'}(z) \right\rangle\!\right\rangle = \underline{\underline{T}}^{\rm eff}(\vec{R}\text{-}\vec{R}'\ ;z)$$

The problem to address then is the derivation of the effective medium terms $\underline{\underline{P}}^{\rm eff}(z)$ and $\underline{\underline{S}}^{\rm eff}(\vec{R}\text{-}\vec{R}'\ ;z)$.

To do this, let us first choose a site $\vec{R}_0$ with its cluster environment $\Xi_{\vec{R}_0}$ (see Fig. 1). In the full augmented space we choose the 'augmented' cluster, that is the cluster $\Xi_{\vec{R}_0}$ and all its possible configurations described by the cardinality sequences $\{\mathcal{C}(\Xi_{\vec{R}_0})\}$ of

the type $\{\emptyset\}$ or $\{\vec{R}_1, \vec{R}_2, \ldots \vec{R}_k\}$ where $1 \leq k \leq n$ (the cluster size) and $\vec{R}_1, \vec{R}_2 \ldots \in \Xi_{\vec{R}_0}$. Let us call the space spanned by $\Xi_{\vec{R}_0} \otimes \{\mathcal{C}(\Xi_{\vec{R}_0}\}$ as $\Psi_{\vec{R}_0}$. This is of rank $n \times 2^n$.

We shall now replace the entire remaining part of the lattice by the effective 'medium' described in Eqn. (4.9). The configuration space now reduces to the dimension 2^n of the configuration space of the cluster $\Xi_{\vec{R}_0}$ alone, spanned by states $\{\mathcal{C}(\Xi_{\vec{R}_0})\}$. In this *far* environment, outside the cluster, the configuration space collapses, as the effective medium is no longer random and there is just one configuration. We shall denote this collapsed augmented space by Ψ'.

We shall partition the collapsed augmented space Ψ' into the space, $\Psi_{\vec{R}_0}$ and the far environment ($\bar{\Psi}_{\vec{R}_0} = \Psi' \backslash \Psi_{\vec{R}_0}$).

The picture is now as follows : at the centre of our system is the site $\vec{R}_0$ at which the occupations are random. In its immediate or *near* environment is made up of the rest of the sites of the cluster $\Xi_{\vec{R}_0}$. The Hamiltonian associated with the near environment is also random. Beyond that is the *far* environment which has been approximated by the non-random mean-field, effective medium. If we now look at the "Hamiltonian" given in Eqn. (4.9) we note that it remains invariant under the translation operator $\mathbf{T}_\chi$ where, $\mathbf{T}_\chi |\vec{R}, \{\vec{R}_1, \vec{R}_2, \ldots \vec{R}_k\}\rangle = |\vec{R} + \chi, \{\vec{R}_1 + \chi, \vec{R}_2 + \chi, \ldots \vec{R}_k + \chi\}\rangle$. Consequently it is immaterial where we choose the cluster centre $\vec{R}_0$. We shall proceed to calculate the effect on the site $\vec{R}_0$ of its environment, both *near* and *far*. Since the procedure does not depend upon the choice of $\vec{R}_0$, its results for the configuration average should be lattice translationally invariant. This result is crucially dependent on the homogeneity of disorder. If the probability density $p(n_{\vec{R}})$ depended upon $\vec{R}$ the above statement would not be true.

The effects of the far and near environments are estimated through repeated downfoldings : first the far environment on the near environment and then the latter onto $\vec{R}_0$. The details of the mathematics can be obtained from EPAPS (72). We shall quote here the main results. The downfolding of the far environment leads to :

$$\begin{aligned} \widetilde{\mathcal{T}}_0^\beta(z) &= (\mathcal{A}_1 - \mathcal{B})^{-\mathcal{P}_{\Psi_{\vec{R}_0}}} \\ \mathcal{A}_1 &= \mathcal{P}_{\Psi_{\vec{R}_0}} \left[\widetilde{\mathcal{T}}_0^\beta(z)^{-1}\right] \mathcal{P}_{\Psi_{\vec{R}_0}} \end{aligned} \tag{4.9}$$

The effect of the far environment is contained in $\mathcal{B}$. If we define the self-energies as :

$$\begin{aligned} \underline{\underline{P}}^{\text{eff}}(z) &= \left\langle\!\!\left\langle P^\beta \right\rangle\!\!\right\rangle + \underline{\underline{\Sigma}}_0(z) \\ \underline{\underline{S}}^{\text{eff}}(\vec{R} - \vec{R}'; z) &= \underline{\underline{S}}^\beta(\vec{R} - \vec{R}') + \underline{\underline{\Sigma}}(\vec{R} - \vec{R}'; z) \end{aligned}$$

then it can be shown that :

$$\mathcal{B}(\vec{k},z) = \underline{\underline{S}}^{\text{eff}}(\vec{k},z)\ \underline{\underline{g}}(\vec{k},z)\ \underline{\underline{S}}^{\text{eff}}(\vec{k},z) \tag{4.10}$$

where

$$\underline{\underline{g}}(\vec{k},z) = \underline{\underline{T}}^{\text{eff}}(\vec{k},z)\ \left(\underline{\underline{I}} + \underline{\underline{\Delta}}(\vec{k},z)\ \underline{\underline{T}}^{\text{eff}}(\vec{k},z)\right)^{-1}$$

and $$\underline{\underline{\Delta}}(\vec{k},z) = \underline{\underline{\Sigma}}_0(z) + \underline{\underline{\Sigma}}(\vec{k},z)$$

It is obvious from Eqn. (4.10) that the matrix elements of $\mathcal{B}$ are themselves functionals of $\underline{\underline{P}}^{\text{eff}}$ and $\underline{\underline{S}}^{\text{eff}}$:

$$\mathcal{B} = \sum_{R\in\Xi_{R_0}} \underline{\underline{B}}_0\left[\underline{\underline{P}}^{\text{eff}}(z);\underline{\underline{S}}^{\text{eff}}(z)\right]\ \mathcal{P}_{\vec{R}}\ldots$$
$$\ldots - \sum_{R,R'\in\Xi_{R_0}} \underline{\underline{B}}\left(R\text{-}R';\underline{\underline{P}}^{\text{eff}}(z);\underline{\underline{S}}^{\text{eff}}(z)\right)\ \mathcal{T}_{\vec{R}\vec{R}'}$$

and

$$\underline{\underline{T}}^{\text{eff}}(\vec{R}\text{-}\vec{R}';z) = \int \frac{d^3\vec{k}}{8\pi^3}\ \mathrm{e}^{i\vec{k}\cdot(\vec{R}\text{-}\vec{R}')}\ \left[\underline{\underline{P}}^{\text{eff}}(z) - \underline{\underline{S}}^{\text{eff}}(\vec{k},z)\right]^{-1}$$
$$\underline{\underline{B}}(\vec{R}\text{-}\vec{R}'\ ;z) = \int \frac{d^3\vec{k}}{8\pi^3}\ \mathrm{e}^{i\vec{k}\cdot(\vec{R}\text{-}\vec{R}')}\ \underline{\underline{B}}(\vec{k};z) \tag{4.11}$$

Having downfolded the effect of the 'far' environment on to the cluster chosen, the augmented space has been reduced to Ψ_0 of rank $n\times 2^n$ where n is the size of $\Xi_{\vec{R}_0}$. The next step would be to partition Ψ_0 to a space Φ of rank n , spanned by the states $|\vec{R}\in\Xi_{\vec{R}_0}\otimes\emptyset\rangle$ and its complement $\bar{\Phi}$ in Ψ_0.

$$\widetilde{\mathcal{T}}_0 = \left(\begin{array}{c|c} \mathcal{D}_1 & \mathcal{D}' \\ \hline \mathcal{D}^T & \mathcal{D}_2 \end{array}\right)$$

The downfolding theorem gives :

$$\mathcal{D}_1^{-\mathcal{P}_\Phi} = \left(\mathcal{D}_1 - \mathcal{D}'\ \mathcal{D}_2^{-\mathcal{P}_{\bar{\Phi}}}\mathcal{D}'^T\right)^{-\mathcal{P}_\Phi} \tag{4.12}$$

We now are working in the vastly reduced augmented space of dimension m. All inverses will now refer to this m-dimensional Hilbert space.

Again, with a little mathematics (details of which can be accessed from EPAPS (72)), we obtain the self-consistency equations for the self-energies :

$$\begin{aligned} \underline{\underline{\Sigma}}_0(z) &= \underline{\underline{B}}_0(z) + \left\langle \vec{R} \right\| \mathcal{K} \left\| \vec{R} \right\rangle \\ \underline{\underline{\Sigma}}\left(\vec{R}\text{-}\vec{R}'; z\right) &= \underline{\underline{B}}(\vec{R}\text{-}\vec{R}'; z) + \left\langle \vec{R} \right\| \mathcal{K} \left\| \vec{R}' \right\rangle \end{aligned}$$

where $\vec{R}, \vec{R}' \in \Xi_{\vec{R}_0}$; $\mathcal{D}_2^{-\mathcal{P}_{\bar{\Phi}}} = \mathcal{K}$ and

$$\begin{aligned} \left\langle \vec{R} \right\| &= \sum_{\vec{R}'' \neq \Xi_{\vec{R}_0}} \underline{\underline{\sigma}}(\vec{R}\text{-}\vec{R}''; z) \langle \vec{R}'' \otimes \{\emptyset\}| + \ldots \\ &\quad \ldots + F(\underline{\underline{P}}^{\beta}) \langle \vec{R} \otimes \{\vec{R}\}| \end{aligned}$$

$$\underline{\underline{\sigma}}\left(\vec{R}\text{-}\vec{R}'; z\right) = \underline{\underline{S}}^{\beta}(\vec{R}\text{-}\vec{R}') - \underline{\underline{B}}\left(\vec{R}\text{-}\vec{R}'; z\right)$$

The matrix elements in Eqns.(4.13) are written in terms of the matrix elements of $\mathcal{K}$:

$$\begin{gathered} \langle \vec{R}_p \otimes \{\emptyset\} | \mathcal{K} | \vec{R}_{p'} \otimes \{\emptyset\} \rangle \ , \ \langle \vec{R} \otimes \{\emptyset\} | \mathcal{K} | \vec{R}_p \otimes \{\vec{R}_p\} \rangle \\ \text{and } \langle \vec{R}_p \otimes \{\vec{R}_p\} | \mathcal{K} | \vec{R}_{p'} \otimes \{\vec{R}_{p'}\} \rangle \qquad \text{where} \quad p, p' = 0, 1 \end{gathered}$$

Since the subspace $\bar{\Phi}$ of the full augmented space is of finite rank, these matrix elements of $\mathcal{K}$ can be obtained by a simple matrix inversion of $\mathcal{D}_2$ in this subspace.

The two downfolding procedures are best illustrated by the schematic figure 4.1 shown here.

These are the equations for the CCPA self-energies. We again emphasize that the choice of $\vec{R}_0$ is immaterial and in the absence of anisotropy in the Hamiltonian, so is the choice of $\vec{R}_1$. The effective medium off-diagonal matrix element in the direction of $\vec{R}_2 - \vec{R}_0$ is related to that in the direction $\vec{R}_1 - \vec{R}_0$ by a rotation matrix :

$$\underline{\underline{S}}^{\text{eff}}(\vec{R}_0 - \vec{R}_2; z) = \underline{\underline{U}}^T \ \underline{\underline{S}}^{\text{eff}}(\vec{R}_0 - \vec{R}_1; z) \ \underline{\underline{U}}$$

Finally, we need to calculate the other average terms in Eqns. (4.4) and (4.9). For this we partition the $\widetilde{\mathcal{T}}_0^{\beta}$ into a subspace π of rank 1, spanned by the state $|\vec{R}_0 \otimes \emptyset\rangle$ and its complement $\bar{\pi}$ in Ψ_0.

$$\widetilde{\Gamma}_0 = \left(\begin{array}{c|c} \mathcal{E}_1 & \mathcal{E}' \\ \hline \mathcal{E}'^T & \mathcal{E}_2 \end{array} \right)$$

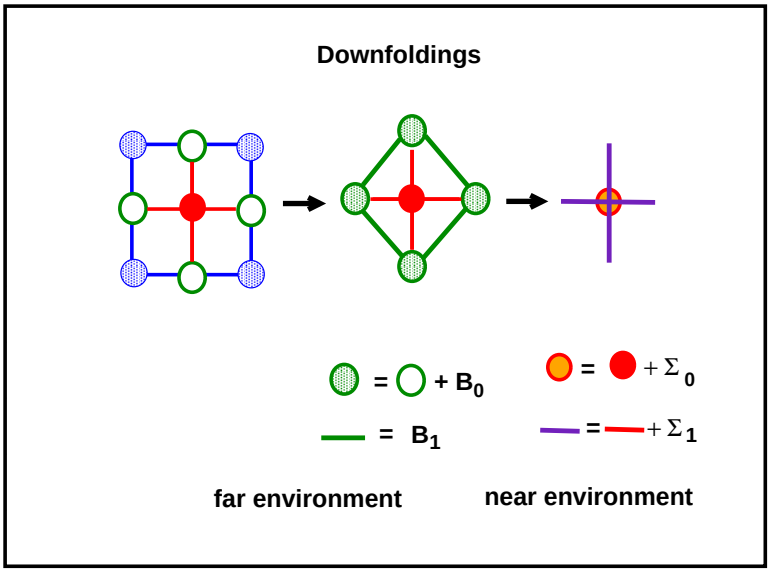

Figure 4.1: Downfolding - The downfoldings of the far and near environments. The cluster centre is shown in red, the near environment in green and the far environment in blue. Successive downfoldings renormalize the Hamiltonian matrix elements.

Downfolding and taking appropriate matrix elements (see EPAPS (72)) we get :

$$\begin{aligned}
&\langle \vec{R}_0 \otimes \{\emptyset\} | \underline{\underline{\mathcal{T}}}^{\beta} | \vec{R}_0 \otimes \{\vec{R}_0\} \rangle = \\
&\left\langle\!\!\left\langle \underline{\underline{T}}^{\beta}_{\vec{R}_0,\vec{R}_0} \right\rangle\!\!\right\rangle \left[F(\underline{\underline{P}}^{\beta})\ \underline{\underline{\Gamma}}^{(2)}_{\vec{R}_0,\vec{R}_0} + \sum_{\vec{R}\neq\vec{R}_0} \underline{\underline{\sigma}}(\vec{R}_0\text{-}\vec{R};z)\ \underline{\underline{\Gamma}}^{(1)}_{\vec{R},\vec{R}_0} \right] \\
&= \left\langle\!\!\left\langle \underline{\underline{T}}^{\beta}_{\vec{R}_0,\vec{R}_0} \right\rangle\!\!\right\rangle\ \underline{\underline{W}}_{\vec{R}_0,\vec{R}_0}
\end{aligned}$$

$$\langle \vec{R}_0 \otimes \{\vec{R}_0\} | \underline{\underline{\mathcal{T}}}^{\beta} | \vec{R}_0 \otimes \{\emptyset\} \rangle = \underline{\underline{W}}_{\vec{R}_0,\vec{R}_0}\ \left\langle\!\!\left\langle \underline{\underline{T}}^{\beta}_{\vec{R}_0,\vec{R}_0} \right\rangle\!\!\right\rangle$$

$$\begin{aligned}
&\langle \vec{R}_0 \otimes \{\vec{R}_0\} | \underline{\underline{\mathcal{T}}}^{\beta} | \vec{R}_0 \otimes \{\vec{R}_0\} \rangle = \\
&\qquad \underline{\underline{\Gamma}}^{(2)}_{\vec{R}_0,\vec{R}_0} + \underline{\underline{W}}_{\vec{R}_0,\vec{R}_0}\ \left\langle\!\!\left\langle \underline{\underline{T}}^{\beta}_{\vec{R}_0,\vec{R}_0} \right\rangle\!\!\right\rangle \underline{\underline{W}}_{\vec{R}_0,\vec{R}_0}
\end{aligned}$$

where

$$\begin{aligned}
\underline{\underline{\Gamma}}^{(2)}_{\vec{R}_0,\vec{R}_0} &= \langle \vec{R}_0 \otimes \{\vec{R}_0\} | \underline{\underline{\mathcal{E}}}_2^{-\mathcal{P}_{\bar{\pi}}} | \vec{R}_0 \otimes \{\vec{R}_0\} \rangle \\
\underline{\underline{\Gamma}}^{(1)}_{\vec{R},\vec{R}_0} &= \langle \vec{R} \otimes \{\emptyset\} | \underline{\underline{\mathcal{E}}}_2^{-\mathcal{P}_{\bar{\pi}}} | \vec{R}_0 \otimes \{\vec{R}_0\} \rangle
\end{aligned}$$

Now substituting in Eqns. (4.4) and (4.9) we get :

$$\left\langle\!\left\langle \underline{\underline{G}}_{\vec{R}_0\vec{R}_0} \right\rangle\!\right\rangle = \left\langle\!\left\langle \underline{\underline{\lambda}}_{\vec{R}_0} \right\rangle\!\right\rangle + \underline{\underline{\mu}}^{\text{eff}}_{\vec{R}_0} \left\langle\!\left\langle \underline{\underline{T}}^{\beta}_{\vec{R}_0\vec{R}_0} \right\rangle\!\right\rangle \underline{\underline{\mu}}^{\text{eff}}_{\vec{R}_0} \cdots$$
$$+\underline{\underline{\delta\mu}}\ \underline{\underline{\Gamma}}^{(2)}_{\vec{R}_0\vec{R}_0}\ \underline{\underline{\delta\mu}}$$
$$\text{where :}\quad \underline{\underline{\mu}}^{\text{eff}}_{\vec{R}_0} = \left\langle\!\left\langle \underline{\underline{\mu}} \right\rangle\!\right\rangle + \sqrt{xy}\ \underline{\underline{\delta\mu}}\ \underline{\underline{W}}_{\vec{R}_0\vec{R}_0}$$

4.4 Configuration averaged spectral functions and complex band-structures

Going back to Eqns. (4.2) and (4.13) we note the following : homogeneity of disorder leads to $\underline{\underline{\mu}}^{\text{eff}}_{\vec{R}_0} = \underline{\underline{\mu}}^{\text{eff}} = \left\langle\!\left\langle \underline{\underline{\mu}} \right\rangle\!\right\rangle + \sqrt{xy}\ \underline{\underline{\delta\mu}}\ \underline{\underline{W}}$ and

$$\left\langle\!\left\langle \underline{\underline{G}}(R_0\text{-}R_1\ ;z) \right\rangle\!\right\rangle = \underline{\underline{\mu}}^{\text{eff}}(z)\ \left\langle\!\left\langle \underline{\underline{T}}^{\beta}(R_0\text{-}R_1\ ;z) \right\rangle\!\right\rangle\ \underline{\underline{\mu}}^{\text{eff}}(z)$$

Spatial homogeneity gives :

$$\left\langle\!\left\langle \underline{\underline{G}}(\vec{k}\ ;z) \right\rangle\!\right\rangle = \underline{\underline{\mu}}^{\text{eff}}(z)\ \left\langle\!\left\langle \underline{\underline{T}}^{\beta}(\vec{k}\ ;z) \right\rangle\!\right\rangle \underline{\underline{\mu}}^{\text{eff}}(z) \tag{4.13}$$

where

$$\left\langle\!\left\langle \underline{\underline{T}}^{\beta}(\vec{k}\ ;z) \right\rangle\!\right\rangle = \left(\left\langle\!\left\langle \underline{\underline{P}}^{\beta} \right\rangle\!\right\rangle - \underline{\underline{S}}^{\beta}(\vec{k}) + \underline{\underline{\Sigma}}_0(z) - \underline{\underline{\Sigma}}(\vec{k}\ ;z) \right)^{-1} \tag{4.14}$$

The self-energy in reciprocal space may be obtained from Eqn. (4.13) by Fourier transformation :

$$\underline{\underline{\Sigma}}(\vec{k};z) = \sum_{\vec{\chi}} \underline{\underline{\Sigma}}(\vec{\chi};z)\ \exp(i\vec{k}\cdot\vec{\chi}) \tag{4.15}$$

where $\vec{\chi}$ are the vectors joining any two sites in the cluster. We should note that although the Hamiltonian may have only nearest neighbour matrix elements, because of downfolding of the far environment, the self-energies, in general, connect all sites of the cluster.

The configuration averaged spectral function is given by :

$$\left\langle\!\left\langle A(\vec{k},E) \right\rangle\!\right\rangle = -\frac{1}{\pi}\ \lim_{\delta\to 0}\ \Im m\ \mathrm{T}r \left\langle\!\left\langle \underline{\underline{G}}(\vec{k}\ ;E+i\delta) \right\rangle\!\right\rangle \tag{4.16}$$

Unlike the periodic solid where the spectral function is a bunch of delta functions at the eigenvalues of the periodic Hamiltonian, for disordered systems aperiodicity in the

potential leads to scattering of the Bloch like functions. Consequently the complex self-energy gives both a shift and a Lorenzian width to the delta functions.

The complex band structure of random systems is obtained directly from the spectral functions. For ordered materials for a given $\vec{k}$ the spectral function $A(\vec{k}, E)$ is a bunch of delta functions at $E = E(\vec{k})$. For disordered materials the configuration averaged spectral functions have peaks at $E(\vec{k})$ which locate the position of the bands. If we fit Lorenzians around these peaks, the half-widths will measure the spread or "fuzziness" of the bands. This has been plotted in Fig. 3. We should note that the spectral function near a peak may have considerable asymmetry. In such cases we really cannot fit it to a Lorenzian near the peak. This description becomes inaccurate in those circumstances.

4.5 Comments

We stress again that the downfolding approach here differs significantly from the earlier proposed cluster coherent potential approximations. We do not begin by partitioning the Hilbert space into clusters. There were always objections that the procedure was not unique and the results violated the translation symmetry of averaged quantities : replacing it by a cluster translational symmetry. Rather, our approach focuses on any site and estimates the effect of configuration fluctuations of its environment on the local properties at that point, using a downfolding technique. In the augmented space, if the disorder is homogeneous, the environment of every site is identical. Thus our choice of the central site is immaterial and the formulation maintains the lattice translational symmetry of configuration averaged quantities. In case the system has more than one atom per unit cell, we can generalize our ideas concentrating on a unit cell (instead of a site) and estimating the effect of configuration fluctuations of the environment of the cell by the downfolding technique.

We distinguish both the immediate or near environment and retain its randomness *exactly* and the far environment which we approximate by an effective medium. We go on to obtain this effective medium self-consistently using successive downfoldings. Razee and Prasad (60) have shown that if we consider the entire environment of a site as an effective far environment we recover the single-site CPA. In that sense the formulation is a generalization of the CPA.

In a formal paper Razee *et.al.*(73) have shown that the downfolding generalization retains the Herglotz analytic properties of the approximated averaged Green function. This is an essential property of any successful generalization of the CPA.

The CCPA proposed here is closely related to the TB-LMTO-ASR (74, 75), which is based on the recursion method (11). It is known that the recursion method successively partitions the full augmented space into subspaces which are successively the further and further shell-environments of the starting site. The continued fraction expansion of the Green function is generated by repeated downfolding using successive applications of the partitioning theorem. In the TB-LMTO-ASR the near environment is the number of recursion steps one carries out *exactly* and the far environment is estimated approximately through the *terminator* (76). In our present formulation, the far environment is estimated in a more transparent self-consistent mean-field approach. The formulation also has close affinities with the itinerant cluster coherent potential (ICPA) proposed by Leath (61). Since the idea of approximation is very similar, it would be interesting to work out an exact relationship between the two. Similarities with the traveling cluster approximation (TCA) of Mills *et.al.*(77, 78) is also apparent, although the TCA approached the problem from a multiple scattering approach. For the CPA, the mean-field and the multiple scattering approaches give identical results. It would be interesting to examine whether this is true also for this CCPA and the TCA. We propose to examine these relationships in a subsequent communication.

4.6 Short ranged order

In the previous section we have described a CCPA approach based on the augmented space formalism for substitutional alloys whose occupation probabilities are homogeneously and independently distributed. However, most disordered alloys have a certain degree of short-ranged order (SRO) dictated by the local chemistry of the constituents. Such SRO cannot be described by single-site mean field approximations. On the other hand, the approach suggested by us, where the effect of the environment of any chosen site is estimated by a downfolding procedure, is ideal for such a description. Short ranged order is described by correlated distribution of the site occupation variable of any chosen site with those of its near environment. In an earlier communication Mookerjee and Prasad (79) had generalized the augmented space formalism to include such

SRO. In the downfolding procedure to obtain the self-consistent equations for the self-energies, we had partitioned the augmented space into one spanned by $|\vec{R}_0 \otimes \emptyset\rangle$ and $|\vec{R}_0 \otimes \{\vec{R}_0\}\rangle$. We shall do this again, but this time the augmented space operator $\widehat{N}_{\vec{R}_0}$ given in Eqn. (4.5) will be replaced by Eqn. (17) of Mookerjee and Prasad (79) :

$$\begin{aligned}\widehat{N}_{\vec{R}_0} = y\ \widehat{I} + (x-y)\ \widehat{\mathcal{P}}^{01}_{\vec{R}_0\vec{R}_1} + (X-y)\ \widehat{\mathcal{P}}^{10}_{\vec{R}_0\vec{R}_1} + \ldots \\ +(X'-y)\ \widehat{\mathcal{P}}^{11}_{\vec{R}_0\vec{R}_1} + B_1\ \widehat{\mathcal{Q}}^{0,01}_{\vec{R}_0\vec{R}_1} + B_2\ \widehat{\mathcal{Q}}^{1,01}_{\vec{R}_0\vec{R}_1} + \ldots \\ +B_3\widehat{\mathcal{Q}}'^{\,01,0}_{\vec{R}_0\vec{R}_1} + B_4\ \widehat{\mathcal{Q}}'^{\,01,1}_{\vec{R}_0\vec{R}_1} + B_5\ \widehat{\widehat{R}}^{01,01}_{\vec{R}_0\vec{R}_1}\end{aligned} \tag{4.17}$$

where,

$$\begin{aligned}\widehat{\mathcal{P}}^{\lambda\lambda'}_{\vec{R}_0\vec{R}_1} &= I \otimes \ldots \mathcal{P}^{\lambda}_{\vec{R}_0} \otimes \ldots \mathcal{P}^{\lambda'}_{\vec{R}_1} \otimes \ldots \\ \widehat{\mathcal{Q}}^{\lambda,\lambda'\lambda''}_{\vec{R}_0\vec{R}_1} &= I \otimes \ldots \mathcal{P}^{\lambda}_{\vec{R}_0} \otimes \ldots \mathcal{T}^{\lambda',\lambda''}_{\vec{R}_1} \otimes \ldots \\ \widehat{\mathcal{Q}}'^{\,\lambda'\lambda'',\lambda}_{\vec{R}_0\vec{R}_1} &= I \otimes \ldots \mathcal{T}^{\lambda'\lambda''}_{\vec{R}_0} \otimes \ldots \mathcal{P}^{\lambda}_{\vec{R}_1} \otimes \ldots \\ \widehat{\widehat{\mathcal{R}}}^{\lambda\lambda',\lambda\lambda'}_{\vec{R}_0\vec{R}_1} &= I \otimes \ldots \mathcal{T}^{\lambda,\lambda'}_{\vec{R}_0} \otimes \ldots \mathcal{T}^{\lambda\lambda'}_{\vec{R}_1} \otimes \ldots\end{aligned}$$

where $\lambda, \lambda', \lambda'' = 0, 1$ and

$$\begin{aligned}X &= y - \alpha(y-x) \qquad X' = x + \alpha(y-x) \\ B_1 &= y\sqrt{(1-\alpha)x(y+\alpha x)} + x\sqrt{(1-\alpha)y(x+\alpha y)} \\ B_2 &= x\sqrt{(1-\alpha)x(y+\alpha x)} + y\sqrt{(1-\alpha)y(x+\alpha y)} \\ B_3 &= \alpha\sqrt{xy} = -B_4 \\ B_5 &= \sqrt{xy}\left[\sqrt{(1-\alpha)x(y+\alpha x)} - \sqrt{(1-\alpha)y(x+\alpha y)}\right]\end{aligned}$$

The rest of the downfolding procedure follows exactly as before and leads to the self-consistency equations :

$$\begin{aligned}\underline{\underline{\Sigma}}_{\vec{R}_0}(z) &= \underline{\underline{B}}_0(z) + \left\langle\ \vec{R}_0\ \right\|\mathcal{K}\left\|\ \vec{R}_0\ \right\rangle \\ \underline{\underline{\Sigma}}(\vec{R}_0\text{-}\vec{R}_1; z) &= \underline{\underline{B}}(\vec{R}_0\text{-}\vec{R}_1; z) + \left\langle\ \vec{R}_0\ \right\|\mathcal{K}\left\|\ \vec{R}_1\ \right\rangle\end{aligned}$$

where,

$$\left\langle\ \vec{R}_0\ \right\| = \sum_{\vec{R}'' \neq \Xi_{\vec{R}_0}} \underline{\underline{\sigma}}(\vec{R}_0\text{-}\vec{R}''; z)\langle\vec{R} \otimes \{\emptyset\}| + \ldots$$

$$+F_1(\underline{\underline{P}}^{\beta})\langle\vec{R}_0\otimes\{\vec{R}_0\}| + F_2(\underline{\underline{P}}^{\beta})\langle\vec{R}_0\otimes\{\vec{R}_1\}|$$
$$+F_3(\ll\underline{\underline{P}}^{\beta}\gg)\langle\vec{R}_0\otimes\{\vec{R}_0\vec{R}_1\}| \quad ‘$$

$$\left\langle\ \vec{R}_1\ \right\| = \sum_{\vec{R}\neq\Xi_{\vec{R}_0}} \underline{\underline{\sigma}}(\vec{R}_1\text{-}\vec{R};z)\langle\vec{R}\otimes\{\emptyset\}| +$$
$$+F(\underline{\underline{P}}^{\beta})\langle\vec{R}_1\otimes\{\vec{R}_1\}|$$

where,

$$\begin{aligned} F_1\left(\underline{\underline{P}}^{\beta}\right) &= B_4(\underline{\underline{P}}^{\beta}_A - \underline{\underline{P}}^{\beta}_B) \quad F_2\left(\underline{\underline{P}}^{\beta}\right) = B_2(\underline{\underline{P}}^{\beta}_A - \underline{\underline{P}}^{\beta}_B) \\ F_3\left(\underline{\underline{P}}^{\beta}\right) &= B_5(\underline{\underline{P}}^{\beta}_A - \underline{\underline{P}}^{\beta}_B) \quad F\left(\underline{\underline{P}}^{\beta})\right) = \sqrt{xy}\ (\underline{\underline{P}}^{\beta}_A - \underline{\underline{P}}^{\beta}_B) \end{aligned}$$

The Eqn. (4.18) then replaces the earlier Eqn. (4.13). It is clear that the SRO affects the self-consistent far environment through the self-consistency equations. Our approach is thus superior to some earlier approaches where the cluster with SRO was immersed in a single-site CPA medium.

Finally the expression for $\underline{\underline{W}}_{\vec{R}_0\vec{R}_0}$ is replaced by :

$$\begin{aligned} \underline{\underline{W}}_{\vec{R}_0\vec{R}_0} &= F_1\left(\underline{\underline{P}}^{\beta}\right)\underline{\underline{\Gamma}}^{(2)}_{\vec{R}_0\vec{R}_0} + F_2\left(\underline{\underline{P}}^{\beta}\right)\underline{\underline{\Gamma}}^{(3)}_{\vec{R}_0\vec{R}_0} + \ldots \\ &\quad +F_3(\left(\underline{\underline{P}}^{\beta}\right)\underline{\underline{\Gamma}}^{(4)}_{\vec{R}_0\vec{R}_0} + \sum_{\vec{R}\neq\vec{R}_0}\underline{\underline{\sigma}}(\vec{R}_0\text{-}\vec{R};z)\ \underline{\underline{\Gamma}}^{(1)}_{\vec{R}\vec{R}_0} \end{aligned}$$

where the new matrix elements of $\underline{\underline{\mathcal{E}}}_2^{-\mathcal{P}_\pi}$ are :

$$\begin{aligned} \underline{\underline{\Gamma}}^{(3)}_{\vec{R}_0\vec{R}_0} &= \langle\vec{R}_0\otimes\{\vec{R}_1\}|\underline{\underline{\mathcal{E}}}_2^{-\mathcal{P}_\pi}|\vec{R}_0\otimes\{\vec{R}_0\}\rangle \\ \underline{\underline{\Gamma}}^{(4)}_{\vec{R}_0\vec{R}_0} &= \langle\vec{R}_0\otimes\{\vec{R}_0\vec{R}_1\}|\underline{\underline{\mathcal{E}}}_2^{-\mathcal{P}_\pi}|\vec{R}_0\otimes\{\vec{R}_0\}\rangle \end{aligned}$$

With these changes, the CCPA can self-consistently include the effects of SRO in its calculation of the averaged Green functions.

4.7 Off-diagonal disorder

In a substitutional alloy with local lattice distortions, the random off-diagonal structure matrices $\underline{\underline{S}}^{\beta}_{\vec{R}\vec{R}'}$ between the sites $\vec{R}$ and $\vec{R}'$ can be written, within the end-point

approximation, in terms of the site occupation numbers $\{n_{\vec{R}}\}$ as :

$$\begin{aligned}\underline{\underline{S}}^{\beta}_{\vec{R}\vec{R}'} &= \underline{\underline{S}}^{\beta}_{BB}(\vec{R}\text{-}\vec{R}') + \Big(\underline{\underline{S}}^{\beta}_{AA}(\vec{R}\text{-}\vec{R}') + \underline{\underline{S}}^{\beta}_{BB}(\vec{R}\text{-}\vec{R}')\ldots \\ &\ldots \quad -2\underline{\underline{S}}^{\beta}_{AB}(\vec{R}\text{-}\vec{R}')\Big)\ n_{\vec{R}}n_{\vec{R}'} + \Big(\underline{\underline{S}}^{\beta}_{AB}(\vec{R}\text{-}\vec{R}')\ldots \\ &\ldots \quad -\underline{\underline{S}}^{\beta}_{BB}(\vec{R}\text{-}\vec{R}')\Big)\ (n_{\vec{R}} + n_{\vec{R}'}) \end{aligned} \tag{4.18}$$

The downfolding procedure now follows exactly as before (details again are to be found in (72)). We shall quote here the final equations for the self-energies :

$$\begin{aligned}\underline{\underline{\Sigma}}_0(z) &= \underline{\underline{B}}_{\vec{R}_0}(z) + \left\langle\ \vec{R}_0\ \right\|\mathcal{K}\left\|\ \vec{R}_0\ \right\rangle \\ \underline{\underline{\Sigma}}(\vec{R}_0\text{-}\vec{R}_1;z) &= \underline{\underline{B}}(\vec{R}_0\text{-}\vec{R}_1;z) + \left\langle\ \vec{R}_0\ \right\|\mathcal{K}\left\|\ \vec{R}_1\ \right\rangle \end{aligned} \tag{4.19}$$

where

$$\begin{aligned}\left\langle \vec{R}_0 \right\| &= \underline{\underline{S}}^{(2)}(R_0\text{-}R_1)\langle\vec{R}_1\otimes\{\vec{R}_0\}| + \ldots \\ &+ \underline{\underline{S}}^{(2)}(R_0\text{-}R_1)\langle\vec{R}_1\otimes\{R_1\}|\ldots \\ &+ \underline{\underline{S}}^{(5)}(R_0\text{-}R_1)\langle\vec{R}_1\otimes\{\vec{R}_0\vec{R}_1\}|\ldots \\ &+ \sum_{\vec{R}\neq\vec{R}_0\vec{R}_1}\underline{\underline{\sigma}}(\vec{R}_0\text{-}\vec{R};z)\langle\vec{R}\otimes\{\emptyset\}|\ldots \\ &+ F(\underline{\underline{P}}^{\beta})\langle\vec{R}_0\otimes\{\vec{R}_0\}| \end{aligned}$$

$$\begin{aligned}\left\langle \vec{R}_1 \right\| &= \underline{\underline{S}}^{(2)}(R_0\text{-}R_1)\langle\vec{R}_0\otimes\{\vec{R}_1\}|\ldots \\ &+ \underline{\underline{S}}^{(2)}(R_0\text{-}R_1)\langle\vec{R}_0\otimes\{\vec{R}_0\}| + \ldots \\ &+ \underline{\underline{S}}^{(5)}(R_0\text{-}R_1)\langle\vec{R}_0\otimes\{\vec{R}_0\vec{R}_1\}|\ldots \\ &+ \sum_{\vec{R}\neq\vec{R}_1\vec{R}_0}\underline{\underline{\sigma}}(\vec{R}_1\text{-}\vec{R};z)\langle\vec{R}\otimes\{\emptyset\}|\ldots \\ &+ F(\underline{\underline{P}}^{\beta})\langle\vec{R}_1\otimes\{\vec{R}_1\}| \end{aligned}$$

where,

$$\begin{aligned}\underline{\underline{S}}^{(1)}(\vec{R}\text{-}\vec{R}') &= (x-y)\ \underline{\underline{\Phi}}^{(1)}(\vec{R}\text{-}\vec{R}') \\ \underline{\underline{S}}^{(2)}(\vec{R}\text{-}\vec{R}') &= \sqrt{xy}\ \underline{\underline{\Phi}}^{(1)}(\vec{R}\text{-}\vec{R}') \\ \underline{\underline{S}}^{(3)}(\vec{R}\text{-}\vec{R}') &= (x-y)^2\ \underline{\underline{\Phi}}^{(2)}(\vec{R}\text{-}\vec{R}') \end{aligned}$$

$$\begin{aligned}
\underline{\underline{S}}^{(4)}(\vec{R}\text{-}\vec{R}') &= \sqrt{xy}\ (x-y)\ \underline{\underline{\Phi}}^{(2)}(\vec{R}\text{-}\vec{R}') \\
\underline{\underline{S}}^{(5)}(\vec{R}\text{-}\vec{R}') &= xy\ \underline{\underline{\Phi}}^{(2)}(\vec{R}\text{-}\vec{R}')
\end{aligned}$$

and

$$\begin{aligned}
\underline{\underline{\Phi}}^{(1)}(\vec{R}\text{-}\vec{R}') &= y\ \underline{\underline{S}}^{\beta}_{AA}(\vec{R}\text{-}\vec{R}') - x\ \underline{\underline{S}}^{\beta}_{BB}(\vec{R}\text{-}\vec{R}') + \ldots \\
&+ (x-y)\ \underline{\underline{S}}^{\beta}_{AB}(\vec{R}\text{-}\vec{R}') \\
\underline{\underline{\Phi}}^{(2)}(\vec{R}\text{-}\vec{R}') &= \underline{\underline{S}}^{\beta}_{AA}(\vec{R}\text{-}\vec{R}') + \underline{\underline{S}}^{\beta}_{BB}(\vec{R}\text{-}\vec{R}') - 2\underline{\underline{S}}^{\beta}_{AB}(\vec{R}\text{-}\vec{R}')
\end{aligned}$$

Following the exact similar steps, the new expression for $\underline{\underline{W}}_{\vec{R}_0\vec{R}_0}$ becomes :

$$\begin{aligned}
\underline{\underline{W}}_{\vec{R}_0\vec{R}_0} &= \Big[F(\underline{\underline{P}}^{\beta})\ \underline{\underline{\Gamma}}^{(2)}_{\vec{R}_0,\vec{R}_0} + \ldots \\
&+ \sum_{\vec{R}\neq\vec{R}_0} \underline{\underline{\sigma}}(\vec{R}_0\text{-}\vec{R};z)\ \underline{\underline{\Gamma}}^{(1)}_{\vec{R},\vec{R}_0} + \underline{\underline{S}}^{(2)}(R_0\text{-}R_1)\underline{\underline{\Gamma}}^{(5)}_{\vec{R}_1\vec{R}_0} + \ldots \\
&+ \underline{\underline{S}}^{(2)}(R_0\text{-}R_1)\underline{\underline{\Gamma}}^{(6)}_{\vec{R}_1\vec{R}_0} + \underline{\underline{S}}^{(5)}(R_0\text{-}R_1)\underline{\underline{\Gamma}}^{(7)}_{\vec{R}_1\vec{R}_0}\Big]
\end{aligned} \tag{4.20}$$

where,

$$\begin{aligned}
\underline{\underline{\Gamma}}^{(5)}_{\vec{R}_1\vec{R}_0} &= \langle \vec{R}_1 \otimes \{\vec{R}_0\} | \underline{\underline{\mathcal{E}}}^{-\mathcal{P}_\pi} | \vec{R}_0 \otimes \{\vec{R}_0\} \rangle \\
\underline{\underline{\Gamma}}^{(6)}_{\vec{R}_1\vec{R}_0} &= \langle \vec{R}_1 \otimes \{\vec{R}_1\} | \underline{\underline{\mathcal{E}}}^{-\mathcal{P}_\pi} | \vec{R}_0 \otimes \{\vec{R}_0\} \rangle \\
\underline{\underline{\Gamma}}^{(7)}_{\vec{R}_1\vec{R}_0} &= \langle \vec{R}_1 \otimes \{\vec{R}_0\vec{R}_1\} | \underline{\underline{\mathcal{E}}}^{-\mathcal{P}_\pi} | \vec{R}_0 \otimes \{\vec{R}_0\} \rangle
\end{aligned}$$

4.8 Application to the equi-atomic CuZn alloy.

As an application of the above methodology we shall study the electronic structure of the equi-atomic CuZn alloy. The reason for this choice is that a considerable body of earlier work on CuZn exists using a plethora of different techniques. As a means of trying out the usefulness of our methodology, this system will provide enough other results for comparison.

The earliest first-principles density functional based study of the electronic properties of disordered CuZn was the single-site coherent potential approximation work of Bansil *et.al.*(80). The authors had studied the complex bands of α-phase of CuZn using the Korringa-Kohn-Rostocker (KKR) method. They commented on the significant effects of charge transfer on the electronic structure.

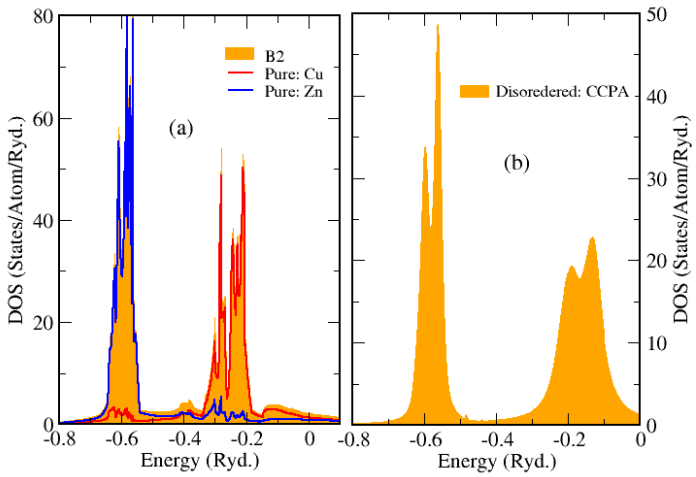

Figure 4.2: DOS - (left panel) Atom projected and total DOS for Cu,Zn in ordered B2 CuZn (right panel) total DOS for disordered bcc CuZn

Later, using the much more sophisticated *locally self-consistent Green function* (LSGF) approach based on the TB-LMTO technique Abrikosov *et.al.*(81) also studied CuZn alloys. The authors argued that earlier studies of the mixing enthalpies of CuZn using the standard CPA approaches (82),(83) showed significant discrepancy with experiment. Part of the discrepancy was assumed to be from neglect of charge transfer effects and part from the effects of short ranged ordering (SRO). Like our work, the main thrust of this technique, which was based on an earlier ideas of a locally self-consistent multiple scattering (LSMS) by Wang *et.al.*(84), was to go beyond the CPA and include the effects of the near environment of an atom in the solid. The LSMS gave an excellent theoretical estimate of the ordering energy in CuZn : 3.37 mRy/atom as compared to the experimental value of 3.5 mRy/atom.

Bruno *et.al.*(85) proposed a modification of the CPA taking into account the local field and showed that charge transfer effects can be taken into account accurately as compared to the O(N) methods just described. They applied their approach to the CuZn alloys.

We ourselves have applied the TB-LMTO-ASR technique to study CuZn (86). The idea is very similar to this work. The effect of the configuration fluctuations of the

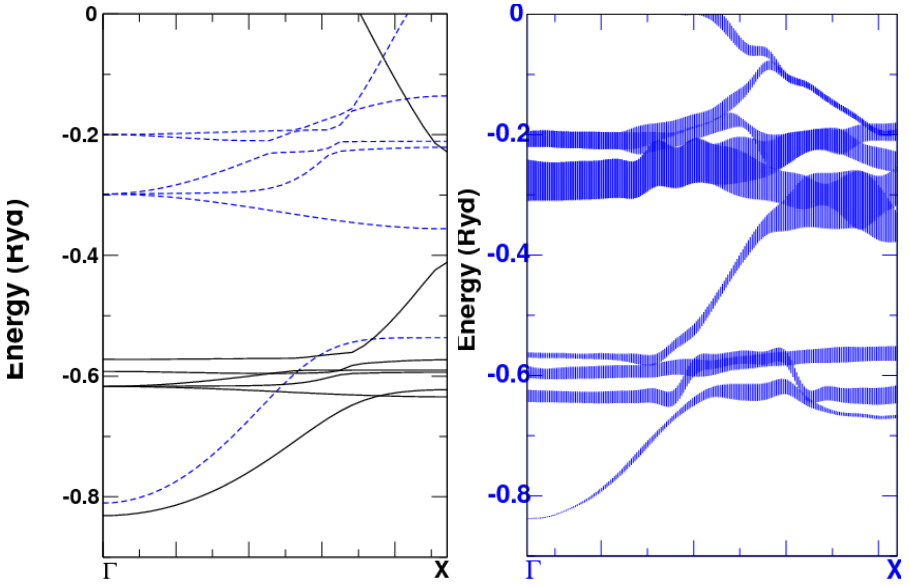

Figure 4.3: (left) Bands for Cu and Zn in a bcc lattice (right) Diffuse bands of disordered bcc CuZn alloy

environment of a site was captured through the recursion method. The effective medium was not 'self-consistent' in the sense of a mean-field theory. In this paper we have suggested a way of obtaining this self-consistent effective medium. For CuZn it would be interesting to address the effects of charge transfer and short-ranged ordering. In this application we shall address exactly these two points.

We have carried out the TB-LMTO-ASR calculations on CuZn with a lattice constant of 2.85 **r**A. The Cu and Zn potentials are self-consistently obtained via the LDA self-consistency loop. All reciprocal space integrals are done by using the generalized tetrahedron integration for disordered systems introduced by us earlier (87).

The left panel in the Fig.4.2 shows the atom projected densities of states for the pure Zn (blue lines) and Cu (red lines) in ordered B2 structure CuZn. This may be compared with disordered bcc 50-50 CuZn alloy in the right panel. We first note that in the ordered B2 alloy there is a considerable narrowing of the Zn as well as the Cu *d*-like bands. In the disordered alloy on the other hand, although disorder scattering introduces life-time effects which washes out the sharp structures seen in the ordered system, the resemblance to the pure metals is evident. This is a feature of split band alloys, where the d-bands of the constituents do not overlap and hybridize.

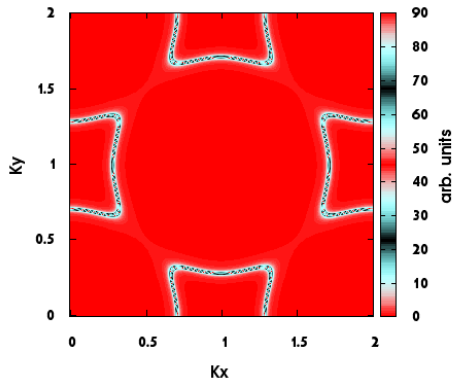

Figure 4.4: Fermi Surface - The (220) cross section of the Fermi surface for the 50-50 CuZn alloy

We have used the CCPA to obtain the complex bands from the spectral functions for the CuZn alloy. This is shown in Fig.4.3. In this figure compare the band structures of pure Cu and pure Zn metals in the same bcc lattice as the 50-50 alloy. We note that the *s*-like bands of Cu and Zn stretch from -0.8 Ry, while the *d*-like states of Zn and Cu, whose degeneracies are lifted by the cubic symmetry of the bcc lattice are more localized and reside in the neighbourhood of -0.6 Ry and between -0.3 to -0.2 Ry respectively. The complex bands of the solid clearly reflect the same band structure. However, the bands are slightly shifted and broadened because of the disorder scattering of Bloch states in the disordered alloy. The scattering lifetimes are maximum for the Cu *d*-like bands, less for the Zn *d*-like bands and minimum for the lower *s*-like bands. This is expected, since the delocalized *s*-like states straddle large volumes of the lattice space and are therefore less sensitive to the local configuration fluctuations of the substitutional alloy.

We comment here that the complex band structure very closely resembles that obtained through the TB-LMTO-ASR by us earlier (86). This is expected because the two approaches are very similar, differing only in the way the effect of the far environment is taken into account.

Recent development in the electron theory of alloys has suggested that the fine structure is a reflex of the flatness of the alloy Fermi surface. The fermi surface of a

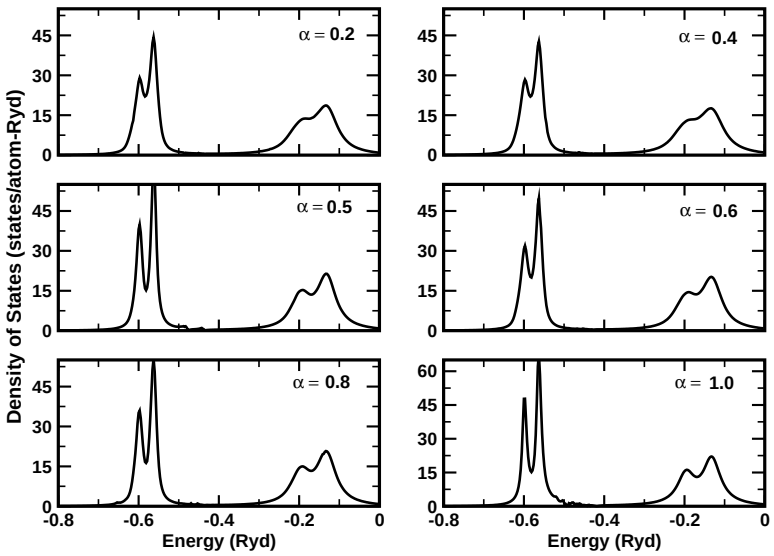

Figure 4.5: SRO-clustering - Densities of states with different degrees of SRO leading to clustering

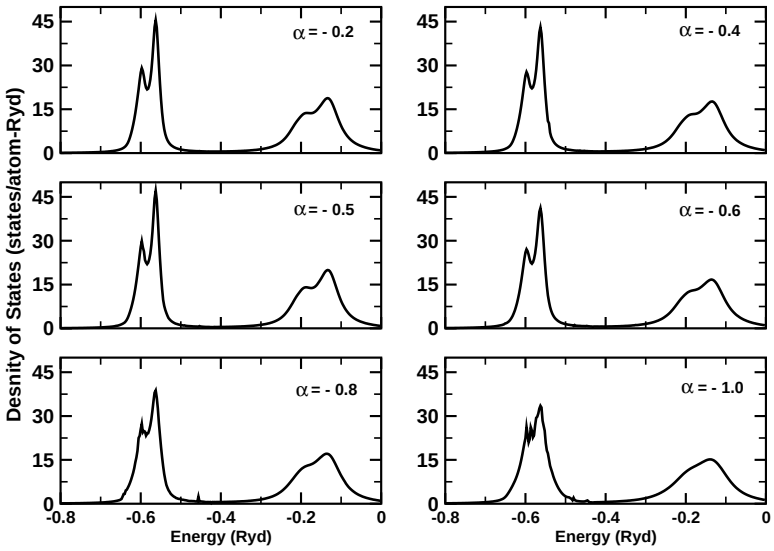

Figure 4.6: SRO-ordering - Densities of states with different degrees of SRO leading to ordering

random binary alloy is thought to be well defined when the interband energy distances are much larger than the energy uncertainty $\hbar/\tau$ introduced by disordered, or equivalently when the wave vector uncertainty δk is much smaller than the linear sizes of the Fermi surface that is the size of the bellies, necks or pockets that might exist on the Fermi surface. In Fig. 4.4, we have sketched a (220) cross section of the Fermi surface of random CuZn alloys in the extended zone scheme. The holes are plainly visible. The gap across the cubic zone boundary gives rise to the discontinuity in the Fermi surface between zones.

Let us now turn to the study of the effect of SRO, leading, on one hand, to ordering ($\alpha < 0$) and, on the other, to segregation ($\alpha > 0$). We shall look at Figs.4.5 and 4.6 for segregating and ordering respectively. The complex band structure (shown in Fig.4.3) indicates that the system is a *split band* alloy. The positions of the *d*-bands of Cu and Zn are well separated in energy below the fermi energy 0eV. This implies that the "electrons travel more easily between Cu or between Zn sites than between unlike ones" (65). So when the alloy orders and unlike sites sit next to each other, the overlap integral between the like sites decrease. This leads to a narrowing of the bands associated with Cu and Zn. A comparison between the top left and top right panels of Fig.4.2 clearly shows that the bands in the latter are narrower as compared to the former. This is the main effect of the onset of order. On the other hand, when the alloy is completely disordered, the bands gets broadened by disorder scattering and the sharp structure in the density of states are smoothed.

The left three panels of Fig.4.5 show the density of states with increasing positive α. Positive α indicates a clustering tendency. Comparing with Fig.4.2 we note that as clustering tendency increases the density of states begins to show the structures seen in the pure metals in both the split bands. For large positive α there is still residual long-ranged disorder. This causes smoothing of the bands with respect to the pure materials. For these large, positive α-s, we notice the development of the structure around -0.25 Ry.

The bottom three panels of Fig.4.6 show the density of states with increasing negative α which indicates increasing ordering tendency. On the bcc lattice at 50-50 composition we expect this ordering to favor a B2 structure. With increasing ordering tendency, both the split bands narrow and lose structure. The feature around -0.25

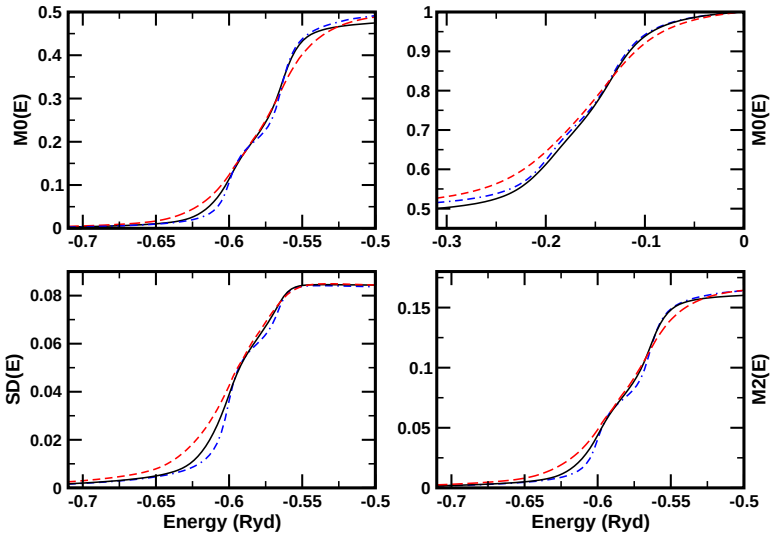

Figure 4.7: NOS - (top panels) The integrated density of states for the two bands of CuZn. (bottom) The variation and second moment of the density of states of the lower energy band. Black full curves refer to the case without SRO, red dashed curves refer to α =1 (clustering) and blue dashed-dotted curves to α=-1 (ordering).

Ry disappears. This band narrowing and suppression of the feature around -0.25 Ry is clearly seen in the ordered B2 alloy shown in Fig.4.2.

A more quantitative analysis of the effect of SRO on the shape of the density of states uses the moment functions :

$$M_n(E) = \int_{-\infty}^{E} dE' \ (E')^n \ n(E')$$

In particular one may use the integrated density of states $M_0(E)$ and the second moment and 'variation' of spectral distribution $M_2(E)$ and $SD(E) = M_2(E) - M_1^2(E)$. These are shown in Fig.4.7 for the case of no SRO, perfect clustering α=1 and ordering α=-1. $M_0(E)$ shows a left shift of spectral weight towards -0.6 Ry in the lower band as clustering tendency increases. In the upper band there is a spectral shift around -2.0 to -3.0 Ry range, which gives rise to the characteristic shoulder around those energies. For ordering $M_0(E)$ indicates a right shift of spectral weight towards -0.55 Ry. $SD(E)$ indicates a distribution of spectral weight away from the mean on clustering and a bunching of spectral weight towards the mean on ordering. The latter indicates a narrowing of the density of states. Use of moment functions quantifies the comparison of the changes in the shapes of the density of states with clustering or ordering.

4.9 Application to the body-centered cubic equi-atomic NiAl alloy

As an application of the new CCPA scheme, we shall choose a body-centered cubic alloy 50-50 NiAl. The relatively narrow Ni *d*-bands lie on the Al *sp*-bands and hybridize with them. At low temperatures this alloy orders into a B2 intermetallic phase which is a simple cubic lattice with two atoms per unit cell : an Al atom at position at the cube edge and a Ni atom at the cube center. This is a very stable structure that remains ordered until nearly the melting temperature. NiAl alloys are attaractive for many application due to their favourable oxidation, carburization and nitridation resistance; as well as their high thermal and electrical conductivity. They are currently used to make electronic metallizations in advanced semi-conductor heterostructures, surface catalysts and high current vacuum circuit breakers. Additionally, these alloys are attractive for aerospace structural applications due to their low density ($5.98\ g/cm^3$) and high melting temperatures. In the Fig. 4.8 we have plotted essentially the contour

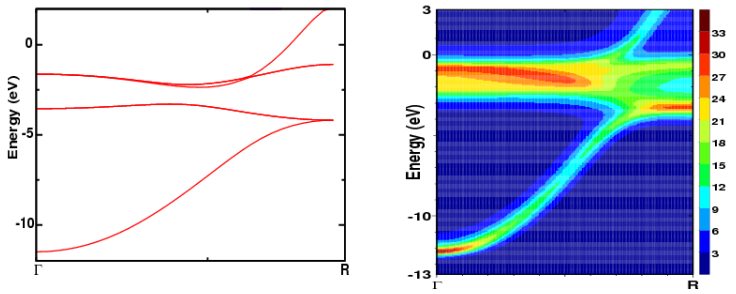

Figure 4.8: Spectral function - (left) Bands for ordered B2 of NiAl and (right) Diffuse bands of disordered NiAl alloy

diagram for the configuration averaged spectral functions $\ll A(\vec{k}, E) \gg$ for disordered NiAl also along the Γ to H direction. The peaks in the spectral function indicate the complex band centers and fitting Lorenzians to the peaks give us the disorder induced widths. The width of the *sp*-states are narrow, since these rather extended states which average out the local disordered scattering effects. The widths of the localized *d*-states are much wider. We also note that throughout the $\vec{k}$ range, there is very little asymmetry in the spectral function widths. A definition of Fermi surface of alloy can

be given in terms of bloch spectral functions $A_B(E;k)$, as the loci of the peaks of the Lorentzian-like bloch spectral function for a constant energy $E = E_F$ in reciprocal space. However, this is only valid if the bloch spectral function fits well to a Lorentzian sum, which is correct in the limit of small disorder. The intersection of the Fermi level with the band structure allows an approximate mapping of important cross sections of each Fermi surface. The Fermi surface is associated not only with the first zone but also with second, third and fourth zone of NiAl alloys in 4.9

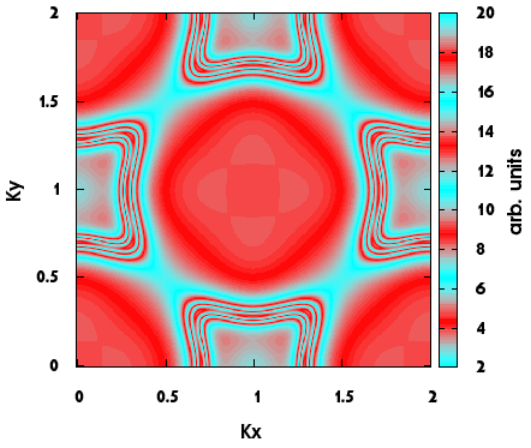

Figure 4.9: Fermi Surface - (220) cross section of the Fermi surface for random NiAl alloys

Comparison between the two panels indicate that other than disorder induced broadening, the basic band structure remains unaltered when the ordered B2 alloy is disordered. This is also reflected in the densities of states. Fig. 4.10 compares the densities of states for ordered B2 and disordered bcc NiAl alloys. The basic two peaked structure arising out of the Ni *d*-states, one around -0.25 Ry and another around -0.12 Ry is maintained when the alloy is disordered. The sharp structures seen in the ordered ally are smoothed out by disorder broadening. There is hardly any energy shift of the structures, indicating that there is hardly any extra charge transfer effects on disordering. An earlier first-principles density functional based study of the electronic properties of disordered CuAu and NiAl was the non-local coherent potential approximation

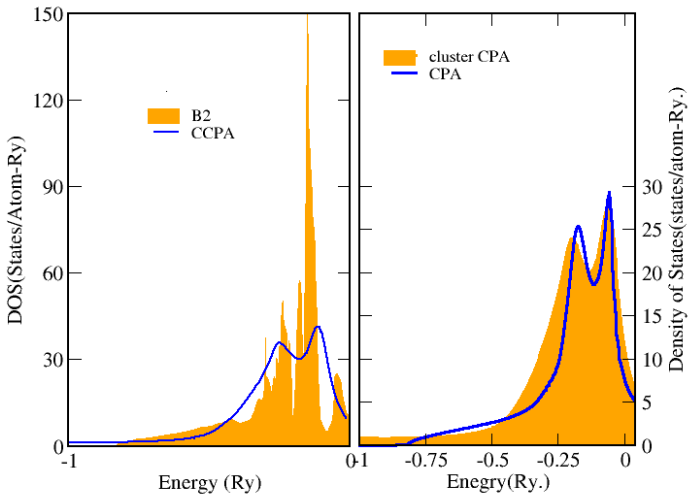

Figure 4.10: DOS - Density of states of NiAl: (left panel) ordered B2 with random CCPA and (right panel) random single site CPA with random CCPA

(NL-CPA) work of Biava *et.al.*(88). The authors had studied the local environment effects on NiAl using the Korringa-Kohn-Rostocker (KKR) method. We ourselves had studied NiAl using augmented space recursion. Our CCPA results closely resemble the results of both these works. This further confirms our earlier assertion(91) that the results of the other four most successful CPA generalizations : NL-CPA(64, 65, 88) , ICPA(61), SQS(63) and ASR(74, 75) should closely resemble each other. This work confirms the same for the CCPA.

In the left panel of Fig 4.11 we show the effect of short-range ordering or clustering on the density of states. A more quantitative analysis of the effect of SRO on the shape of the density of states uses the moment functions(76) :

$$M_n(E) = \int_{-\infty}^{E} dE' \ (E')^n \ n(E')$$

and the three shape measures : standard deviation σ, sknewness μ and kurtosis κ :

$$\begin{aligned} \overline{E} &= \int_{-\infty}^{E_F} dE \ E \ n(E) = M_1(E_F) = \widehat{M_1} \\ \sigma^2 &= \int_{-\infty}^{E_F} dE \ (E - \overline{E})^2 \ n(E) = \widehat{M_2} - \widehat{M_1^2} \ \left(2 - \widehat{M_0}\right) \end{aligned}$$

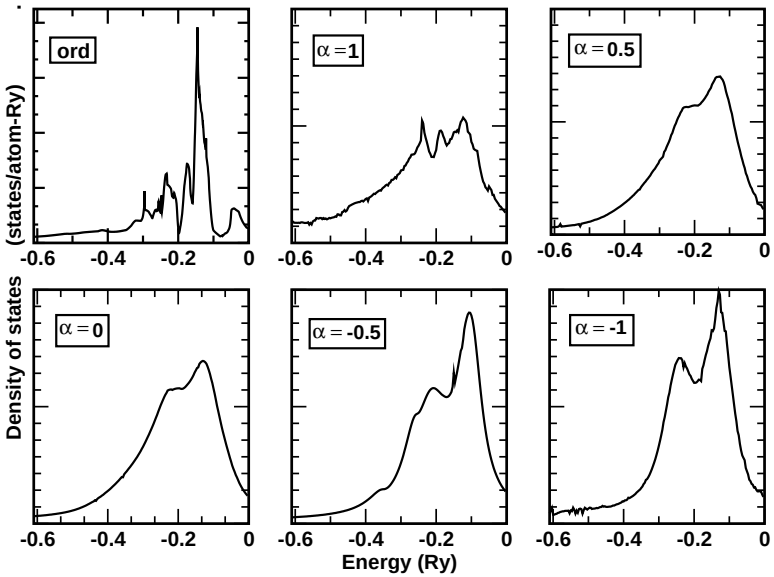

Figure 4.11: SRO - Densities of states for NiAl (top, left) ordered B2 (top, centre and right) with different degrees of SRO leading to clustering (bottom, left) fully disordered and (bottom, centre and right) with different degrees of SRO leading to ordering

α	σ^2	μ	κ
-1.0	2.3763	0.4325	-2.7111
0.0	2.4495	0.4320	-2.8110
1.0	3.5463	0.4099	-2.8304

Table I. The shape parameters for NiAl with Warren-Cowley parameters $\alpha = 0,\pm 1$

$$\mu = \frac{1}{\sigma^3}\left\{\int dE\ (E-\overline{E})^3\ n(E)\right\} = \frac{1}{\sigma^3}\left\{\widehat{M}_3 - 3\widehat{M}_2\widehat{M}_1 + \widehat{M}_1^3\ \left(3-\widehat{M}_0\right)\right\}$$

$$\kappa = \frac{1}{\sigma^4}\left\{\int_{-\infty}^{E_F} dE\ \left[(E-\overline{E})^4 - 3\sigma^4\right]\ n(E)\right\} = \frac{1}{\sigma^4}\left\{\widehat{M}_4 - 4\widehat{M}_3\widehat{M}_1 + \ldots \right.$$
$$\left. \ldots 6\widehat{M}_2\widehat{M}_1^2 - \widehat{M}_1^4\ \left(4-\widehat{M}_0\right) - 3\sigma^4\ \widehat{M}_0\right\}$$

The standard deviation σ measures how spread the shape is around the mean. If skewness $\mu < 0$ the shape is skewed to the left of the mean, while $\mu > 0$ indicates that the shape is skewed to its right. Kurtosis $\kappa > 0$ shows that the shape is more peaked than a Gaussian, while $\kappa < 0$ shows that is it flatter.

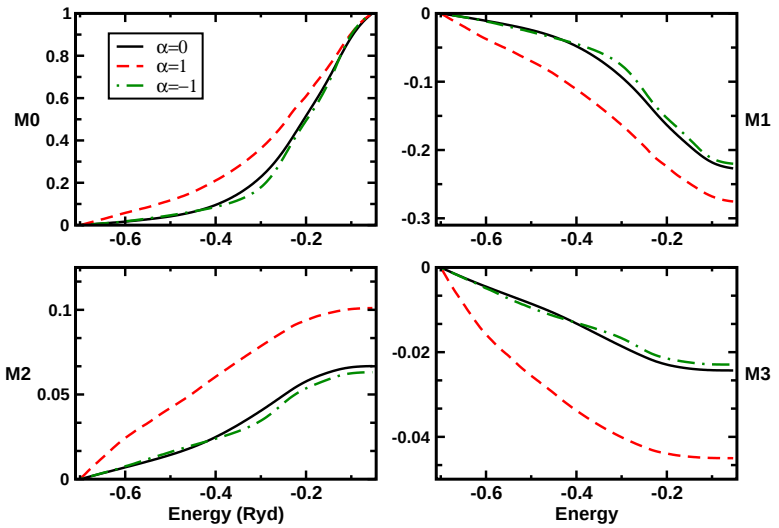

Figure 4.12: Moments - Comparison of the moment functions $M^p(E)$ $p = 0 \ldots 3$ for the densities without SRO and with $\alpha = 1$ and -1.

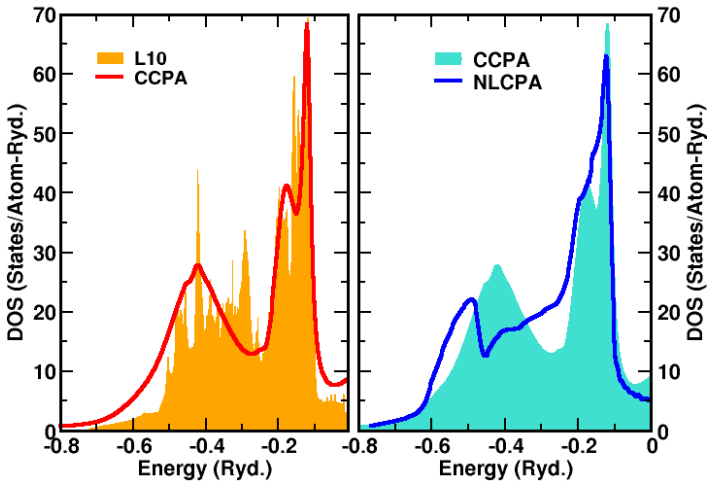

Figure 4.13: DOS - (Color Online) The density of states for fcc CuAu in left panel ordered $L1_0$ with random CCPA and right panel random CCPA with random NLCPA.

The first four moment functions for the cases with extreme SRO Warren-Cowley parameters $\alpha = \pm 1$ and that with no SRO are shown for comparison in the right panel of Fig. 4.12. The corresponding shape parameters are shown in Table 4.9.

As α increases from 0 to its maximum value 1, the Ni and Al atoms tend to segregate and the density of states simply begins to resemble the direct sum of the density of states of Al and Ni. The moments $M_0(E)$ and $M_1(E)$ both indicate that there is a shift of weight towards more negative energies. $M_2(E)$ being larger indicates that the spread of the DOS over the spectrum increases. In agreement with the above, the standard deviation increases, indicating that the spectral spread is greater around the mean. The skewness is less positive, indicating spectral weight shift to the left (to more negative values). Finally the kurtosis becomes more negative, showing that the shape becomes flatter. These statements are evident from the Fig. 4.12.

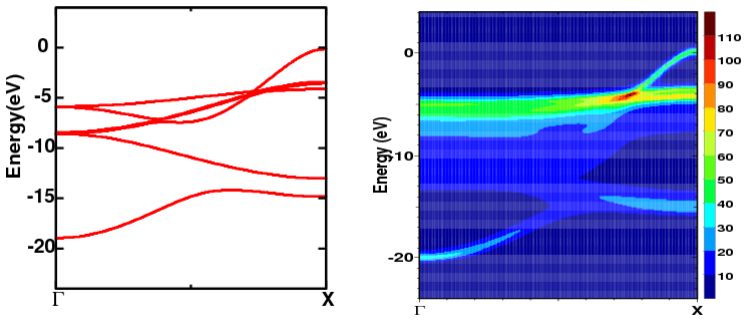

Figure 4.14: Spectral Function - (left) Bands for ordered $L1_0$ and (right) Bloch spectral function of CuAu alloy with 50-50 concentration

On the other hand, as the Warren-Cowley parameter increases towards its negative maximum $\alpha = -1$, the DOS begins to resemble the ordered alloy. The spectral weight shifts towards the right and the spread decreases. Decrease in spread is confirmed by the decrease in the standard deviation and the peakiness from from the fact that the kurtosis becomes less negative. In this case there is little change in the skewness parameter.

The state $\alpha = -1$ has maximum SRO, but no long-ranged order. Thus although its DOS begins to resemble the ordered alloy, there is still residual disorder scattering induced broadening. There are there (2-fold degenerate) bands that cross the Fermi

	σ^2	μ	κ
Ordered	9.2920	0.3054	-2.9065
NLCPA	8.2217	0.3071	-2.9055
CCPA	9.2232	0.3012	-2.9091

Table II. The shape parameters for CuAu ordered,CPA and CCPA.

energy and so the resulting Fermi surface is reflected in the contour plot of Fermi surface in Fig.4.15. The features that are of particular interest here are 'tube like' sections that occur along (220) cross section in the reciprocal space. They are generated by states on the uppermost band and partially by states on the next-uppermost band.

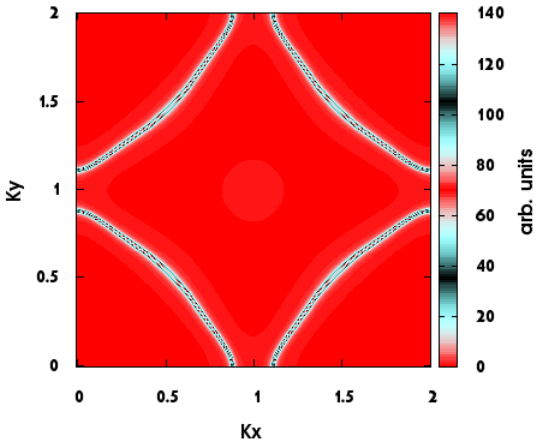

Figure 4.15: Fermi Surface - Fermi surface along (220) cross section of CuAu alloys for 50-50 composition

4.10 Application to the face-centered cubic equi-atomic CuAu alloy

The left panel of Fig 4.14 shows the band structure of the ordered L_{10} CuAu alloy along the direction Γ to X . The overlapping d bands of Cu and Au straddle the s-band of the

alloy. Unlike our earlier study of CuZn(92), where the d bands of Cu and Zn do not overlap and we have a split-band alloy, here the d bands of Cu and Au overlap. The overall structure is maintained in the spectral functions of the disordered alloy. The resulting complex bands are shown in the right panel of Fig. 4.14. These overlapping bands, disorder broadened, straddle the entire energy range [-7.5 eV,-1.5 eV]

It is important to see the shape of farmi surface in order to study of short-range order effects in CuAu alloys(90). The fermi surface Brillouin zone boundary construction introduced by Sato and Toth(89), a symmetrical variation of the 110 diameter of the fermi surface must be assumed with respect to the equiatomic composition. The fermi surface contour plot of CuAu alloys for 50-50 centration is shown in Fig. 4.15. In CuAU alloys the fermi surface of Cu and Au have the same shape.

In the Fig. 4.13 compares the DOS for the ordered L_{10} CuAu and the fcc based disordered CuAu within the non-local CPA (NLCPA) and CCPA approximations. We have also compared the moment functions in Fig.4.16. The CCPA reproduces the ordered peak at -0.2Ry more faithfully than the NLCPA. The CCPA shows clearly the energy split between the d-like structures around [-0,5,-0.3] and the d-like structures around [-0.2,-0.1], which can be interpreted as the disorder broadened bonding and anti-bonding states between Cu and Au. On the other hand, NLCPA being also muti site approximation (65) via reciprocal space cannot reflect this. As a result, in the CCPA there is a shift of spectral weights towards the lower energies, a larger spread in spectral weight as well as smaller skewness, as shown in the moment function comparisons shown in the right panel of Fig. 4.13 and in the Table 4.9. The positive skewness parameter indicates that the spectral weights are higher on the right side of the mean. The NLCPA has the maximum skewness, while the CCPA which better compares with the spectral distribution of the ordered structure with spectral weight balances to the left has the minimum. Negative kurtosis for all DOS shows that they are flatter than a Gaussian, with the CCPA having the flattest shape.

4.11 Concluding Remarks

We have carried forward the CCPA proposed in an earlier work(92) and applied it to two alloys,specially chosen such that one involves short-ranged ordering and the other a split-band case. We wished to benchmark our results against earlier work. We have

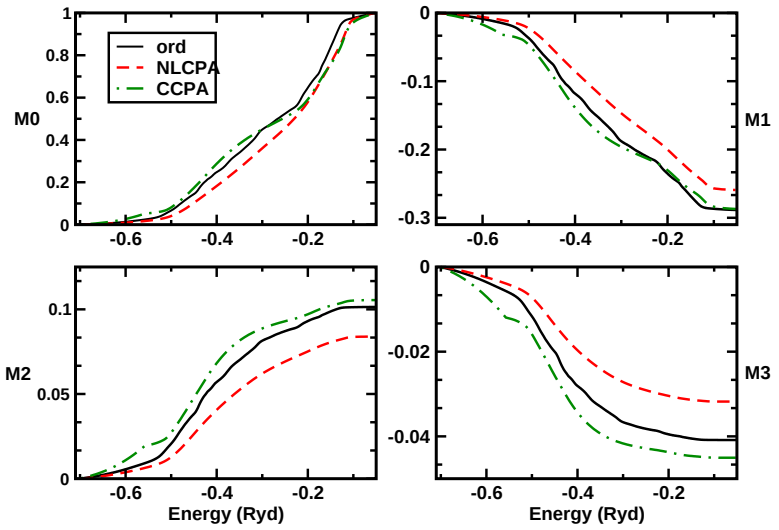

Figure 4.16: Moments - Comparison of the moment functions $M^p(E)$ $p = 0 \ldots 3$ for the densities of states for 50-50 CuAu ordered L10, the NLCPA disordered and CCPA disirdered.

shown that for CuZn, NiAl and CuAu, our CCPA results compare very favourably with the four successful generalizations of the CPA, three of which (ICPA, TCA and ASR) are all based on the augmented space formalism. We expect our CCPA to win over the other methods (in the sense of easier computability) when we deal with complex compounds with more than one interpenetrating lattices and different degrees of disorder in each sub-lattice (as in partially disordered Heusler alloys(93)). Now that we are confident about the accuracy and applicability of our CCPA, our future aim will be its application to such complex compounds and ones with off-stoichiometric compositions.

Chapter 5

Order-Disorder Phase Transition of FeCo alloys

5.1 Introduction

FeCo alloys posses a unique combination of magnetic and mechanical properties, which make them indispensable as materials for advanced motors and electrical generators in aviation and special power applications (94). In particular, they are characterized by exceptionally high saturation magnetization, low coercivity and high Curie temperature ($> 820^0$C). The elevated Curie temperatures of the alloys makes them especially attractive for various high temperature applications. However, at around 730^0C, the disordered body-centered cubic Fe_xCo_{1-x} alloys undergo an ordering phase transition into the B2 structure (space group Pm3m) in the composition range $\sim 0.3 \leq x \leq 0.7$ (95, 96, 97, 98), which significantly affects their magnetic and mechanical properties.

There exist numerous investigations of phase equilibria in the Fe-Co system; in particular, the order-disorder phase transition(96). This has been observed for the first time by Seehra and Silinsky (95), who measured the electrical resistivity in FeCo alloys and found near $T_c = 1006$K a change in the slope of the temperature dependent resistivity curve indicating an order-disorder phase transition. Oyedele and Collins (96) investigated the order-disorder phase transition in FeCo alloys by the neutron-powder diffraction techniques for the composition range of 30 to 70 at.% of Co. Montano and Seehra (97) used Mössbauer spectroscopy to identify the order-disorder phase transition. They found the transition temperature about $T_c = 1006$K for the equiatomic

composition. Ohnuma *et al.*(99) investigated the phase equilibria in the Fe-Co system both experimentally, using transmission electron microscopy for thin-film samples and X-ray and electron diffractometer for the bulk system, and theoretically by the CALPHAD method, which was modified by considering chemical interactions dependent on the magnetic state.

The coupling of magnetism and atomic short-range order (SRO) in Fe-Co, up to 25 at.% of Co, have been investigated experimentally by Pierron-Bohnes *et al.*(100, 101, 102) using neutron diffuse scattering and nuclear magnetic resonance techniques. For the first time, the influence of the magnetism on the atomic SRO was clearly evident from an abrupt change in the temperature dependence of the local order at the Curie temperature. The theoretical analysis of the coupling between the magnetic and chemical degrees of freedom based on the mean-field approximation of a combined Ising-Heisenberg Hamiltonian was done by Pierron-Bohnes *et al.*(100). They have shown that the magnetic contribution to the effective interactions should be roughly proportional to the square of the magnetization.

The FeCo system has been theoretically studied by using a wide variety of phenomenological methods as well as with first principles techniques. In an early phenomenological treatment of the A2-B2 transition, Beinenstock and Lewis (103) employed a low temperature expansion of the Ising model to calculate a phase diagram with nonmagnetic components. This phenomenological approach resulted in a B2 phase field symmetric about the 50-50 composition and somewhat narrower than that found experimentally. Real space renormalization group was used by Racz and Collins (104) to study the slight asymmetry in the A2-B2 phase boundary. In the context of a nonmagnetic nearest-neighbor Ising model, they found that a small three-body interaction could account for the experimentally observed asymmetry.

The coupling of magnetism and atomic short-range order (SRO) in Fe-Co, up to 25 at.% of Co, have been investigated experimentally by Pierron-Bohnes *et al.*(100, 101, 102) using neutron diffuse scattering and nuclear magnetic resonance techniques. For the first time, the influence of the magnetism on the atomic SRO was clearly evident from an abrupt change in the temperature dependence of the local order at the Curie temperature. The theoretical analysis of the coupling between the magnetic and chemical degrees of freedom based on the mean-field approximation of a combined Ising-Heisenberg Hamiltonian was done by Pierron-Bohnes *et al.*(100). They have shown that

the magnetic contribution to the effective interactions should be roughly proportional to the square of the magnetization.

The FeCo system has been theoretically studied by using a wide variety of phenomenological methods as well as with first principles techniques. In an early phenomenological treatment of the A2-B2 transition, Beinenstock and Lewis (103) employed a low temperature expansion of the Ising model to calculate a phase diagram with nonmagnetic components. This phenomenological approach resulted in a B2 phase field symmetric about the 50-50 composition and somewhat narrower than that found experimentally. Real space renormalization group was used by Racz and Collins (104) to study the slight asymmetry in the A2-B2 phase boundary. In the context of a nonmagnetic nearest-neighbor Ising model, they found that a small three-body interaction could account for the experimentally observed asymmetry.

The coupling of magnetism and atomic short-range order (SRO) in Fe-Co, up to 25 at.% of Co, have been investigated experimentally by Pierron-Bohnes *et al.*(100, 101, 102) using neutron diffuse scattering and nuclear magnetic resonance techniques. For the first time, the influence of the magnetism on the atomic SRO was clearly evident from an abrupt change in the temperature dependence of the local order at the Curie temperature. The theoretical analysis of the coupling between the magnetic and chemical degrees of freedom based on the mean-field approximation of a combined Ising-Heisenberg Hamiltonian was done by Pierron-Bohnes *et al.*(100). They have shown that the magnetic contribution to the effective interactions should be roughly proportional to the square of the magnetization.

The FeCo system has been theoretically studied by using a wide variety of phenomenological methods as well as with first principles techniques. In an early phenomenological treatment of the A2-B2 transition, Beinenstock and Lewis (103) employed a low temperature expansion of the Ising model to calculate a phase diagram with nonmagnetic components. This phenomenological approach resulted in a B2 phase field symmetric about the 50-50 composition and somewhat narrower than that found experimentally. Real space renormalization group was used by Racz and Collins (104) to study the slight asymmetry in the A2-B2 phase boundary. In the context of a nonmagnetic nearest-neighbor Ising model, they found that a small three-body interaction could account for the experimentally observed asymmetry.

5.2 Methodology

5.2.1 Effective cluster interactions for finite magnetization

The PDLM state, which represents the partially ordered magnetic state for a given global magnetization m, can be introduced as a straightforward generalization of disordered local moment (DLM)(120, 121) model. The magnetic binary Fe_xCo_{1-x} alloy is described in terms of a four component alloy $Fe^{\uparrow}_{ux}Fe^{\downarrow}_{dx}Co^{\uparrow}_{u(1-x)}Co^{\downarrow}_{d(1-x)}$, where $u = (1+m)/2$ and $d = (1-m)/2$, respectively. Fe and Co atoms with up and down spin orientation are distributed randomly relative to one another on the underlying lattice. In the adiabatic approximation adopted in this paper, the dynamics of the spins and its coupling with other types of thermal excitations has been neglected. One can see, that this model gives the ferromagnetic state for $m = 1$ and the DLM state for $m = 0$.

Using the fact that thermally induced fluctuations of the local magnetic moment orientations are much faster than the atom-vacancy exchanges associated with equilibrating the atomic short-range order, one can define "spin-averaged" effective pair interactions (EPI's) for a binary Fe_xCo_{1-x} alloy in the PDLM states as(122)

$$< V_{ij}^{\mathrm{FeCo}} >= \frac{1}{16} \sum_{\sigma_1,\sigma_2,\sigma_3,\sigma_4} p_{\sigma_1} p_{\sigma_2} p_{\sigma_3} p_{\sigma_4} \bar{V}_{ij}^{\mathrm{Fe}^{\sigma_1},\mathrm{Fe}^{\sigma_2},\mathrm{Co}^{\sigma_3},\mathrm{Co}^{\sigma_4}}, \tag{5.1}$$

The PDLM state, which represents the partially ordered magnetic state for a given global magnetization m, can be introduced as a straightforward generalization of disordered local moment (DLM)(120, 121) model. The magnetic binary Fe_xCo_{1-x} alloy is described in terms of a four component alloy $Fe^{\uparrow}_{ux}Fe^{\downarrow}_{dx}Co^{\uparrow}_{u(1-x)}Co^{\downarrow}_{d(1-x)}$, where $u = (1+m)/2$ and $d = (1-m)/2$, respectively. Fe and Co atoms with up and down spin orientation are distributed randomly relative to one another on the underlying lattice. In the adiabatic approximation adopted in this paper, the dynamics of the spins and its coupling with other types of thermal excitations has been neglected. One can see, that this model gives the ferromagnetic state for $m = 1$ and the DLM state for $m = 0$.

Using the fact that thermally induced fluctuations of the local magnetic moment orientations are much faster than the atom-vacancy exchanges associated with equilibrating the atomic short-range order, one can define "spin-averaged" effective pair interactions (EPI's) for a binary Fe_xCo_{1-x} alloy in the PDLM states as(122)

$$< V_{ij}^{\mathrm{FeCo}} >= \frac{1}{16} \sum_{\sigma_1,\sigma_2,\sigma_3,\sigma_4} p_{\sigma_1} p_{\sigma_2} p_{\sigma_3} p_{\sigma_4} \bar{V}_{ij}^{\mathrm{Fe}^{\sigma_1},\mathrm{Fe}^{\sigma_2},\mathrm{Co}^{\sigma_3},\mathrm{Co}^{\sigma_4}}, \tag{5.2}$$

5.2.2 Details of the first principles calculations

We have used three related first-principles techniques for our calculations:

(i) the Korringa-Kohn-Rostoker Green function method in the atomic sphere approximation (KKR-ASA)(124, 125). This was used for the calculation of the densities of states and magnetic moments of the alloys at different compositions ;

(ii) the locally self-consistent Green's function (LSGF) method (126, 127) based on the KKR-ASA method for the determination of the on-site and inter-site screening constants needed for the electrostatic part of the screened generalizied purturbation method (SGPM) effective pair interactions ; and

(iii) the exact muffin-tin orbital (EMTO) method within the full charge density formalism(128) for the total energy and cluster interaction calculations.

Randomness has been treated using the coherent potential approximation (CPA) (17, 125, 126, 129): the KKR-ASA-CPA and the EMTO-CPA. The local density approximation (LDA) (130) has been used for the exchange-correlation potential.

The KKR-ASA Green function and LSGF methods have been used to determine the screening constants which enter the DFT-CPA formalism in the single-site approximation (in the so-called "isomorphous" CPA model). In this formalism, the on-site screened electrostatic potential V_{scr}^i and energy E_{scr}^i are determined as suggested by Ruban(30) and Ruban *et al.*(31):

$$\begin{aligned} V_{\mathrm{scr}}^i &= -e^2 \alpha_{\mathrm{scr}} \frac{q_i}{S} \\ E_{\mathrm{scr}}^i &= -e^2 \frac{1}{2} \alpha_{\mathrm{scr}} \beta_{\mathrm{scr}} \frac{q_i^2}{S}. \end{aligned} \tag{5.3}$$

Here, q_i is the net charge of the atomic sphere of the ith alloy component, S the Wigner-Seitz radius, α_{scr} and β_{scr} the on-site screening constants. Their values, which are $\alpha_{\mathrm{scr}} = 0.81, 0.84, 0.88$ and $\beta_{\mathrm{scr}} = 1.15, 1.17, 1.18$, have been determined from the

corresponding supercell LSGF calculations of random $Fe_{30}Co_{70}$, $Fe_{50}Co_{50}$ and $Fe_{70}Co_{30}$ alloys, respectively.

The screening charge has also been used to determine the inter-site screening constants, $\alpha_{\rm scr}(R)$, needed in the calculations of the electrostatic part of the SGPM effective pair interactions (30, 131), the intersite screened Coulomb interactions for the i and j sites, which in the case of a binary A-B alloy can be defined as

$$V_{ij}^{\rm scr} \;=\; e^2\alpha_{\rm scr}(\mathbf{R}_{ij})\frac{q_{\rm eff}^2}{S}, \tag{5.4}$$

where $q_{\rm eff} = q_A - q_B$ is the effective charge transfer in the case of a binary alloy and $\mathbf{R}_{ij}$ is the vector connecting sites i and j. The whole SGPM interaction is then

$$V_{ij}^{(2)} = V_{ij}^{\rm one-el} + V_{ij}^{\rm scr}, \tag{5.5}$$

where $V_{ij}^{(2)}$ is the SGPM interaction at the ith coordination shell and $V_{ij}^{\rm one-el}$ the one electron contribution to the SGPM interaction.

Experimental lattice parameters (98) have been used in the first-principles calculations of the electronic structure and effective interactions of Fe_xCo_{1-x} alloys. The Monkhorst-Pack grid(132) with subdivisions along each reciprocal lattice vector 31×31×31 has been used for integration over the Brillouin zone in the LDA self-consistent and SGPM calculations.

5.3 Results and discussion

5.3.1 Electronic structure and magnetic properties of Fe-Co alloy

The electronic structure and magnetic properties of Fe-Co alloys have been calculated previously by MacLaren *et al.*(133) by the KKR-CPA method. In this paper we use a similar Green's function KKR-ASA-CPA method (124, 125) for the calculations of the electron density of states (DOS) and magnetic moments. The experimental(98) lattice spacing varying with composition from a=2.835 **r**A to 2.863 **r**A has been used in our LDA self-consistent calculations.

In Fig. 5.1 we show the electronic density of states (DOS) of pure bcc Fe and Co as well as B2-ordered FeCo alloy calculated for the same lattice parameter, a=2.86 **r**A. The majority bands of pure Fe and Co are shifted relative each other, which is a consequence of the fact that this band is filled in Co but unoccupied to some degree

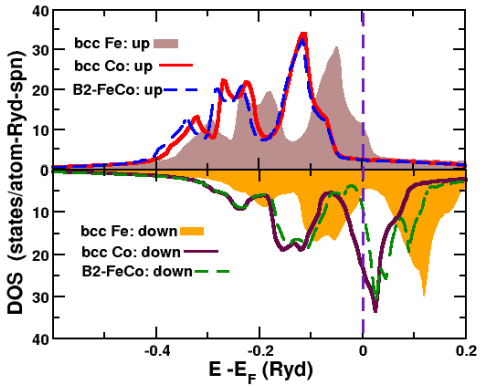

Figure 5.1: DOS - Density of states of bcc Fe, Co, and ordered B2-FeCo alloy

in Fe. The completely filled majority d-band in Co becomes inert or non-bonding and moves down with energy closer to the bottom of the valence band. There is also a substantial difference in the position of the minority band of Co and Fe, which is due to the difference in the number of the occupied states in this band.

What may however seem a bit unusual is the fact that the position and the form of the majority and minority bands of the ordered B2-FeCo almost coincide with those of bcc Co almost up to the Fermi energy. Only approximately 0.05 eV below the Fermi energy, the minority band of FeCo becomes different from that of Co by forming a an additional valley and redistributing the states above the Fermi energy. To explain the electronic structure of the B2-FeCo, it is useful to see what happens with electronic states at the local level, inside atomic spheres of Fe and Co.

In Fig. 5.2a we show the local DOS of Co and Fe atoms in the ordered B2-FeCo alloy. The local DOS of the majority Fe and Co states are practically the same. The difference in the minority DOS of Fe and Co is more pronounced, although they still have a similar form and position up to the Fermi energy. Such a strong similarity of the local Fe and Co bands can be understood, in its turn, in terms of the average bond model, proposed by Ruban *et al.*(134).

Let us note first that the B2 structure is quite special in respect that every Fe atom is completely surrounded by Co atoms at the first coordination shell and vice versa. In

this case, the Fe and Co nearest neighbors form a common *bond* between themselves due to the strong hybridization of the d-states. Since the d-states are quite localized, the influence of more distant coordination shells on the electronic structure is small, and thus the DOS of the ordered alloy is vey similar to that of pure metals, as has been demonstrated by Ruban *et al.*(134) for the case of non-magnetic 4d-metal alloys. The position of majority and minority states in the B2-FeCo can be then explained by the shift of the majority d-band of FeCo due to its complete filling and the consequent hybridization of the minority band with the majority one. Such a coherent behaviour

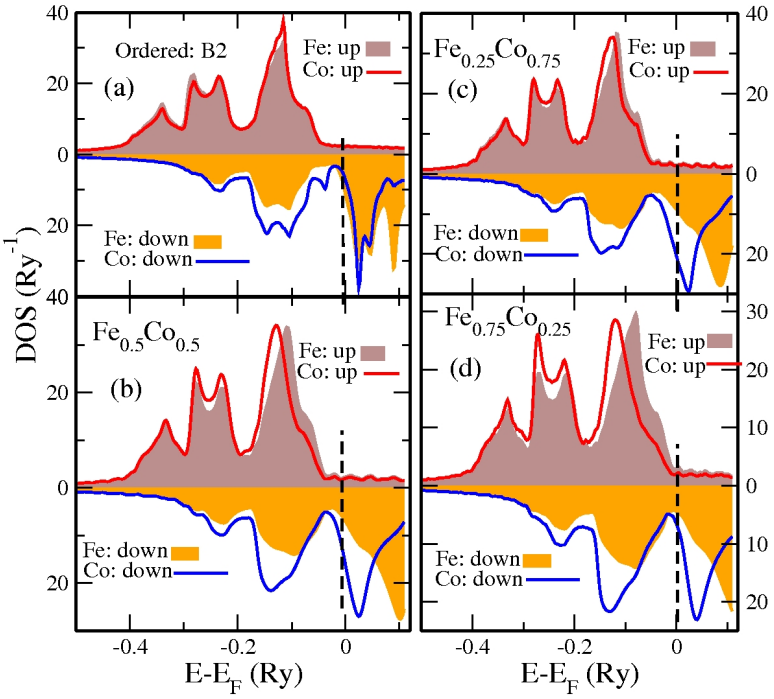

Figure 5.2: DOS - DOS of Fe and Co in ordered-B2 and random alloys

of the local DOS of Fe and Co appears to be disturbed by the randomness in random alloys, which can be clearly see in Fig. 5.2b where we present the local DOS of random $Fe_{0.5}Co_{0.5}$ alloy. The positions of the peaks of the local DOS of Fe and Co atoms are shifted relative to each other, which is a manifestation of the fact the they have on average equal number of Fe and Co atoms at the first coordination shell. In particular, the minority DOS of Co strongly increases at the Fermi energy, as it should be when Co atoms has Co nearest neighbors at the fist coordinations shell (see the DOS of pure Co

in the bcc structure in Fig. 5.1). This makes such an atomic configuration unfavorable compared to the ordered B2 structure and this is the main source origin of the ordering behaviour of Fe-Co alloys.

Now, it is easy to understand the reason for the changes of the DOS with variations of the composition of random alloys, which is shown in Fig. 5.2c and d for $Fe_{0.25}Co_{0.75}$ and $Fe_{0.75}Co_{0.25}$ alloys, respectively. In the case of $Fe_{0.25}Co_{0.75}$ alloy (Fig. 5.2c), the average number of Fe atoms surrounded each Fe atom decreases, and the local DOS of Fe mainly follows that of Co, especially in the case of the majority band. At the same time, the average number of Co atoms surrounded each Co atom increases, and this again leads to the increase of the Co minority DOS at the Fermi energy. Vice versa, in the case of the $Fe_{0.75}Co_{0.25}$ alloy, the effective number Fe atoms at the first coordination shell of increases thereby pushing the Fe majority band to the Fermi energy as in pure bcc Fe ((see Fig. 5.1 for Fe). At the same time, Co atoms become surrounded mostly by Fe atoms and this makes possible to rearrange their minority band in a way to have a valley at the Fermi energy similar to the case of the B2 phase. As disscussed in Richter

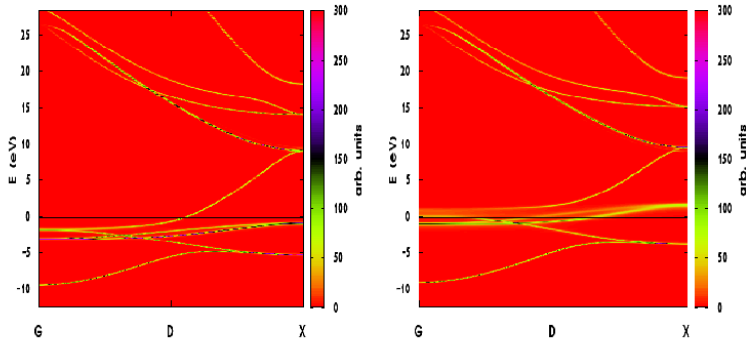

Figure 5.3: Spectral Function - Bloch spectral function of random $Fe_{0.75}Co_{0.25}$ alloys. Left panel for up spin and right panel for the down spin

et al.(135), the different magnetitudes of the individual self-energy components cause an anisotropic broadening of the states in the Brillouin zone. This can be seen best in the Bloch spectral function. For ordered systems, at a given wavevector K, it id defined as the set of delta functions at the energy eigenvalues. In the disordered alloy the peaks

are broadened due to the lack of translational invariance, indicating the finite lifetime of initial Bloch states. The bloch spectral function is plotted in Fig.5.3 for $\Gamma - X$ direction of boths spin. We see the spectral lines are more broadened for down spin than for up spin states. We have also calculated concentration variation of the Fermi surface of random $Fe_{1-x}Co_x$ alloys for boths spin-up and spin-down by using the fixing the energy at Fermi lavel of Block spectral function $B_f(E_f; K)$. The Fermi surface cross section is shown in Fig.5.4 along (220) cross section. A single energy 'band' crosses the Fermi level, as we see in the Bloch spectral function for spin-up, which is clearly reflected in fermi surface and the remains unchanged in the whole concentration range. The concentration effects are only evident in the spin-down bands and the reflection of concentration effects is obvious in the spin-down Fermi surface in Fig. 5.4, which is smeared out due to the effect of alloy disorder.

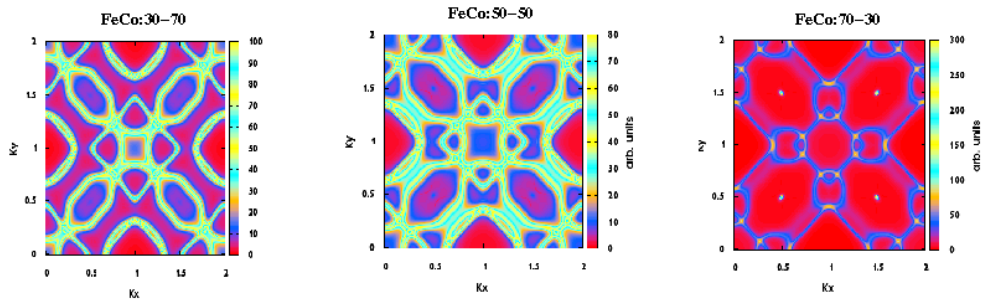

Figure 5.4: Fermi Surface - Concentration variation of Fermi surface for spin-down along (220) cross section of random $Fe_{x-1}Co_x$ alloys.

The concentration dependence of the average magnetic moment of Fe-Co alloys exhibit the Slater-Pauling behavior and it was discussed in details by MacLaren *et al.*(133). In Fig. 5.5 we compare our results for the average and local magnetic moments in Fe-Co random alloys with the first-principles calculations by MacLaren *et al.*(133) and experimental data (137). One can see that our results follow the same trend as MacLaren *et al.*(133), but closer to the experimental data. The difference arises due to the use of different lattice spacings, since we have used experimental data. Our calculated magnetic moments a bit lower than the experimental data. The reason for the this discrepancy is most probably related to atomic short range order effects neglected in our single-site CPA calculations, and which may exist and be pronounced

in the experimental samples. Let us also note, that Co-rich FeCo alloys are not a good candidates for neutron experiments (140), first, because of their higher neutron absorption cross-section and also because of their high magnetic anisotropy. FeCo alloys exhibit the weakest environment effects compared to other Fe-based alloys. In addition Co has small but significant orbital magnetism that makes the system more complicated.

According to the neutron-diffraction studies (137), the complete occupation of the majority band of Fe by the addition of Co leads to a maximum mean magnetic moment 2.45 μ_B per atom at the composition c_{Co}=0.3. Fig. 5.5 shows that our the KKR-CPA calculations reproduce well the experimental trend of magnetization with composition. One can notice quite a peculiar behaviour of the local magnetic moments. The local moment on the Co atom remains nearly the same in the whole concentration range. At the same time, the local magnetic moment of Fe increases with increasing Co concentration from 2.2μ_B in bcc Fe to the unusually large magnitude of about 2.62 μ_B at c_{Co}=0.5 and then remains almost constant. The addition of Co to Fe leads to a redistribution of the electrons such that the total system becomes a strong ferromagnet. The local moment of Fe is environment dependent. It increases with the number of Co nearest neighbors and takes its maximum value when all eight nearest neighbor sites have been occupied by Co. This happens in the B2 structure.

5.3.2 Effective cluster interactions and ordering energies in the FM state

The effective cluster interactions in this work has been determined by the SGPM method. This method yields only a "chemical" contribution to the effective interactions, which determine the configurational energetics on a fixed ideal lattice. The contribution related to the possible local lattice relaxations should however be small in the Fe-Co alloys due to small atomic size mismatch of Fe and Co. We have also ignored contribution from lattice vibrations, which we expect to be insignificant in this system at least relative to quite large chemical interactions.

The SGPM interactions are concentration and volume dependent. In Fig.5.6, we show the EPI for three different alloy compositions: $Fe_{0.3}Co_{0.7}$, $Fe_{0.5}Co_{0.5}$, and $Fe_{0.7}Co_{0.3}$ in the FM state. As one can see, the strongest EPI is at the first coordination shell for

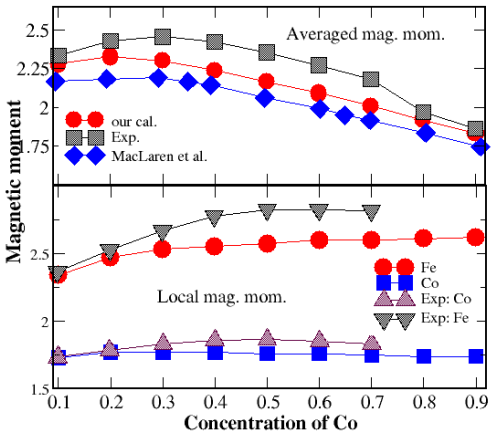

Figure 5.5: Magnetic Moments - Magnetic moments of FeCo alloys. The experimental data have taken from Bardos *et al.*(139) and Collins*et al.*(137) and the theoretical data have taken from MacLaren *et al.* (133)

all the alloy compositions. Other significant interactions are at the first five coordination shells and at the eleventh coordination shell, which is in the closed-packed [111] direction. One can also notice that the nearest neighbor EPI is changing almost by a factor of two in the concentration range of $0.3 < c_{Co} < 0.7$, decreasing for Co-rich alloys. It is clear, that such a dependence should affect the order-disorder transition temperature too.

We have also calculated the three- and four-site interactions. In Fig. 5.7,5.8 we show some of the strongest multisite interactions in $Fe_{0.5}Co_{0.5}$ alloy in the ferromagnetic state. The interaction index is given by the coordination shell numbers of the sides of the corresponding cluster. In the case of the four-site interactions, the order of indexes matters, so the choice is the following: the first four indexes are the coordination shells of the sides of a closed loop through all the four sites, and the last two are the coordination shells of remaining sides of the cluster. It is clear that many-body interactions do not vary systematically, however in most cases the strongest multisite interactions are along the line in the close-packed direction such as, for instance, $V^{(3)}_{1-1-5}$ in the case of 3-site interactions and $V^{(4)}_{1-5-11-1-5-1}$ in the case of four-site interactions. The discussion of the trends for multisite ECI can be found in Ref. (141).

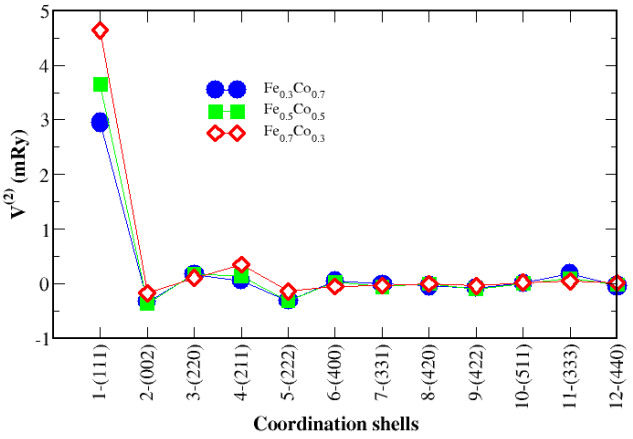

Figure 5.6: EPI - Composition variation of EPI's for FM state Fe_xCo_{1-x} alloys

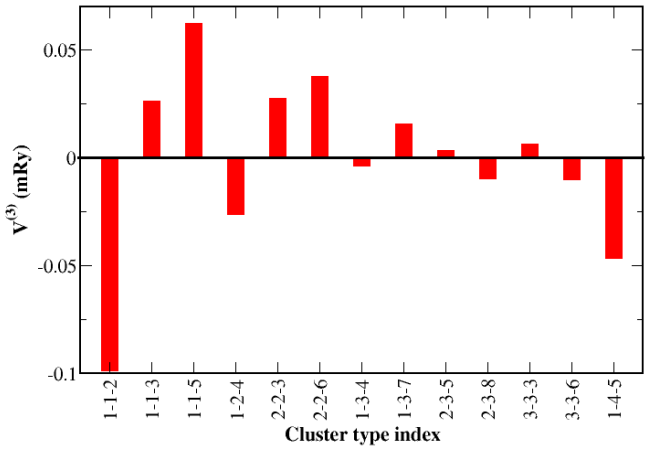

Figure 5.7: ECI - Three-site ECI for $Fe_{0.5}Co_{0.5}$ alloy in the FM state.

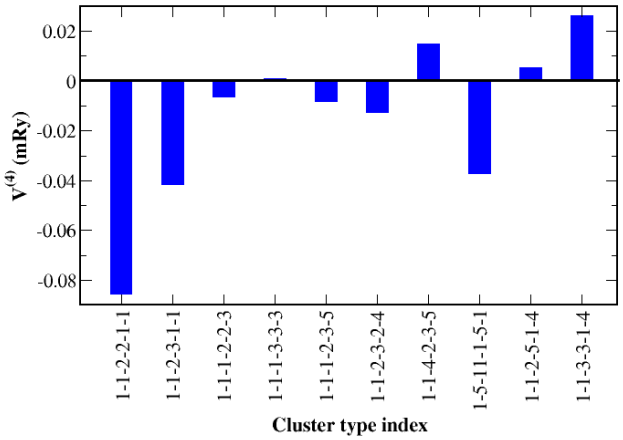

Figure 5.8: ECI - Four-site ECI for $Fe_{0.5}Co_{0.5}$ alloy in the FM state.

In order to check the validity of the SGPM effective cluster interactions, we have calculated the ordering energy of a set of ordered structures α, determined as the difference of the total energies of the ordered random alloys, $\Delta E^{\alpha}_{\rm ord} = E^{\rm ord}_{tot} - E^{random}_{tot}$ from both the direct total energy calculations using this formula as well as from the SGPM interactions. In Table 5.1 we show the ordering energies of FeCo for four different ordered phases: A11, B11, B2 and B32. The agreement seems to be quite good, especially taking into consideration the fact that the SGPM interactions are obtained in the random state, where magnetic state, including, for instance, the local magnetic moments of Fe and Co atoms, is different from those in the ordered structures.

Structure	SGPM(mRy)	Total energy (mRy)
A11	-0.231	-0.639
B11	0.200	0.649
B2	-5.051	-4.614
B32	0.634	0.509

Table 5.1: The ordering energy calculated from the SGPM ECI and from the direct total energy calculations.

5.3.3 Order-disorder phase transition in the reduced ferromagnetic state

Accurate phase equilibria calculations in magnetic systems becomes highly non-trivial at temperatures close to the point of a phase transition when magnetic and configurational interactions are of the same order, i.e. when magnetic and configurational degrees of freedom becomes strongly coupled and complexly interconnected. In Fe-Co alloys the order-disorder phase transition is only 100 C below the magnetic phase transition, which means that magnetic thermal excitations should affect the order-disorder phase transition.

Unfortunately, there is no simple and accurate first-principles based approach to the description of the thermally excited ferromagnetic state of the itinerant magnets, like Fe-Co alloys. Thus, the only way to proceed is to use a simplified model, hopefully not too simple, to the description of the magnetic state. As has been mentioned above, we use the PDLM model for treating the alloy in the ferromagnetic state with a reduced magnetization. Since the magnetic excitations are much faster than atomic configurational, which are connected to the quite slow process of the atomic diffusion, we can separate out the magnetic degree of freedom. In the single-site mean field consideration adopted in this work, the magnetic state is given by the reduced magnetization m.

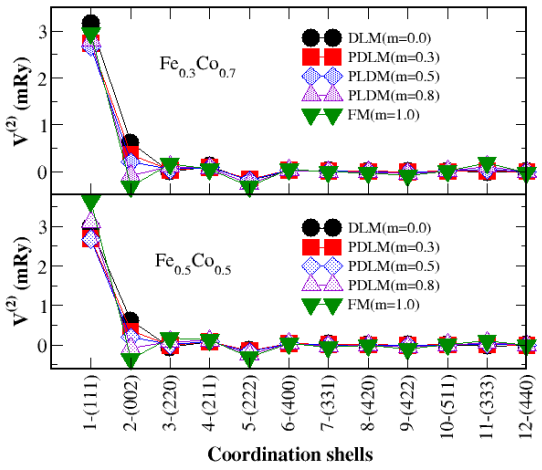

Figure 5.9: EPI - The magnetization dependent EPI's of $Fe_{0.3}Co_{0.7}$ (upper panel) and $Fe_{0.5}Co_{0.5}$ (lower panel) alloys

The variation of the EPI with magnetization from the DLM state ($m = 0$) to the FM state is shown in Fig.5.9 for two different alloy compositions. It is clear that the mostly affected EPI's are for the first and second coordination shells. This is so since the connection between interactions in different magnetic states is roughly determined by the magnetic exchange interaction parameters, which have approximately the same hierarchy as the chemical interactions (113). One can also see that the nearest neighbor EPI changes non-monotonically with magnetization. The most dramatic change with the magnetization is however for the next nearest neighbor EPI: it changes the sign from negative in the FM state to positive in the DLM state. In fact, this change in the EPI for the next nearest neighbor affects very strongly the order-disorder transition temperature.

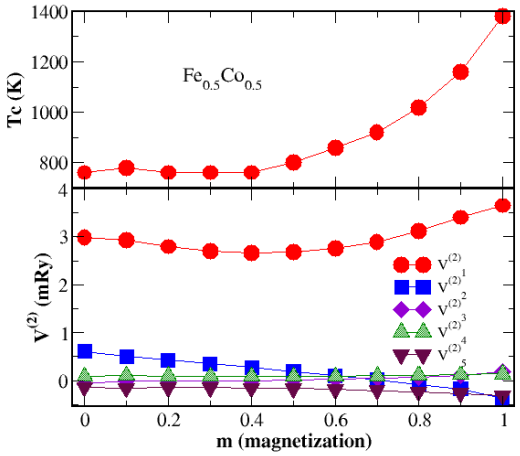

Figure 5.10: Transition - The order-disorder transition temperature (upper panel) and EPI's (lower panel) of $Fe_{0.5}Co_{0.5}$ alloy as a function of magnetization

The order-disorder transition temperatures in Fe-Co alloys in the concentration range of $0.3 < c_{Co} < 0.7$ has been determined in the Monte Carlo simulations. The following ECI have been used in this case: The EPI at the first 30 coordination shells, 13 for three-site and 10 four-site strongest ECI. In Fig. 5.10 we show the calculated order-disorder transition temperature of $Fe_{0.5}Co_{0.5}$ as a function of magnetization together with the EPI at the first five coordination shells. It is clear, that transition temperature is very sensitive to the magnetization. One can also see, that the depen-

dence of the transition temperature from the magnetic state is not entirely related to the magnetization dependence of the EPI at the first coordination shell. In fact very strong increase of the transition temperature close to the FM state is also related to the decrease of the EPI at the second coordination shell. This is so, since the second coordination shell in the B2 structure consists of the atoms of the same type, and therefor negative interaction at this coordination shell is stabilizing the B2 structure.

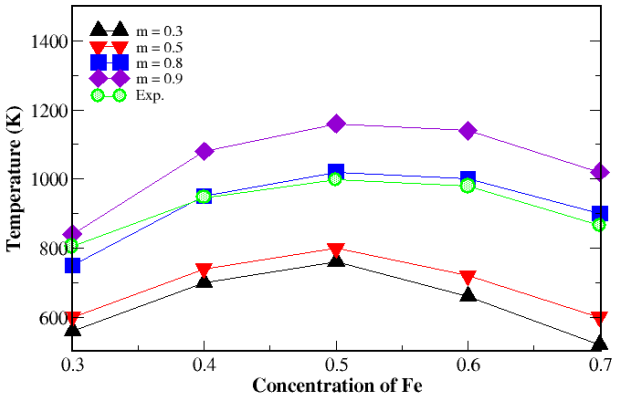

Figure 5.11: Transition - Concentration dependence of the transition temperature for different magnetizations

Finally, in Fig. 5.11 we show the calculated order-disorder transition temperature for several values of magnetization as function of alloy composition together with the experimental data(96). The experimental transition temperature is close to the theoretical prediction for magnetization $m = 0.8$. There are very few experimental data for the magnetization close to the ordering transition. According an early experimental study by Clegg and Buckley (143) and a Mössbauer study by Montano and Seehra(97), the magnetization at the temperature of the ordering transition is $m \simeq 0.83$ for the equiatomic alloy composition. Thus, one can conclude that our results are in very good agreement with experimental data.

Of course, such agreement can to some degree be fortuitous, and further investigations are apparently needed concerning the description of the magnetic state and probably some other contributions, neglected in this work. In particular, a drawback

of our model is that it neglects longitudinal spin fluctuations expected to be important for Co-rich alloys. However, it is clear that our calculations confirm quite strong dependence of the ordering effects on the degree of magnetization, similar to the cases of fcc Fe-Ni (119) and bcc Fe-Cr alloys (118) considered lately.

Chapter 6

Optical properties of FeCo alloys

6.1 Introduction.

Recently there has been much progress in theoretical investigation of electronic properties of ferromagnetic transition metal binary alloys. Optical properties, on the other hand, are far from being fully understood of. At room temperature equiatomic FeCo alloys have CsCl structure (B2 phase with space group Pm3m), where Fe and Co atoms occupy the corners and centers of the cubic cells respectively. The disordered phase is body-centered cubic. Several investigations have been carried out experimentally [(148)] as well as theoretically [(149, 150, 151)] for optical properties of FeCo alloys.

The aim of this work is to propose a formalism for the calculation of configuration averaged optical response functions in disordered binary alloys. Earlier papers [(152, 153)] had proposed the generalized recursion (GR) method as a useful and feasible method for doing so. Here we shall analyze the method in greater detail. Two aspects will be commented on in particular : the combination of GR with the augmented space approach (AS) to deal with disorder, and the inclusion of configuration fluctuations involving essential off-diagonal terms. We shall illustrate the technique by it application to the 50-50 FeCo disordered alloy.

The generalization of the standard recursion method of Haydock *et.al.*[(11, 13)] suggested by Viswanath and Müller [(154)], allows us to obtain continued fraction expressions for correlation functions related to various response functions in solids. We propose a combination of this GR with the AS introduced by us [(25)] as a suitable methodology to study configuration averaged response functions in disordered alloys.

We shall briefly describe the AS and argue that since the disorder in the current operators involved in optical response is essentially off-diagonal, standard single-site mean-field approaches like the CPA are inadequate.

6.2 Methodology.

6.2.1 The generalized recursion.

The idea of a generalized recursion method for obtaining response functions was proposed by Viswanath and Müller [(154)]. The algorithm of recursion is based on linear current response of a system to a perturbing electromagnetic field :

$$\langle \mathbf{J}^{\mu}(t) \rangle = \int_{-\infty}^{\infty} \chi^{\mu\nu}(t-t') \ \mathbf{A}^{\nu}(t') \tag{6.1}$$

where, $\mathbf{A}^{\nu}(t)$ is the vector potential, and the generalized susceptibility can be written as:

$$\chi^{\mu\nu}(t-t') = (i/\hbar) \ \Theta(t-t') \ \langle [\mathbf{J}^{\mu}(t), \mathbf{J}^{\nu}(t')] \rangle \tag{6.2}$$

In lattices with cubic symmetry, $\chi^{\mu\nu} = \chi \ \delta_{\mu\nu}$. The fluctuation-dissipation theorem then relates the imaginary part of the Laplace transform of the generalized susceptibility to the Laplace transform of the current-current correlation function :

$$\chi''(\omega) = (1/2\hbar) \left(1 - \exp^{-\beta\hbar\omega}\right) S(\omega) \tag{6.3}$$

where,

$$S(\omega) = \int_{0}^{\infty} dt \ e^{i(\omega + i\delta)t} \ \mathrm{Tr} \left(\mathbf{J}^{\mu}(t) \ \mathbf{J}^{\mu}(0) \right) \tag{6.4}$$

Since the response function is independent of the direction label μ for cubic symmetry, in the following we shall drop this symbol. Our aim would then be to obtain the correlation function given a Hamiltonian is available to us. For either a system with lattice translational symmetry or for configuration averages in a homogeneously disordered system,

$$S(t) = \frac{1}{N} \sum_{R} \langle R|\mathbf{J}(t)\mathbf{J}(0)|R\rangle = \langle R|\mathbf{J}(t)\mathbf{J}(0)|R\rangle \tag{6.5}$$

In an earlier paper(152) we have described how to obtain the correlation function by a recursive algorithm. For completeness we shall present here the main points. In order to simplify the expressions for the dynamical quantities as produced by the Hamiltonian,

we consider henceforth the modified Hamiltonian $\bar{H} = H - E_0\ I$, whose band energy is shifted to zero. The time evolution of a state $|\psi(t)\rangle = \mathbf{J}(t)\ |\phi\rangle$ is described by the Schrödinger equation

$$-\ i\ \frac{d}{dt}\left\{|\psi(t)\rangle\right\} = \bar{H}|\psi(t)\rangle \tag{6.6}$$

We shall now generate an orthogonal basis $\{|f_k\rangle\}$ for representation of equation (6.6) :

(a) The initial conditions give :

$$|f_{-1}\rangle = 0 \quad ; \quad |f_0\rangle = \mathbf{J}(0)|R\rangle$$

(b) Further members are generated by a three term recurrence :

$$|f_{k+1}\rangle = \bar{H}|f_k\rangle - \alpha_k|f_k\rangle - \beta_k^2|f_{k-1}\rangle;\ \ k \geq 0$$

where mutual orthogonality gives,

$$\alpha_k = \frac{\langle f_k|\bar{H}|f_k\rangle}{\langle f_k|f_k\rangle} \qquad \beta_k^2 = \frac{\langle f_k|f_k\rangle}{\langle f_{k-1}|f_{k-1}\rangle} \tag{6.7}$$

We now expand the state $|\psi(t)\rangle$ in this orthogonal basis :

$$|\psi(t)\rangle = \sum_{k=0}^{\infty} D_k(t)\ |f_k\rangle \tag{6.8}$$

Substituting equation(6.8) into equation(6.6) and using orthogonality of the basis, we get :

$$-\ i\dot{D}_k(t) = D_{k-1}(t) + \alpha_k\ D_k(t) + \beta_{k+1}^2\ D_{k+1}(t) \tag{6.9}$$

and its Laplace transform :

$$(z - \alpha_k)\ d_k(z) - i\delta_{k,0} = d_{k-1}(z) + \beta_{k+1}^2 d_{k+1}(z);\ \ k \geq 0 \tag{6.10}$$

We shall now show that the pair of sequences generated by us, namely, $\{\alpha_k\}$ and $\{\beta_k^2\}$ are enough to generate the correlation function. We first note that :

$$D_0(t) = \langle f_0|\psi(t)\rangle = S(t) \tag{6.11}$$

This set of equations can be solved for $d_0(z)$ as a continued fraction representation :

$$d_0(z) = \cfrac{i}{z - \alpha_0 - \cfrac{\beta_1^2}{z - \alpha_1 - \cfrac{\beta_2^2}{z - \alpha_2 - \ldots}}} \tag{6.12}$$

The structure function, which is the Laplace transform of the correlation function can then be obtained from the above :

$$S(\omega) \;=\; \lim_{\delta\to 0}\; 2\;\Re e\; d_0(\omega + i\delta) \tag{6.13}$$

In case of a disordered alloy we notice that, $S(t) = S[\bar{H}(\{n_R\})]$ is a function of random variable n_R and we need to calculate the configuration averaged value. Therefore we use the augmented space formalism and applying the augmented space theorem [(25)] we can write :

$$\ll S(t) \gg \;\;=\;\; \langle R\otimes\{\emptyset\}\;\Big|\;\widetilde{\mathbf{J}}(t)\widetilde{\mathbf{J}}(0)\;\Big|\;R\otimes\{\emptyset\}\rangle = S[\widetilde{H}(\{\widetilde{N}_R\})] \tag{6.14}$$

where the augmented space Hamiltonian $\widetilde{H}$ and the current operators $\widetilde{\mathbf{J}}(t)$ are constructed by replacing every random variable n_R by the corresponding operator $\widetilde{N}_R$. The recursion may now be modified step by step in the full augmented space :

$$\widetilde{D}_0(t) = \langle\widetilde{f}_0|\{\emptyset\}\otimes\psi(t)\rangle = \ll S(t)\gg \tag{6.15}$$

where $|\widetilde{f}_0\rangle = \widetilde{\mathbf{J}}(0)|R\otimes\{\emptyset\}\rangle$ and,

$$\widetilde{d}_0(z) \;=\; \cfrac{i}{z-\widetilde{\alpha}_0-\cfrac{\widetilde{\beta}_1^2}{z-\widetilde{\alpha}_1-\cfrac{\widetilde{\beta}_2^2}{z-\widetilde{\alpha}_2-\ldots}}} \tag{6.16}$$

The configuration averaged structure function, which is the Laplace transform of the averaged correlation function can then be obtained from the above :

$$\ll S(\omega)\gg \;=\; \lim_{\delta\to 0}\; 2\;\Re e\;\widetilde{d}_0(\omega+i\delta) \tag{6.17}$$

6.2.2 Construction of the Hamiltonian and current operators in augmented space.

As a first step we need to construct the Hamiltonian and the current operator in augmented space. This goes in as an initial input in the recursion process. We shall begin by obtaining the effective Hamiltonian for a random alloy represented in the minimal basis of a tight-binding linear muffin-tin orbitals method (TB-LMTO). This is obtained through a density functional theory (DFT) self-consistent run of an augmented space recursion package (TB-LMTO-ASR). This procedure has been discussed amply

earlier and the interested reader is referred to our review [(26)]. The Hamiltonian is of the form :

$$H = \sum_{RL} C_{RL}\mathbf{P}_{RL} + \sum_{RL}\sum_{R'L'} \Delta^{1/2}_{RL} S_{RL,R'L'} \Delta^{1/2}_{R'L'} \mathbf{T}_{Rl,R'L'} \tag{6.18}$$

where L is the composite index $(\ell m\sigma)$, $\ell m\sigma$ are the angular momenta-spin indices, and R labels the unit cell. For a random binary alloy :

$$\begin{aligned} C_{RL} &= C^A_{RL} n_R + C^B_{RL}(1-n_R) = C^B_{RL} + \delta C_{RL} n_R \\ \Delta^{1/2}_{RL} &= \Delta^{A1/2}_{RL} n_R + \Delta^{B1/2}_{RL}(1-n_R) = \Delta^{B1/2}_{RL} + \delta\Delta^{1/2}_{RL} n_R \end{aligned} \tag{6.19}$$

The ASR prescription gives the Hamiltonian in augmented space as :

$$\widetilde{H} \;=\; \sum_{RL} \widetilde{C}_{RL} \otimes \mathbf{P}_{RL} + \sum_{RL}\sum_{R'L'} \widetilde{\Delta}^{1/2}_{RL} \otimes \widetilde{S}_{RL,R'L'} \otimes \widetilde{\Delta}^{1/2}_{R'L'} \otimes \mathbf{T}_{Rl,R'L'} \tag{6.20}$$

where,

$$\widetilde{C}_{RL} = C^B_{RL}\widetilde{I} + \delta C_{RL}\widetilde{N}_R \qquad \widetilde{\Delta}^{1/2}_{RL} = \Delta^{B1/2}_{RL}\widetilde{I} + \delta\Delta^{1/2}_{RL}\widetilde{N}_R \tag{6.21}$$

The wavefunctions are expressed as linear combinations of the linearized basis functions of the LMTO :

$$\Phi_{j\mathbf{k}}(\mathbf{r}) \;=\; \sum_{RL} c^{j\mathbf{k}}_{RL} \left[\phi_{RL}(\mathbf{r}, E_{\nu\ell}) + \sum_{R'L'} h_{RLR'L'} \dot{\phi}_{R'L'}(\mathbf{r}, E_{\nu\ell}) \right] \tag{6.22}$$

where j is the band index. In this basis, the matrix elements of the current operator can be written as

$$\begin{aligned} J^{\mu}_{RL,R'L'} \;=\; & \Bigg[V^{(1),\mu}_{RL,RL'}\delta_{RR'} + \sum_{L''} \left\{ V^{(2),\mu}_{RL,RL''} h_{RL'',R'L'} + h_{RL,R'L''}\; V^{(3),\mu}_{R'L'',R'L'} \right\} + \ldots \\ & \sum_{R''L''}\sum_{L'''} h_{RL,R''L'''} V^{(4),\mu}_{R''L''',R''L''}\; h_{R''L'',R'L'} \Bigg] \end{aligned} \tag{6.23}$$

where

$$\begin{aligned} V^{(1),\mu}_{RL,RL'} &= \int_{r<s_R} d^3\mathbf{r}\; \phi^*_{RL'}(\mathbf{r}, E_{\nu\ell})\; (-i\nabla^{\mu})\; \phi_{RL}(\mathbf{r}, E_{\nu\ell}) \\ V^{(2),\mu}_{RL,RL'} &= \int_{r<s_R} d^3\mathbf{r}\; \dot{\phi}^*_{RL'}(\mathbf{r}, E_{\nu\ell})\; (-i\nabla^{\mu})\; \phi_{RL}(\mathbf{r}, E_{\nu\ell}) \\ V^{(3),\mu}_{RL,RL'} &= \int_{r<s_R} d^3\mathbf{r}\; \phi^*_{RL'}(\mathbf{r}, E_{\nu\ell})\; (-i\nabla^{\mu})\; \dot{\phi}_{RL}(\mathbf{r}, E_{\nu\ell}) \\ V^{(4),\mu}_{RL,RL'} &= \int_{r<s_R} d^3\mathbf{r}\; \dot{\phi}^*_{RL'}(\mathbf{r}, E_{\nu\ell})\; (-i\nabla^{\mu})\; \dot{\phi}_{RL}(\mathbf{r}, E_{\nu\ell}) \end{aligned}$$

We shall use the prescription of Hobbs [(155)] to obtain the above matrix elements. For details we again refer to reader to the above reference. The next step should be to calculate pair-wise currents where the two end sites are occupied by atom pairs AA, BB and AB embedded in the disordered medium. The current operator in the binary disordered system, unlike the Hamiltonian parameters which were local, lead to off-diagonal disorder. Intrinsically the single site coherent potential approximation is unable to deal with such problems. The strength of the augmented space method comes to the fore. The current can be written as

$$\vec{\mathbf{J}} = \sum_{RL} \vec{J}_{RL,RL}\ \mathbf{P}_{RL} + \sum_{RL,R'L'} \vec{J}_{RL,R'L'}\ \mathbf{T}_{RL,R'L'} \tag{6.24}$$

The diagonal term of the current operator can be written as :

$$\vec{J}_{RL,RL} = \vec{J}^{AA}_{RL,RL} n_R + \vec{J}^{BB}_{RL,RL}(1 - n_R) \tag{6.25}$$

while the off-diagonal term may be written as :

$$\begin{aligned} \vec{J}_{RL,R'L'} &= n_R n_{R'} \vec{J}^{AA}_{RL,R'L'} + (1 - n_R)(1 - n_{R'})\ \vec{J}^{BB}_{RL,R'L'} \\ \ldots &+ [n_R(1 - n_{R'}) + n_{R'}(1 - n_R)]\ \vec{J}^{AB}_{RL,R'L'} \end{aligned} \tag{6.26}$$

We need to express this current operator in augmented space. Replacing n_R by the corresponding operator $\widetilde{N}_R$ we get :

$$\widetilde{\vec{J}}_{RL,RL} = \vec{J}^{BB}_{RL,RL}\ \widetilde{\mathbb{I}} + \vec{J}^{(1)}_{RL,RL}\ \widetilde{N}_R \tag{6.27}$$

these operators either count or create/annihilate configuration fluctuations locally at sites R and

$$\widetilde{\vec{J}}_{RL,R'L'} = \vec{J}^{BB}_{RL} \widetilde{I} + \vec{J}^{(2)}_{RL}(\widetilde{N}_R + \widetilde{N}_{R'}) + \vec{J}^{(3)}_{RL} \widetilde{N}_R \otimes \widetilde{N}_{R'} \tag{6.28}$$

where

$$\vec{J}^{(1)}_{RL} = \vec{J}^{AA}_{RL} - \vec{J}^{BB}_{RL} \qquad \vec{J}^{(2)}_{RL} = \vec{J}^{AB}_{RL} - \vec{J}^{BB}_{RL} \qquad \vec{J}^{(3)}_{RL} = \vec{J}^{AA}_{RL} + \vec{J}^{BB}_{RL} - 2\vec{J}^{AB}_{RL} \tag{6.29}$$

It is easy to check that all the factors above vanish when the structure matrices are independent of site occupation (i.e. not random). The first two operators in the first line of equation (6.28) either count or create/annihilate configuration fluctuations at either of the two sites R and R'. The last operators in the of equation (6.28) either counts or

creates/annihilates configuration fluctuations *simultaneously* at both the sites R and R'. These operators are essentially *non-local* and cannot be dealt with in a local (single-site) mean-field approximation. Once the Hamiltonian is set up as in equation (6.20) and the current operators are set up, as in equations. (6.27-6.28), we go back to our formulation of augmented space recursion described and carry out the calculation for the configuration averaged optical response functions. We use the augmented current operator to construct the starting state

$$|\psi(0)\rangle \;=\; \widetilde{\mathbf{J}}^{\mu}\;|R\otimes\{\emptyset\}\rangle$$

and perform the recursion in augmented space to calculate the configuration averaged correlation function $\ll S(\omega) \gg$. Finally the imaginary part of the dielectric function is related to this correlation function through :

$$\epsilon_2(\omega) = 4\pi\frac{\ll S(\omega)\gg}{\omega^2} \tag{6.30}$$

The real part of the dielectric function $\epsilon_1(\omega)$ is related to the imaginary part $\epsilon_2(\omega)$ by a Kramer's Krönig relationship :

$$\epsilon_1(\omega) = \frac{1}{4\pi}\int_{-\infty}^{\infty}\; d\omega'\;\frac{\epsilon_2(\omega')}{\omega-\omega'} \tag{6.31}$$

All optical response functions may now be derived from these. The optical conductivity follows :

$$\sigma(\omega) = \frac{\omega\epsilon_2(\omega)}{4\pi}$$

The complex refractive index is related to the dielectric function by :

$$n(\omega) + i\kappa(\omega) = \sqrt{\epsilon(\omega)}$$

The imaginary part of the complex refractive index is the extinction coefficient. If we assume the orientation of the crystal surface to be parallel to the optic axis, the reflectivity $R(\omega)$ follows directly from Fresnel's formula :

$$R(\omega) \;=\; \left|\frac{\sqrt{\epsilon(\omega)}-1}{\sqrt{\epsilon(\omega)}+1}\right|^2 \tag{6.32}$$

where $\epsilon(\omega) = \epsilon_1(\omega) + i\epsilon_2(\omega)$ is the complex dielectric function

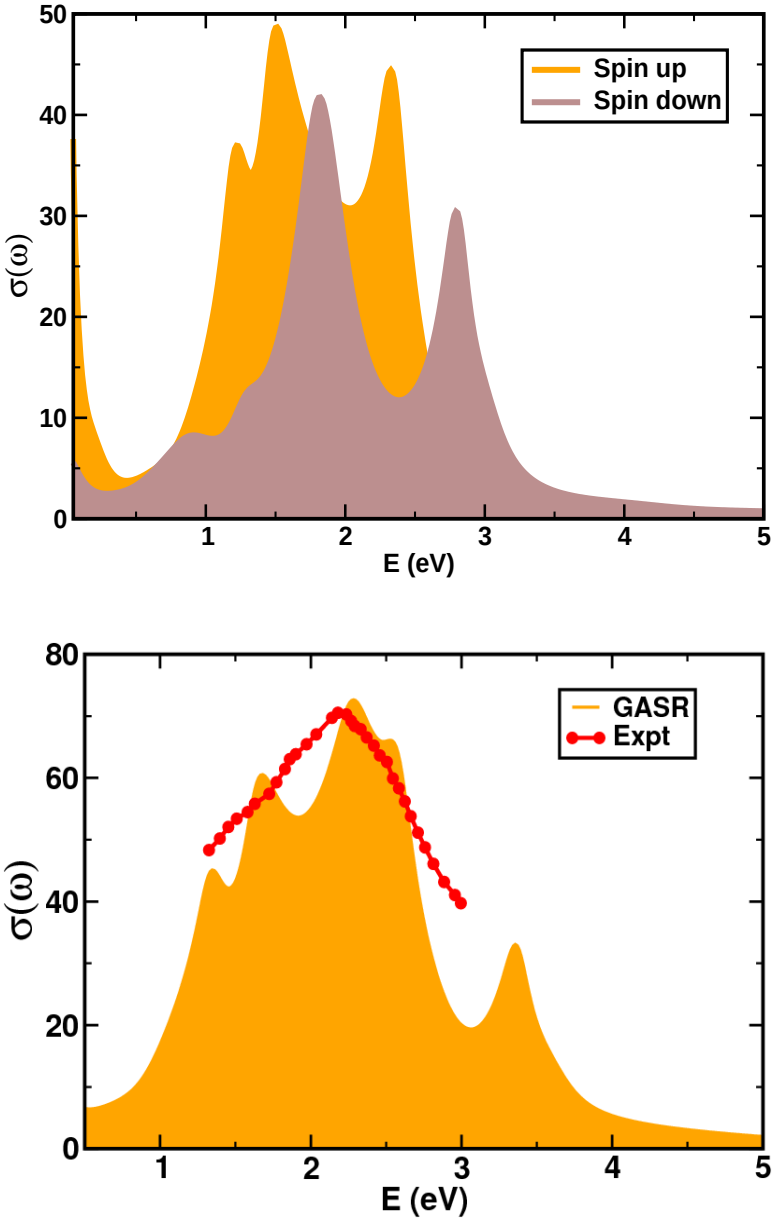

Figure 6.1: (Top panel) The spin projected optical conductivities of FeCo (top panel) and (bottom panel) Comparison of the total optical conductivity with experimental data taken from Sasovskaya *et.al.* [(148)]

6.3 Application to disordered FeCo alloys.

The main feature of interest for later analysis of optical properties is the fact that in FeCo , for the up-spin states the Fermi energy straddles the low density due to *sp* bands. So for low photon energies we expect a Drude like $1/\omega$ behaviour of the optical conductivity. The optical conductivity picks up around photon energies 1.0 eV for the up-spin band and 1.5 eV for the down-spin bands when transitions begin to occur between the *d*-like occupied states to the unoccupied ones. The real part of the dielectric function and the optical conductivity for bcc FeCo disordered alloy at 50-50 composition is shown in Fig. 6.1. For optical conductivity, the structures can be analyzed directly from the densities of states. At low photon energies the optical intra-band transitions are between *sp*-like states and the behaviour is Drude-like. Since the *d*-like structures nearest the Fermi energy that contribute to inter-band transitions are about 1.4 eV (0.1 Ry) below it, the Drude behaviour is only at photon energies below this value. At higher photon energies the inter-band transitions from the occupied*d*-bands to the unoccupied ones provide the structures in optical conductivity. The broad structure between 1.5 - 2.7 (eV) ($\sim$ 0.1 - 0.2 Ry) below the Fermi energy lead to the main structural peak in optical conductivity. Weaker structures between 4-5 eV (0.3 - 0.4 Ry) are dampened by the $1/\omega$ asymptotic behaviour of the optical conductivity. Experimental data are available for ordered $Fe_{50}Co_{50}$ in the CsCl structure [(149), (148)]. Both the works exhibit a broad absorption structure around 1-2.5 eV. A similar structure is also seen in pure Fe at 2.5 eV and in pure Co around 0.8 eV. This has been attributed to inter-band transitions between occupied *d* and unoccupied *p* bands [(151)]. The absorption structures seen in the disordered alloy straddles almost the same photon energies. The structures are broadened by the imaginary part of the disorder induced configuration fluctuation scattering self-energy, as expected. However, the general features are very similar to that of the ordered compound. Interested readers may refer to Figs. (2) and (4) of Kim *et.al.*[(151)] and Fig. 1 of Sasovskaya and Knyazev [(148)] and compare the experimental results with our theory. The agreement is good throughout the photon energy range 0-4 eV.

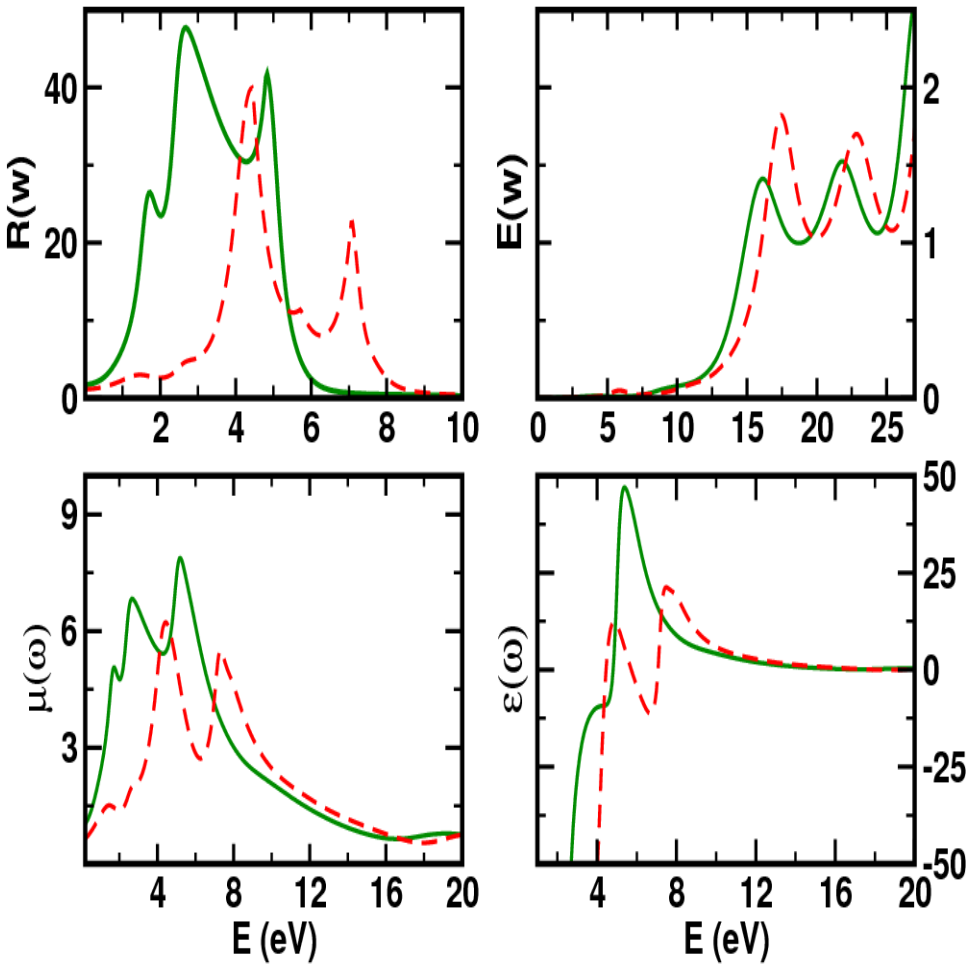

Figure 6.2: Component projected and total (top,left) Reflectivities (top, right) Extinction coefficients (bottom,left) Real part of the refractive index and (bottom, right) Real part of the dielectric function for the disordered FeCo alloy. Full lines for the majority and dashed lines for the minority spins.

Chapter 7

Conclusion and future directions

7.1 General Conclusions.

The plan of this chapter is to summarize the work in this thesis and provide a guideline for future direction.

The thesis is concerned with several aspects : excited states and the band gap, ground state properties of random binary alloys and order-disorder phase transitions in them. We shall briefly describe the steps we have followed to reach our goal.

The first two chapters, we have overviewed and briefly derived the basic tools for the calculation of electronic structure of ordered and disordered systems.

Density functional theory (DFT) is at the heart of electronic structure calculations. It converts a full many-body problem with immensely large degrees of freedom to one which superficially resembles a single electron problem. We introduce the DFT in the first chapter in some mathematical detail. The choice of basis set and potential is important for any electronic structure calculation involving the solution of the Kohn-Sham equations. We have introduced the KKR and LMTO methods for doing this, also in the first chapter.

The second chapter deals with methods to take care of disorder. It includes single mean-field methods like the CPA. It also describes how to go beyond the single-site and take care of effects of the local environment. We describe the augmented space theorem and describe it as the basis of generalizations of the CPA.

In chapter 3, we have developed excited-state DFT for band-gap determinations of bulk semiconductors. A new exchange-correlation functional has been introduced for

excited-state band energy. The excited-state formalism has been applied to a series of semi-conductors and insulator. The results have shown very good agreement with the available experimental data.

In chapter 4, the cluster coherent potential approximation (CCPA) have introduced for studying of local environmental effects on random substitutional binary alloys. The augmented space formalism and downfolding techniques have been used to get a self-consistent CCPA for random alloys. This CCPA satisfies the necessary Herglotz analytic properties. The CCPA has been applied to three disordered disordered alloys : CuZn, NiAl and CuAu and the results compared with other methods.

A detailed investigation of magnetic FeCo alloys have been carried out in the last two chapters. The electronic structure and order-disorder phase transition of ferromagnetic FeCo alloys have discussed in details in chapter 5. The influence of magnetism at the order-disorder phase transition have been investigated within the disorder local moment (DLM) model. Effective cluster interactions have been used in Monte-Carlo simulations to calculate the order-disorder transition temperatures of. The concentration dependent effective cluster interactions have been calculated by the generalized perturbation method (GPM). This DLM based model has shown that the order-disorder transition of ferromagnetic FeCo alloys is strongly influenced by magnetism.

In the last chapter 6, we have derived the augmented space generalized recursion formalism for the calculation of configuration averaged optical response functions in random binary alloys. The diagonal and off diagonal disorder the current operator have been taken into account. The theoretical results for the optical conductivity of FeCo alloys have been compared with the available experimental data.

7.2 Future directions.

Alloys form an important and fascinating materials problem. Stainless steels, iron, nickel and cobalt alloys, superalloys, titanium alloys, tungsten based alloys, and high-temperature and corrosion-resistant metals are needed extensively for aerospace, medical, automotive machinery, bridges, buildings, and energy applications. Iron alloys have very diverse chemical compositions and properties. These steels can perform under exceedingly rigorous service conditions. They also have good electrical, thermal, and magnetic properties. Stainless steel or other iron alloys require an understanding of

long-range and short range ordering, heat-treating, corrosion-resistivity and electrical resistivity etc.

Physical models of these phenomena remain the subject of intense research and, often, dispute. The mathematical properties of the models have to be studied rigorously. Besides electronic structure for ground states at zero temperature. It is necessary to introduce thermodynamic models coupled with first-principle techniques in order to analyze temperature dependent properties.

A PhD. programme is always time bound and a person's thirst for knowledge may not find it's fulfillment in this limited span of time. But this endeavor may be considered as a training ground for research and it does elevate his thirst for more. I cannot assess how much knowledge of disorder physics I have been able to pick up, but I sincerely believe that this work with all its limitations will encourage me to go on working in this vastly exciting area of materials studies.

References

[1] P. Grosso and P. Parvicini. **Solid State Physics**. *Academic Press*, 2003. 2

[2] P. Hohenberg and W. Kohn. **Phys. Rev.**. *136, 864*, 1964. 3, 8, 13

[3] W. Kohn and L. J. Sham. **Phys. Rev.**. *140, A1133*, 1965. 3, 49, 59

[4] E. H. Lieb. **Int. J. Quant. Chem.**. *24, 243*, 1983. 10, 11, 48

[5] M. Levy. **Phys. Rev. A**. *26,1200*, 1982. 10

[6] C. De Dominicis and P. C. Martin. **J. Math. Phys.**. *5, 14*, 1964. 12

[7] R. Fukuda, T. Kotani, Y. Suzuki, S. Yokojema. **Prog. Theo. Phys.**. *92,4,833*, 1994. 12

[8] H. Hellmann. **Einfuhrung in die Quantenchemie, Leipzig**. *Book*, 1937. 13

[9] R. P. Feynman. **Phys. Rev.** . *56, 340*, 1939. 13

[10] O K Andersen and O. Jepsen. **Phys. Rev. Lett.** . *53, 2571*, 1984. 16

[11] R. Haydock. **thesis.** . *University of Cambridge, U.K.*, 1972. 22, 58, 70, 108

[12] V. Heine. **Solid State Physics**. *vol 35 (Academic Press)*, 1982. 22

[13] Haydock R, Heine V and Kelly M J **J. Phys. C: Solid State Phys.** *5, 2845.*,1972 24, 108

[14] Nex C. M. M. **Comput. Phys. Commun.** *53, 141*,1989 26

[15] Luchini M. U. and Nex C. M. M. **J. Phys. C: Solid State Phys.** *20, 3125*,1987. 26, 27

[16] Haydock R., Nex C. M. M. and Wexler G. **J. Phys. A: Math. Gen** *37, 161*,2004. 26

[17] P. Soven. **Phys. Rev.** . *156, 809*, 1967. 33, 94

[18] D. W. Taylor. **Phys. Rev.** . *156, 1017*, 1967. 33

[19] R.J. Elliott, J. A. Krumhansl and P.L. Leath. **Rev. Mod. Phys.** . *46, 465*, 1974. 36

[20] Nickel B. and Krummhansl J. A **Phys. Rev. B:** *4, 4353*,1971 36

[21] Tsukuda M. **J. Phys. Soc. Jpn** *26, 684*,1969. 36

[22] Tsukuda M. **J. Phys. Soc. Jpn** *32, 1475*,1972. 36

[23] Butler W. H. **Phys. Rev. B** *31, 3260*, 1985. 36

[24] Kaplan T. and Gray L. J. **Phys. Rev. B** *15, 3260*, 1977. 37

[25] A. Mookerjee. **J. Phys. C: Solid State.** . *6, 1340*, 1973. 38, 60, 62, 108, 111

[26] A. Mookerjee. **in Electronic Structure of cluster, surfaces and disordered solids ed. A. Mookerjee and D.D. Sarma.** . *Taylor Francis*, 2003. 38, 60, 112

[27] J. Kudrnovský and V. Drchal. **Phys. Rev. B** . *41, 7515*, 1990. 45

[28] Johnson D.D., Nicholson D.M., Pinski F.J., Gyorffy B.L and Stocks G.M., **Phys. Rev. Lett.:** *56, 2088*,1986. 45

[29] Johnson D.D., Nicholson D.M., Pinski F.J., Gyorffy B.L and Stocks G.M., Phys. Rev. B.: 41, 9701,1990. 45

[30] A.V. Ruban and H. L. Skriver. **Phys. Rev. B** . *66, 024201*, 2002. 45, 94, 95

[31] A. V. Ruban, S. Shallcross, S. I. Simak, P. A. Korzhavyi and H. L. Skriver. **Phys. Rev. B** . *66, 024202*, 2002. 45, 94

[32] R. M. Martin . **Electronic Structure: basic theory and practical calculation** . *Published 2004, Cambridge University Press*, 2004. 47

[33] J.P. Perdew, R.G. Parr, M. Levy and J.L. Balduz Jr.. **Phys. Rev. Lett.** . *49, 1691*, 1982. 47

[34] J.P. Perdew and M. Levy. **Phys. Rev. Lett.** . *51, 1184*, 1983. 48

[35] L.J. Sham and M. Schluter. **Phys. Rev. Lett.** . *51, 1888*, 1983. 48

[36] A. Gorling. **Phys. Rev. A** . *59, 3359*, 1999. 48

[37] M. Levy, Á. Nagy. **Phys. Rev. Lett** . *83, 4361*, 1999. 48

[38] Á. Nagy and M. Levy. **Phys. Rev. A** . *63, 052502*, 2001. 48

[39] M. Levy. **Proc. Natl. Acad. Sci. USA** . *76, 6062*, 1979 48

[40] P. Samal and M.K. Harbola. **J.Phys.B: At. Mol. Opt. Phys.**. *39, 4065*, 2006. 48, 55

[41] P. Samal and M.K. Harbola. **J.Phys.B: At. Mol. Opt. Phys.**. *38, 3765*, 2005. 49, 50, 55

[42] P.A.M. Dirac. **Proc. Cambridge Phil. Soc**. *26, 376*, 1930. 50

[43] Andersen O K, Kasowski R V. **Phys. Rev. B** . *4, 1064*, 1971. 53

[44] Kasowski R V, Andersen O K. **Solid State Commun** . *11, 1064*, 1972.

[45] Andersen O K, Woolley R G. **Mol.Phys** . *28, 905*, 1973.

[46] Andersen O K. **Phys. Rev. B** . *12, 3060*, 1975. 53

[47] T. Kotani. **Phys. Rev. B** . *50, 14816*, 1994. 54, 56

[48] T. Kotani. **Phys. Rev. Lett.** . *74, 2989*, 1995. 54, 56

[49] T. Kotani and H. Akai. **Phys. Rev. B** . *54, 16502*, 1996. 54

[50] A.Svane. **Phys. Rev. B** . *35, 5496*, 1987. 54, 56

[51] R.P.Pandey,J.E.Jaffe,and A.B.Kunz. **Phys. Rev. B** . *44, 9228*, 1991. 56

[52] M.S.Hybertsen and S.G.Louie. **Phys. Rev. B** . *34, 5390*, 1986. 56

[53] R.C.Whited,C.J.Flaten,and W.C.Walker. **Solid State Commun** . *13,1903*, 1973. 56

[54] I.N.Remediakis and Efthimios Kaxiras. **Phys. Rev. B** . *59,5536*, 1999. 56

[55] S.C.Abrahams. **Acta Crystallographica B** . *24, 1968*, 1982. 56

[56] K.H.Hellwege and A.M.Hellwege. **Landolt-Börnstein Tables**. *Group III,Vol.7b(Springer,Berlin*, 1975. 56

[57] Kittel,C.. **Introduction to Solid State Physics,6th Ed.,New York:John Wiley**. *p.185*, 1985. 54, 56

[58] R.W. Godby, M. Schluter and L.J. Sham. **Phys. Rev. Lett.** . *56, 2415*, 1986. 54

[59] S.S.A. Razee and R. Prasad. **Phys. Rev. B** . *48, 3265*, 1992. 57, 58

[60] S.S.A. Razee and R. Prasad. **Phys. Rev. B** . *48, 1349*, 1993. 57, 58, 69

[61] S.Ghosh, P.L. Leath and M.H. Cohen. **Phys. Rev. B** . *66, 14206*, 2002. 57, 70, 83

[62] A. Chakrabarti and A. Mookerjee. **E. Phys. J.: B** . *44, 21*, 1993. 57

[63] A. Zunger, S. -H. Wei, L.G. Ferreira and J.E. Bernard. **Phys. Rev. Lett.** . *65, 353*, 1990. 57, 83

[64] M. Jarrell and H.R. Krishnamurthy. **Phys. Rev. B.** . *63, 125102*, 2001. 58, 83

[65] D.A. Rowlands, J.B. Staunton, B.L. Gyorffy, E. Bruno and B. Ginatempo,. **Phys. Rev. B.** . *72, 045101*, 2005. 58, 79, 83, 88

[66] R. Haydock. **Philos. Mag. B.** . *43, 203*, 1981. 58

[67] R. Haydock and R. L. Te . **Phys. Rev. B.** . *49, 10845* , 1981.

[68] N. Beer and D.G. Pettifor. **The Electronic Structure of Complex Systems** . *43, 203*, 1981. 58

[69] A. Gonis and J.W. Garland . **Phys. Rev. B.** . *16, 2424* , 1977. 59

[70] J.S. Faulkner. **Progess in Materials Science, ed. J.W. Christian,P. Hassen and T. Massalski (Pergamon, New York)** . *27, 1* , 1982. 59

[71] O.K. Andersen and O. Jepsen . **Phys. Rev. Lett.** . *53, 2571* , 1984. 59, 60

[72] Moshiour Rahaman and A. Mookerjee . **See EPAPS Document No. E-PRBMDO-79-092901 for details of the derivation of the CCPA equations. For more information on EPAPS** . *see http://www.aip.org/pubservs/epaps.html.* , 2009. 64, 66, 67, 73

[73] S.S.A. Razee, A. Mookerjee and R. Prasad . **JPCM** . *3, 3301* , 1991. 70

[74] T. Saha, I. Dasgupta and A. Mookerjee . **Phys. Rev. B.** . *50, 13267*, 1994. 70, 83

[75] T. Saha, I. Dasgupta and A. Mookerjee . **JPCM.** . *8, 1979* , 1996. 70, 83

[76] R. Haydock. **in Solid State Theory,Academic Press, New York** . *35* , 1980. 70, 83

[77] R. Mills and P. Ratanavararaksa . **Phys. Rev. B.** . *18, 5291*, 1978. 70

[78] R. Mills, L.J. Gray and T. Kaplan . **Phys. Rev. B.** . *27, 3252*, 1983. 70

[79] A. Mookerjee and R. Prasad. **Phys. Rev. B.** . *48, 17724*, 1993. 70, 71

[80] A. Bansil and H. Ehrenreich . **Phys. Rev. B.** . *9, 445*, 1974. 74

[81] I.A. Abrikosov, A.M.N. Niklason, S.I. Simak, B. Johansson, A.V. Ruban and H.L. Skriver. **Phys. Rev. B.** . *76, 014434*, 2007. 75

[82] I.A. Abrikosov, Yu. H. Velikov, P.A. Korzhavyi, A.V. Ruban and L.E. Shilkrot . **Solid State Commun** . *83, 867*, 1992. 75

[83] P.A. Korzhavyi, A.V. Ruban, I.A. Abrikosov and H.L. Skriver. **Phys. Rev. B.** . *51, 5773*, 1995. 75

[84] Y. Wang, G. Stocks, W.A. Shelton and D.M.C Nicolson, Z. Szotek and W.M. Temmerman. **Phys. Rev. Lett..** . *75, 2867*, 1995. 75

[85] E. Bruno, L. Zingales and A. Milici . **Phys. Rev. B.** . *66, 245107*, 2002. 75

[86] K. Tarafder, A. Chakrabarti, K.K. Saha and A. Mookerjee . **Phys. Rev. B.** . *74, 144204*, 2006. 75, 77

[87] K.K. Saha, A. Mookerjee and O. Jepsen. **Phys. Rev. B.** . *71, 094207*, 2005. 76

[88] D.A. Biava, Subhradip Ghosh, D.D. Johnson, W.A. Shelton and A.V. Smirnvo. **Phys. Rev. B.** . *72, 113105*, 2005. 83

[89] H. Sato and R.S. Toth. **Phys. Rev.** . *124, 1833*, 1961. 88

[90] K. Yamagishi, S. Hashimoto and H. Iwasaki . **J. Phys. Soc. Jp.** . *51, 605-611* , 1982. 88

[91] K. Tarafder, S. Ghosh, B. Sanyal, O. Eriksson, A. Mookerjee and A. Charkrabarti . **JPCM** . *20, 445201* , 2008. 83

[92] Moshiour Rahaman and A. Mookerjee . **Phys. Rev. B.** . *79, 054201*, 2009. 88

[93] M. Chakrabarty, A. Chakrabarti and A. Mookerjee . **J. Magn. Mater** . *313, 243*, 2007. 89

[94] T. Sourmail . **Prog. Mat. Sci**. *50, 816*, 2005. 90

[95] M. S. Seehra and P. Silinsky . **Phys. Rev. B.,** *13, 5183*, 1976. 90

[96] J. A. Oyedele and M. F. Collins . **Phys. Rev. B.** . *16, 3208*, 1977. 90, 106

[97] P. A. Montano and M. S. Seehra. **Phys. Rev. B.** . *15, 2437* , 1977. 90, 106

[98] D. Bonnenberg, K.A. Hempel and H.P.J. Wijn . **1.2.1.1** . *Phase diagrams, lattice parameters. H.P.J. Wijn (ed.). Springer Materials - The Landolt-Brnstein Database* . 90, 95

[99] I. Ohnuma, H. Enoki, O. Ikeda, R. Kainuma, H. Ohtani, B. Sundman and K. Ishida,. **Acta Meteriala** . *50, 379*, 2002. 91

[100] V. Pierron-Bohnes, M. C. Cadeville and F. Gautier. **J. Phys. F: Met. Phys.** . *13, 1889-1713* , 1983. 91, 92

[101] V. Pierron-Bohnes, M. C. Cadeville and F. Gautier. **J. Phys. F: Met. Phys.** . *15, 1441-1448* , 1985. 91, 92

[102] V. Pierron-Bohnes, M. C. Cadeville, A. Bieber and F. Gautier. **J. Magn. Magn. Mater** . *54-57, 1027-1028*, 1986. 91, 92

[103] A. Beinenstock and J. Lewis . **Phys. Rev.** . *160, 393*, 1967. 91, 92

[104] Z. Racz and M. F. Collins . **Phys. Rev. B.** . *21, 229*, 1980. 91, 92

[105] R. A. Tahir-Kheli and Kawasaki T.. **JPC** . *10, 7207*, 1977.

[106] L. Billard, P. Villemain and A Chamberod, . **JPC** . *11, 2815*, 1978.

[107] J. L. Morán-Lopez and L. M. Falicov . **JPC** . *13, 1715-23*, 1980.

[108] F. Mieja-Lira, J. Urias and J.L. Moŕan-Lopez, . **Phys. Rev. B.** . *24, 5270* , 1981.

[109] J. Mizial, M.F. Collins and M. Iwamatsu . **J. Phys. F: Met. Phys** . *12, L115-20*, 1982.

[110] J.M. Sanchez and C.H. Lin . **Phys. Rev. B.** . *30, 1448*, 1984.

[111] F. J. Martinez-Herrera, F. Mejia-Lira, F. Aguilera-Granja and J. L. Morán-Lopez . **Phys. Rev. B.** . *31, 1686*, 1985.

[112] F. Ducastelle and F. Gautier . **J.Phys. F: Met.Phys** . *6, 2039* , 1976.

[113] A. Bieber and F. Gautier . **J. Magn. Magn. Mater** . *99, 293*, 1991. 105

[114] M. Sluiter and Y. Kawazoe . **Sci. Rep. RITU A** . *40, pp301-306*, 1995.

[115] J. Kudrnovský, I. Turek, A. Pasturel, R. Tetot, V. Drchal, and P. Weinberger . **Phys. Rev. B.** . *50, 9603*, 1994.

[116] A. Diaz-Ortiz, a, R. Drautzb, M. Fhnleb and H. Doschb . **J. Magn. Magn. Mater** . *780, 272-276* , 2004.

[117] A. Daz-Ortiz, R. Drautz, M. Fähnle, H. Dosch, and J. M. Sanchez. **Phys. Rev. B.** . *73, 224208*, 2006.

[118] A. V. Ruban, P. A. Korzhavyi and B. Johansson. **Phys. Rev. B.** . *77, 094436*, 2008. 107

[119] M. Ekholm, H. Zapolsky, A. V. Ruban, I. Vernyhora and I. A. Abrikosov . **Phys. Rev. Lett.** . *105, 167208*, 2010. 107

[120] M. Cyrot . **Phys. Rev. Lett.** . *25, 871*, 1970. 93

[121] B. L Gyorffy, A. J. Pindor. J. Staunton, G. M. Stocks and H. Winter . **J. Phys. F: Met. Phys.** . *15, 1337-1386* , 1985. 93

[122] A. V. Ruban, S. Shallcross, S. I. Simak and H. L. Skriver . **Phys. Rev. B.** . *70, 125115* , 2004. 93

[123] A. V. Ruban and H. L. Skriver . **Phys. Rev. B.** . *55, 856* , 1997.

[124] I. A. Abrikosov and H. L. Skriver. **Phys. Rev. B.** . *47, 16532*, 1993. 94, 95

[125] A. V. Ruban and H. L. Skriver . **Comput. Mater. Sci**. *15, 119*, 1999. 94, 95

[126] I. A. Abrikosov, A. M. N. Niklasson, S. I. Simak, B. Johansson, A. V. Ruban and H. L. Skriver . **Phys. Rev. Lett..** . *76, 4203*, 1996. 94

[127] I. A. Abrikosov, S. I. Simak, B. Johansson, A. V. Ruban and H. L. Skriver . **Phys. Rev. B.** . *56, 9319* , 1997. 94

[128] L. Vitos . **Phys. Rev. B.** . *64, 014107*, 2001. 94

[129] B.L. Gyorffy. **Phys. Rev. B.** . *5,2382* , 1972. 94

[130] J. P. Perdew and Y. Wang . **Phys. Rev. B.** . *45,13244* , 1992. 94

[131] A. V. Ruban, S. I. Simak, P. A. Korzhavyi and H. L. Skriver . **Phys. Rev. B.** . *66, 024202*, 2002. 95

[132] H. J. Monkhorst and J. D. Pack . **Phys. Rev. B.** . *13, 5188*, 1972. 95

[133] J. M. MacLaren, T. C. Schilthless, W. H. Butler, R. Sutton, and * McHenry . **J. Appl. Phys.** . *85, 4833*, 1999. 95, 99, 101

[134] A. V. Ruban, H. L. Skriver and J. K. Norskov . **Phys. Rev. Lett.** . *80, 1240* , 1998. 96, 97

[135] Richter R, Eschrig H and Velicky B, . **J. Phys. F.: Met. Phys.** . *17, 351* , 1987. 98

[136] K. Schwarz, P. Mohn, P. Blah and J. Kübler, . **J. Phys. F: Met. Phys** . *14, 2659-2671*, 1984.

[137] M. F. Collins, J. B. Forsythe . **Philos. Mag.**. *8, 401*, 1963. 99, 100, 101

[138] J. S. Kouvel . **Magnetism and Metallurgy, ed. A. E. Berkowitz and E. Kneller (Academic, New York, 1969)** . *Vol. 2, p. 523*, 1969.

[139] D. I. Bardos . **J. Appl. Phys.** . *40, 1371* , 1969. 101

[140] M. C. Cadeville and J. L. Moran-Lopez . **Phys. Reports**. *153, 6, 331*, 1987. 100

[141] A. Bieber and F. Gautier . **J. Phys. Soc. Jap** . *53,6, 2061*, 1984. 101

[142] Toru Moriya. **Spin Fluctuations in Itinerant Electron Magnetism** . *Springer-Verlag*, 1985.

[143] D.W. Clegg and R.A. Buckley . **Matal. Sci.** . *7, 48*, 1973. 106

[144] H.G. Baer . **Naturwissenschaflen in German** . *43, 298*, 1956.

[145] H.G. Baer . **Z. Metalik** . *49, 614*, 1958.

[146] I.A. Bagariatskii and I.D. Tiapkin . **Sov.Phys. Doklady** . *3, 1025*, 1958.

[147] R.J Taunt and B. Ralph . **Surf. Sci.** . *47,569-582* 1975.

[148] Sasovskaya I.I. and Knyazev Yu. V., **Zh. Prikladnoi Spektroskopii** *28, 564* (1978) viii, 108, 115, 116

[149] Kim K.J., Lee S.J. and Lynch D.W., **Solid State Commun.** *11, 457* (2000) 108, 116

[150] Kulkova S.E., Valujsky D.V., Jai Sam Kim, Geunsik Lee, Koo Y.M., **Physica B**, *322, 236*, (2002) 108

[151] Kim K.J., Leung T.C., Harmon B.N. and Lynch D.W., **J. Phys. C : Solid State** *6, 5069* (1994) 108, 116

[152] Tarafder K. and Mookerjee A., bf J. Phys. Condens. Matter *17, 6435.*,(2005) 108, 109

[153] Saha K.K. and Mookerjee A., **J. Phys. Condens. Matter** *17, 4559* 2005 108

[154] Viswanath V.S. and Müller G., **in "The user friendly recursion method", (Troisieme Cycle de la Physique, en Suisse Romande, 1993)** 108, 109

[155] Hobbs D., Piparo E., Girlanda R. and Monaca M., **J. Phys. Condens. Matter** *7, 2541* (1995) 113

List of Publications

1. **Study of phase stability in a class of binary alloys using augmented space recursion based orbital peeling technique**
   Kartick Tarafder, Moshiour Rahaman, Durga Paudyal, Biplab Sanyal, Olle Eriksson and Abhijit Mookerjee
   Physica B: **404, 1137-1142**, (2008).
2. **A local-density approximation for the exchange energy functional for excited states: The band-gap problem.**
   Moshiour Rahaman, Shreemoyee Ganguly, Prasanjit Samal, Manoj Kumar Harbola, Tanusri Saha-Dasgupta, Abhijit Mookerjee
   Physica B: **404, 1137-1142**,(2009).
3. **An augmented space based cluster coherent potential approximation for binary random and short-range ordered alloys**
   Moshiour Rahaman and Abhijit Mookerjee
   Phys. Rev.B, **79, 054201**,(2009)
4. **An augmented space based cluster coherent potential approximation : application to CuAu and NiAl alloys**
   Moshiour Rahaman and Abhijit Mookerjee
   Accepted in **IJMPB, to be published in December, 2010**
5. **Magnetic behaviour of AuFe and NiMo alloys**
   Prashant Singh, Rudra Banarjee, Moshiour Rahaman, A.V. Ruban, Biplab Sanyal and A. Mookerjee
   Accepted in **PRAMANA**, (2010)
6. **Magnetic state effect upon the order-disorder phase transition in FeCo alloys: A first-principles study**
   Moshiour Rahaman, A.V. Ruban, A. Mookerjee and B. Johansson
   Submitted in Phys. Rev.B.

[0]The contents of the paper with serial number (1) and (5) are not included in this thesis.